Scholars' Mine

Spring 2018

Proppant transport with varying injection points and its impact on proppant development inside a fracture

Shail Janakbhai Soni

Follow this and additional works at: https://scholarsmine.mst.edu/masters_theses

Part of the Petroleum Engineering Commons

Department:

PROPPANT TRANSPORT WITH VARRYING INJECTION POINTS

AND ITS IMPACT ON PROPPANT DEVELOPMENT INSIDE A FRACTURE

by

SHAIL JANAKBHAI SONI

A THESIS

Presented to the Faculty of the Graduate School of the

MISSOURI UNIVERSITY OF SCIENCE AND TECHNOLOGY

In Partial Fulfillment of the Requirements for the Degree

MASTER OF SCIENCE IN PETROLEUM ENGINEERING

2018

Approved by

Dr. Shari Dunn Norman, Advisor
Dr. Abdulmohsin Imqam, Co-advisor
Prof. Larry K. Britt
Dr. Joseph Smith

ABSTRACT

This study presents experimental work which examines the effect of perforation placement and density on proppant placement within a hydraulic fracture. The study also investigates the effect of proppant angularity.

Experiments were conducted with ceramic proppant injected in a fracture slot model consisting of three injection points at the bottom, middle and top of the fracture slot, and two outlets, at the bottom and top of the fracture model. The effect of single point injection height was investigated by injecting solely at the bottom, middle or top of the apparatus, for both bottom and top outlet conditions. Multiple injection points were investigated with dual and triple injection experiments. Results of these experiments were reported as equilibrium dune height (EDL) and length (EDX) as well as proppant surface area.

Results show that for single point injection, proppant surface area increases with the increase in the injection point height relative to the bottom of the fracture. Reduced slurry velocities for multiple injection points reduces proppant transport. Multipoint injection cases were most similar to single point injection at the middle of the slot.

The effect of proppant angularity was investigated by comparing transport behavior of brown sand to ceramic proppant using single point injection. It has been shown that the shape of the dune is dependent on the friction angle of proppant. Proppant with high sphericity and roundness creates a low angle dune whereas sand creates a greater EDL and EDX.

ACKNOWLEDGMENTS

I would like to thank my advisor Dr. Shari Dunn Norman and co-advisor Dr. Abdulmohsin Imqam for their constant support, commitment, pushing us to work as group, to go beyond conventional methods to fulfil the purpose of the research. financially support, and making me the student I should be and the person I have become.

I admire committee members Prof. Larry Brit and Dr. Joseph Smith for their help with visualization of research and its prospect towards field application as well as the guidance they provided.

Finally, I would like to thank my friends Vivek, Dhurgham for being there, helping each other at lab to make research work a joyful ride, my roommates, and my family back in India for their emotional support throughout my journey.

TABLE OF CONTENTS

LIST OF ILLUSTRATIONS

LIST OF TABLES

NOMENCLATURE

Symbol	Description
g	Gravitational constant, 980 cm/s^2
ρ_p	Particle density, gm/cc
ρ_f	Fluid density, gm/cc
D_p	Particle diameter, cm
μ_f	Fluid viscosity, poise
α, β	Boundary layer coefficients
$V_{equilibrium}$	Equilibrium velocity, ft/min
q_i	Injection rate, bbl/min
$\overline{w}$	Average fracture width, in
h_o	Cross-sectional area above-settled sand, ft
C_{fD}	Dimensionless fracture conductivity
k_f	Fracture permeability, md
W	Fracture width, ft
k	Reservoir permeability, md
x_f	Fracture half length, ft
θ	Angle of repose
l	Fracture length, mm
h_f	Fracture height, mm

v_w Settling rate corrected for presence of walls, cm/s

V_s Settling velocity, cm/s

P Pressure,

ρ Slurry density, m/cc

m_p Proppant mass, gm

m_w Water mass, gm

V_p Proppant volume, cc

V_w Water volume, cc

K_L Loss coefficient, dimensionless

D_e Equivalent diameter, cm

h Slot height, cm

w Slot width, cm

μ Apperent slurry viscosity, poise

Q_s Slurry flowrate, cm^3/s

l Slot length, cm

$V_\varnothing$ Settling rate of concentrated particle, cm/s

$\varnothing$ Proppant concentration (Volume of solid/Volume of mixture)

SPF   Shots per foot

PFP   Preferred hydraulic fracture plane

Δp_{pf} Perforation back pressure

C   Discharge co-efficient

$\dfrac{q}{n}$	Flowrate per perforation in bpm
γ	Geometry factor
G	Elastic shear modulus
E	Young's modulus
v	Poisson's ratio
$V_{s,hindered}$	Hindered settling velocity
C_v	Volume concentration of solid
EDL	Equilibrium dune level, %
EDX	Equilibrium dune length, %
FPV	Fracture Pore Volume

1. INTRODUCTION

The first hydraulic fracture treatment was pumped in a well located in the Hugoton field, which was previously treated with an acid treatment in 1947. It was performed to compare the effect of the hydraulic simulation to acidizing directly. Hydraulic stimulation is the process of pumping fluid (i.e. transport fluid) into the wellbore at a high injection rate and breaking the formation, which creates a fracture. This fracture is kept open using proppant (such as sand or ceramic particles).

Natural gas production in the United States has rapidly increased from shale gas reservoirs in the past decade. Around 28% of the total energy supplied, comes from natural gas and it has been the second largest source of energy since the 1960s in the United States. In 2016, the marketed production of natural gas was 28.5 trillion ft^3 (U.S. Energy Information Administration, 2017) for the United States.

Since natural gas is important and is a cleaner energy source than coal or liquid petroleum, it is desirable to contribute to the improvement of its production. Hydraulic fracturing is a well demonstrated and documented processes to improve the production of this energy source. Its design includes parameters like pump rate, the volume of the treatment, proppant mass, proppant type, fluid type and its properties. The selection process of these materials is coupled with formation type, formation fluid, geomechanical properties, desired fracture dimensions, and economics.

1.1. HYDRAULIC FRACTURING BACKGROUND

Hydraulic stimulation is the process of pumping fluid (i.e. transport fluid) into the wellbore at a high injection rate and breaking the formation, which creates a fracture. These created fractures can have a different type of orientation depending on the in-situ stress (natural stress regime) of the targeted zone.

The different in-situ stress regimes are defined according to the magnitude of the three principal stresses acting at the location of interest. As shown in Figure 1.1, there are three principle stresses acting at a certain location in the earth's crust. They are referred to as vertical stress or overburden stress (σ_v), maximum horizontal stress (σ_H), and minimum horizontal stress (σ_h). Their magnitude depends on factors such as depth, faults, natural fissures, and plate tectonics. The fracture propagates perpendicular to the minimum of these three principal stresses as shown.
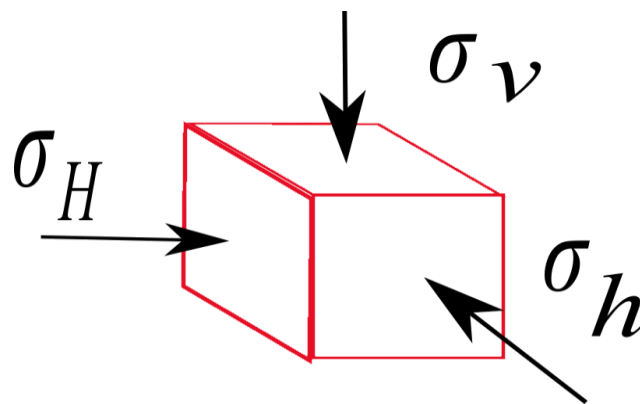
Figure 1.1 Perpendicular principle stresses.

When overburden stress is highest of the three principal stresses i.e. $\sigma_v > \sigma_H > \sigma_h$, then the geological environment is referred as a normal fault regime. In this regime, the created fracture will be oriented perpendicular to the minimum horizontal stress. So, the fracture will be vertical.

When the overburden stress is the least of the three principal stresses i.e. $\sigma_H > \sigma_h > \sigma_v$, then the geological environment is considered to be in reverse or thrust fault regime. As the magnitude of vertical stress is minimum, the fracture will be horizontal. Figure 1.2 a) illustrates vertical well in normal fault regime creating a vertical hydraulic fracture.

Sometimes the magnitude of vertical stress is between the magnitude of two horizontal stresses i.e. $\sigma_H > \sigma_v > \sigma_h$, then the geological environment is considered to be in strike-slip fault regime. Here the created fracture will be vertical, same as the normal stress regime. Figure 1.2 shows a vertical well in (a) a normal fault regime and (b) in a reverse fault regime that creates a horizontal hydraulic fracture.

For a horizontal well, fracture orientation depends on the direction in which the lateral well has been drilled. The hydraulic fractures are always perpendicular to the minimum principal stress. If the horizontal well is oriented in minimum horizontal stress direction, the fractures are perpendicular to the lateral axis, and these types of the fractures are called the transverse fractures. If the horizontal well is oriented in maximum horizontal stress direction, the fracture propagates along the lateral axis, and these types of the fractures are called the longitudinal fractures. Figure 1.3 shows the possible trajectories for a horizontal well and the resulting fracture orientations.
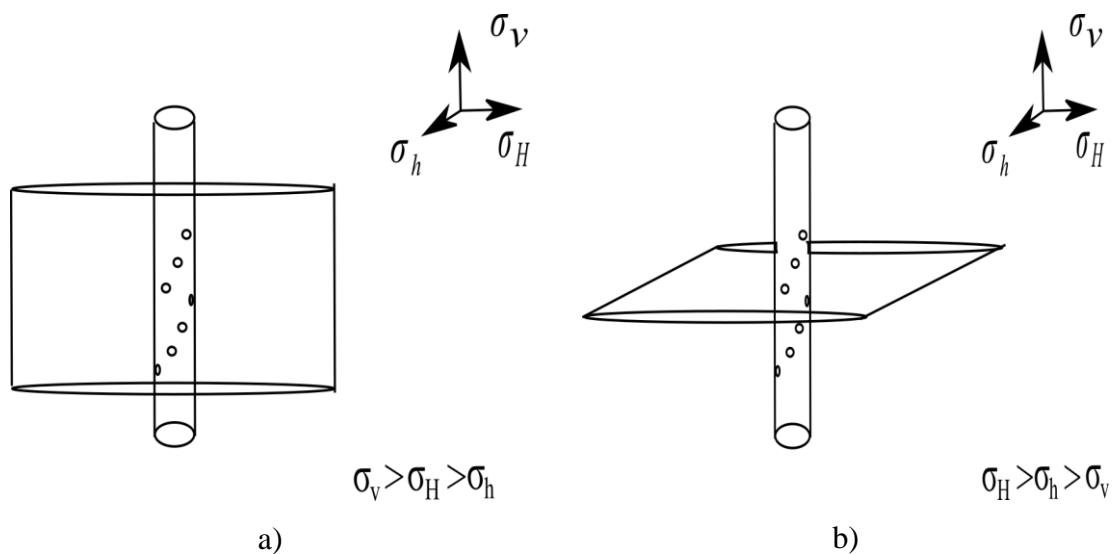
Figure 1.2 Vertical well with a) a vertical fracture, b) a horizontal fracture.
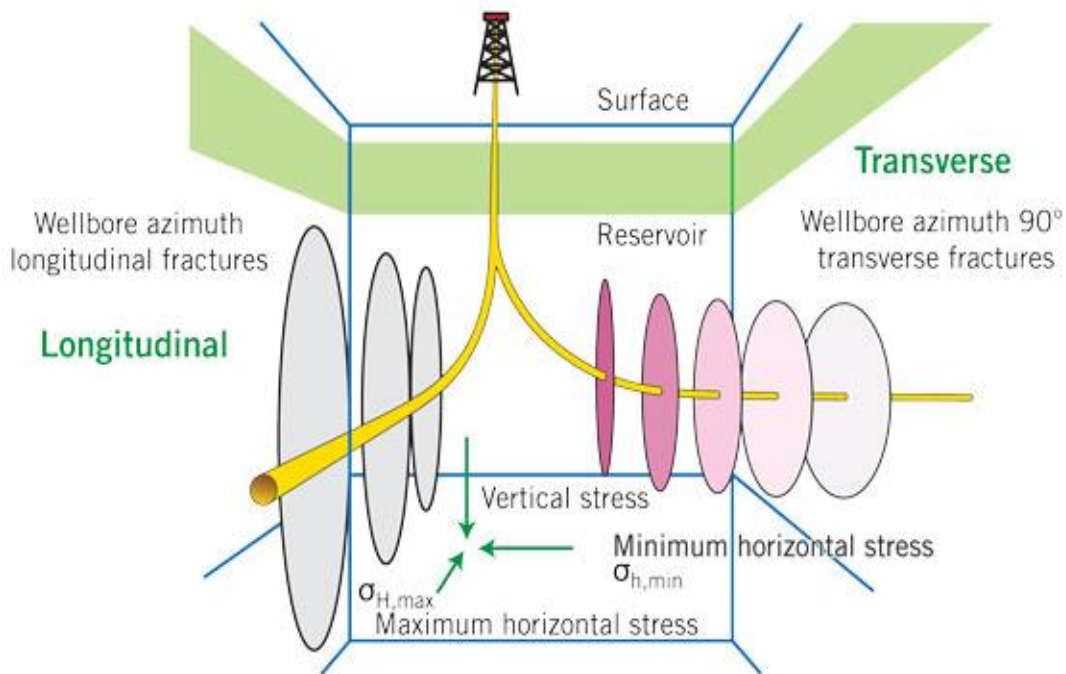
Figure 1.3 Vertical fractures in a horizontal well (Oil and Gas Journal vol.110, issue 5).

Multi-stage fractured horizontal wells are systematically planned considering geomechanical and reservoir properties. For oil and gas shale reservoirs with extremely low permeability, transverse fractures are most commonly created along the length of the lateral, thereby significantly increasing drainage area, production and ultimate reserve recovery.

Proppant (sand or ceramic) is placed in the hydraulic fractures during the treatment. As pumping pressure is released, the created fractures are held open by the proppant to provide fracture conductivity. Typically, the proppant slurry concentration is ramped up during the stimulation i.e. the treatment starts with a low proppant concentration which is increased gradually until reaching the end concentration for the treatment. The treatment may be overflushed to ensure the perforations are not blocked by the injected proppant.

Hydraulic fracturing theory assumes the vertical created fracture will be bi-planar, meaning that two wings of the fracture will emanate symmetrically from the wellbore (lateral for a horizontal well). Fractures created in a vertical well in higher permeability reservoirs are typically planar fractures, but microseismic data for horizontal well multi-stage fractures supports both planar and complex fractures can be created. Figure 1.4 illustrates proppant transport during fracture stimulation treatment in a vertical well with a planar fracture. The well perforations are oriented in the fracture plane.

In 1961, Prats provided pressure profile in a fractured reservoir as a function of the fracture half-length and the relative capacity a, which is defined as

$$a = \frac{\pi k x_f}{2 k_f w} \tag{1}$$
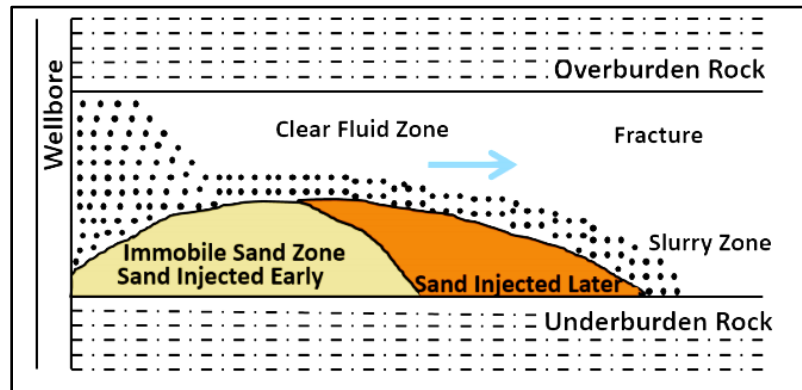
Figure 1.4 Schematic of sand transport in vertical planar fracture (Mohanty et al. 2016).

In subsequent work, Agrawal et al. (1979) and Cinco-Ley and Samaniego (1981) introduced a dimensionless fracture conductivity F_{cd} as a parameter relating fracture performance to the permeability environment where the fracture is placed. Dimensionless fracture conductivity is defined in terms of the fracture half-length, fracture permeability, width of the fracture, and reservoir permeability:

$$F_{cd} = \frac{K_f w}{K x_f} \ . \tag{2}$$

The dimensionless conductivity of the fracture can be related to the effective wellbore radius, as shown in Figure 1.5. A fracture is considered to provide infinite conductivity when F_{cd} is greater than 30. Typically, the value of F_{cd} is wished to be 2 for oil wells in higher permeability formations in pseudo-steady state, while the value of F_{cd} is desired to be 10 for gas wells. (Britt et al. 2009)

The relationship shown in Figure 1.5 shows that in reservoirs having a high permeability (k), it is preferred to have high fracture conductivity ($k_f w$) and a shorter
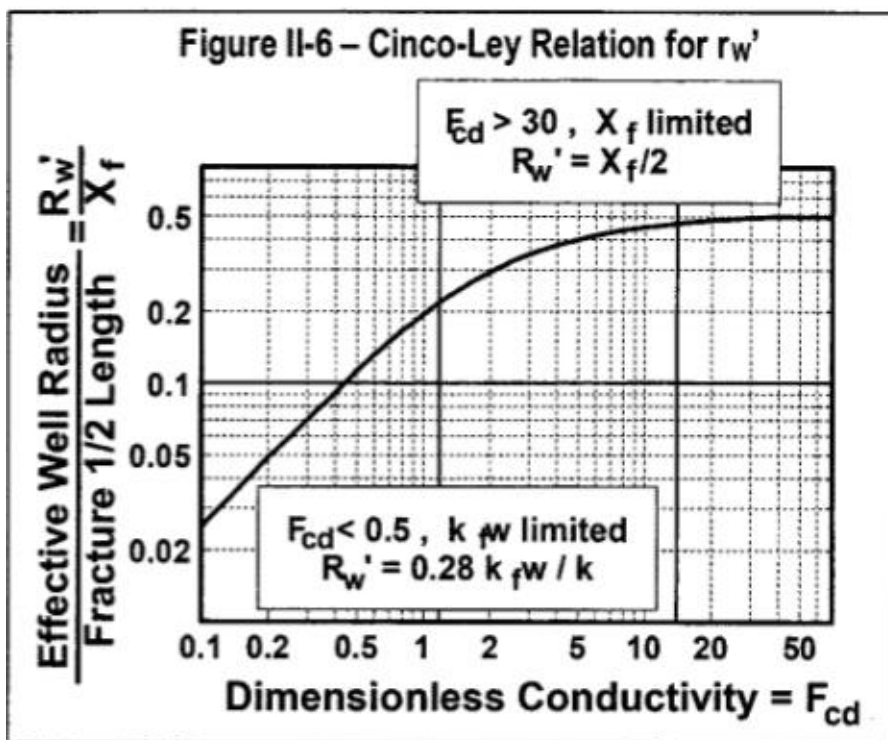
Figure 1.5 Cinco ley relation for effective wellbore radius (Cinco ley et al. 1981).

propped fracture half-length (x_f). In other words, for the production improvement in a high permeability reservoir, a thick, short, and densely packed fracture is needed. But for an unconventional reservoir having a very low permeability (k), a very high propped fracture half-length (x_f) and the low fracture conductivity ($k_f w$) are required. Meaning, for the production improvement in an unconventional reservoir, a thin, long and minimally propped fracture is desired. Hence, in shale type environments only low proppant concentrations (up to 3 ppg) are required to achieve the necessary fracture conductivity.

Perfect proppant transport is shown in Figure 1.6 a) and can be achieved using high viscosity, cross-linked fracturing fluids. The cross-linked fluids are used in high

permeability reservoirs because of their ability to transport high proppant concentrations (~10 ppg) and densely pack the short fractures but these fluids are pumped at lower rates. In extremely low permeability reservoirs, it is desired to develop longer fractures using high injection rates, and only low fracture conductivity is needed. Hence, water slickened with polyacrylamide, referred to as 'slickwater' is used to transport low proppant concentrations in hydraulic fracturing of shale reservoirs. Slickwater is referred to as imperfect proppant transport, which has been characterized as shown in Figure 1.6 b). Low viscosity fluids like slickwater can be pumped at very high rates (~70 bpm) But slickwater has very low carrying capacity so the proppant is settles quickly. Due to the settling of the
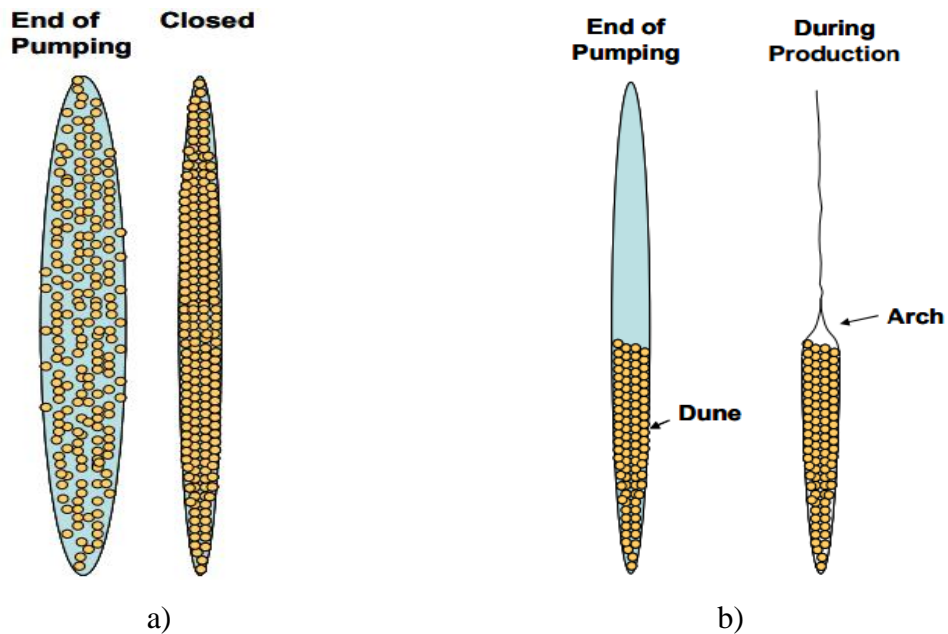
Figure 1.6 Fracture geometry a) perfect transport b) slick water dune (Warpinski et al. 2009).

proppant, the effective fracture half-length is reduced and the unpropped fracture closes as shown in Figure 1.6 b)

Fracture conductivity is affected by proppant type, size, concentration and placement. Proppant transport is as important aspect in creating fracture conductivity which in turn leads to creating the perfect fracture otherwise the created fracture would not have any significant improvement in production.

1.2. COMPLETION ASPECTS

In this section, different completion techniques and their significance in a hydraulic fracturing treatment are discussed.

1.2.1. Perforation. Perforating is an important completion aspect of cased hole hydraulic fracturing. It provides a connection between the wellbore and the formation. In this process, perforating guns are used, which carry explosive charges. The perforating gun is lowered in the well to the targeted zone and activated. The jet charges explode outwards creating holes through the casing, cement and into the formation.

Vertical wells are typically perforated using a perforation gun as shown in Figure 1.7 a). The perforating gun may be run on wireline, or on the tubing as part of the completion (tubing convened perforating, TCP). In all cases, the perforation gun is located in across from the reservoir net pay and detonated. If the well is completed underbalanced with tubing conveyed perforating (TCP), flow goes directly to the production facility. If wireline guns are run overbalanced, then perforating guns are retrieved and the well must be brought on production.

In a cased and cemented horizontal wells, the perforations are created using plug and perf method. In this method, the first stage perforation gun is lowered into the well to the targeted zone using coiled tubing and perforations are created. Subsequent perforations are created from the toe to the heel of the well and wireline guns may be pumped down to perforate the well. Multiple perforation clusters are created in one stage along a lateral. The perforations in each stage are hydraulically stimulated together. After each stage of the hydraulic fracture job is complete, those perforations are isolated from the well using a composite plug, and the process is repeated until all stages have been stimulated. These plugs may be milled out or dissolved with time to enable production.

1.2.2. Limited Entry Perforation. Limited entry perforation is perforation technique applied when multiple zones are to be hydraulically fracture at the same time, and it is desired to ensure each zone is treated at the same injection rate. Limited entry perforating relies solely on equalizing the perforation pressure drop across each perforation cluster to achieve an even injection profile. It has been around for vertical wells since 1967. The production logs from many horizontal wells in shale reservoirs indicate that 30% of perforation clusters do not contribute to production. The stress shadow effect is considered to be one of the main reasons. Limited entry perforation in horizontal wells has been successfully implemented to overcome this inefficiency. This technique promotes perforation friction pressure during reservoir stimulation treatment by limiting the number or size of perforation holes. The perforations act as a choke between the wellbore and formation. For non-crosslink fluids, a given perforation diameter, density of the fluid, and

perforation coefficient can be used to define perforation back pressure (Δp_{pf})(Crump and

Conway, 1988; Economides and Nolte, 2000):

$$\Delta p_{pf} = \frac{0.2369\rho_f}{D_p^4 C^2}\left(\frac{q}{n}\right)^2 \tag{3}$$

where ρ_f is fluid density in ppg, D_p is perforation diameter in inches, C is the discharge

coefficient, $\dfrac{q}{n}$ is the flowrate in bpm per perforation. To achieve enough perforation back

pressure to treat all the intervals, small perforation diameters are desired.

For vertical wells, Equation 2 is used. Initially, the value of the perforation back

pressure is decided and according to this value, the value of flowrate per perforation is

acquired. This value is used to estimate the maximum number of perforations that would

create enough back pressure for hydraulic fracturing to be uniform. Figure 1.8 shows an

application of the limited entry perforation, where formation net-pay height is different.

For the horizontal wells, the most common hydraulic-stimulation completion

technique is plug and perf. The limited entry perforation technique is applied in a different

manner. In plug and perf method, after formation is perforated, the formation is

hydraulically fractured. For the fracturing process, the tubing or the coiled tubing must be

pulled out which increases the number of trips and time required for the well to be

completed. To reduce the number of trips and overall job time, the perforations are shot

multiple times. These created sets of perforations are called perforation clusters. Typically,

2 to 3 perforation clusters are selected per stage.
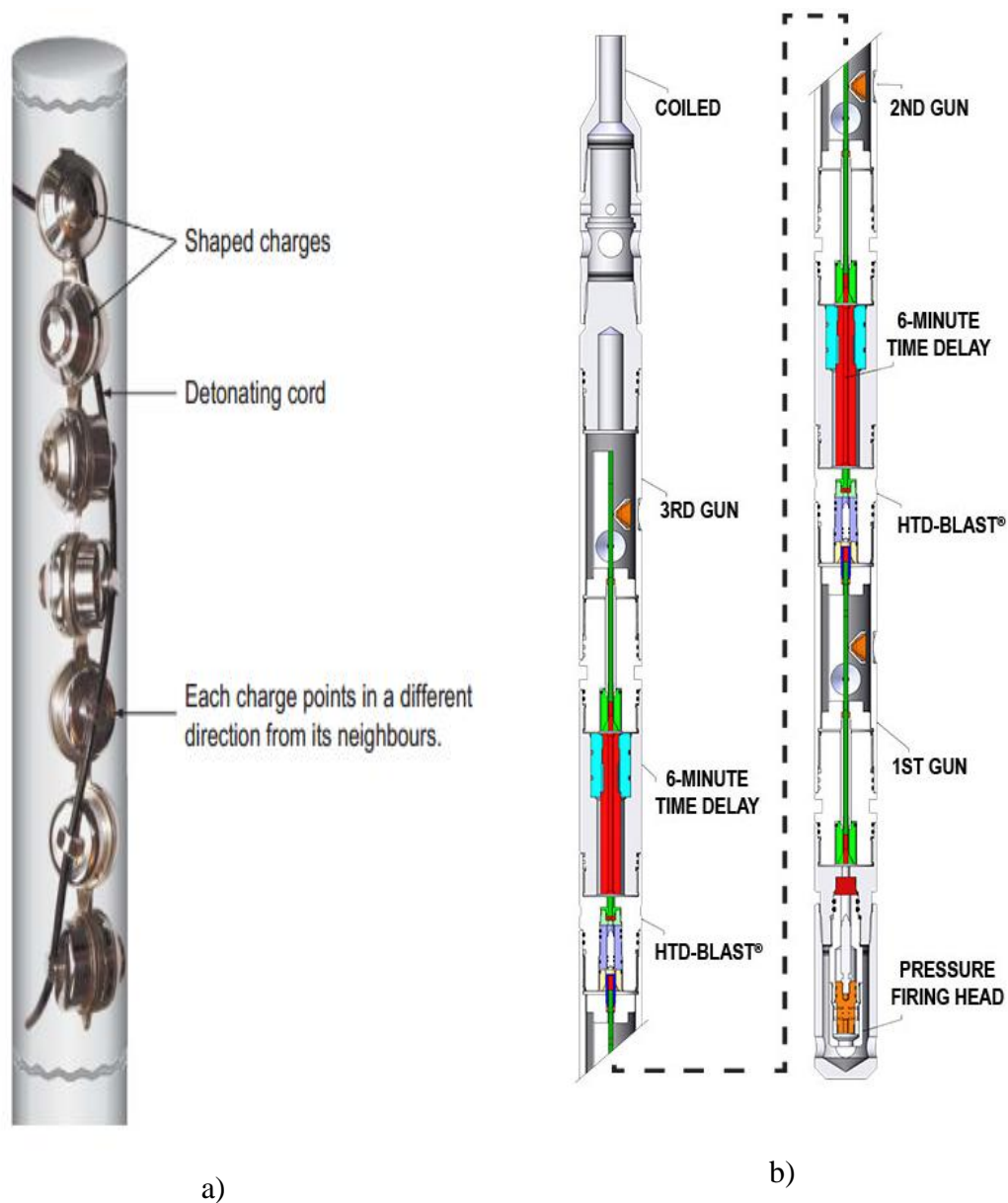
Figure 1.7 Perforating guns a) Wireline conveyed expandable perforating gun (vertical wells) b) Tubing conveyed Horizontal Time Delay Ballistic Assisted Sequential Transfer (core laboratories, 2009).

During the fracturing treatment, due to the friction losses, different treatment pressures are observed at the different clusters according to the cluster spacing, i.e. more

Figure 1.8 Limited entry perforation example.

the distance between two clusters, more the pressure drop. To ensure the same flowrate through each cluster, either the size of the perforations is changed or the number of perforations in each cluster is changed. The pressure drop across the perforation is increased, which accounts for the same flowrate through each cluster. Figure 1.9 shows the application of the limited entry perforation by changing the number of perforations in each perforation clusters.

1.3. FRACTURING MATERIALS

Different fracturing materials, mainly fracturing fluid and proppant are discussed in this section focusing on advancement in technology and commonly used materials.

1.3.1. Fracturing Fluid. Fracture fluids are typically water combined with polyacrylamide, or in the case of cross linked fluids water is mixed with guar or hydroxyethyl-cellulose (HEC). Other additives are used to serve different purposes, mainly

friction reduction, corrosion and erosion control, formation damage control (removing filter cake), fluid loss reduction, clay stabilization, and pH control. The ideal fracturing fluid should be cost-effective and be able to transport the proppant in the fracture, generate enough pressure drop along the fracture to create a conductive fracture, and not damage formation.
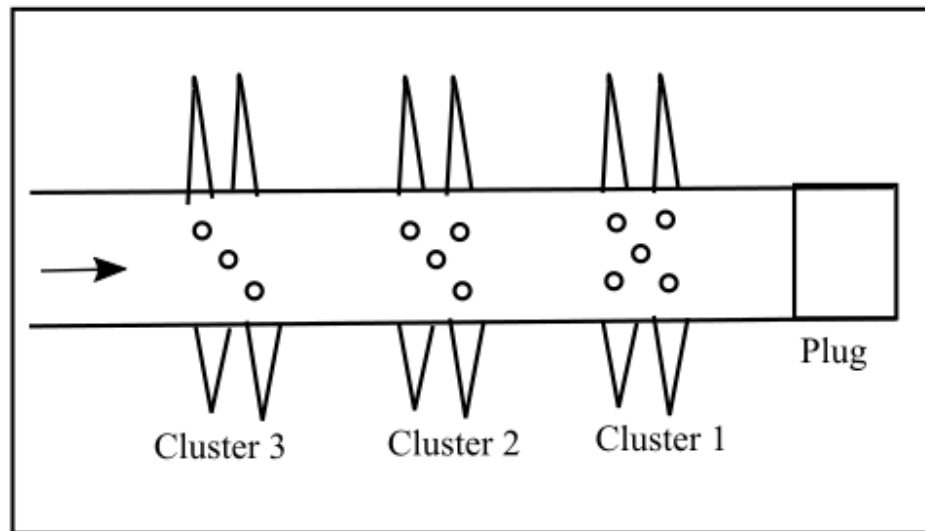
Figure 1.9 Limited entry perforation application during the plug and perf completion.

Below are some of the ingredients of the fracturing fluids with few examples.

- Friction reducers are added to the fracturing fluid to reduce the pressure drop over occurring in the drill pipe, casing, or/and coil tubing according to the design. Anionic copolymers are used, such as polyacrylamide in a 10 pptg concentration.

- Viscosifiers or cross-linkers are used to achieve the required viscosity of the fracturing fluid, which can enhance the typical carrying capacity of these fluids for proppant. Viscosity can also change the pressure drop along the fracture, which contributes to the width and length of the fracture.

- Fluid loss additives increase the fluid efficiency in fracturing treatment. Additives like diesel and fine sand block the high fluid loss regions and improve the pressure loss along the fracture.

- Breakers are added in the fracturing fluid, especially in crosslink gel to break these polymers after the fracturing injection is completed to reduce any damage done to the formation by filter cake formation. The most common breakers are acid, oxidizers, or enzymes.

- A buffer controls the pH of the fracturing fluid and maintains it in the range of 6-8 according to the formation and other additive's compatibility requirements. Sodium bicarbonate and fumaric acid are commonly used buffers.

- Surfactants lower the surface tension and promote the fluid recovery. Fluorocarbon and other nonionic surfactants can be used.

- Clay stabilizers like KCl, NHCL, or KCL substitutes are used to prevent clay swelling in high clay formations or expected sensitive formation encounters during the fracturing treatment.

Even though the above list is long these additives contribute to less than 0.2% of the fracturing fluid in slick water fracturing fluid.

Fluid properties can widely affect proppant transport and fracture creation. Fluids with a higher viscosity create the fractures that are smaller in length and wider compared to that of a low-density fluid. This is due to a high-pressure drop across the fracture length in high viscosity fracturing fluid. The average fracture width is related to viscosity and flowrate by a quarter-root relation. The following are two commonly used two-dimensional models to predict fracture width of the fracture;

PKN model:

$$\overline{w} = 2.31 \left[\frac{q_i \mu (1-v) x_f}{G} \right]^{1/4} \left(\frac{\pi \gamma}{4} \right) \tag{4}$$

KGD model:

$$\overline{w} = 2.27 \left[\frac{q_i \mu (1-v) x_f^2}{G h_f} \right]^{1/4} \left(\frac{\pi}{4} \right). \tag{5}$$

In the models, $\overline{w}$ is the average width, q_i is the injection rate, v is the Poisson ratio, μ is the apparent viscosity, x_f is the fracture half-length, h_f is the fracture height, γ is the geometry factor, which is approximately equal to 0.75, and G is the elastic shear modulus which is related to Young's modulus, E, by

$$G = \frac{E}{2(1+v)} \tag{6}$$

1.3.2. Proppant. Proppant is important for successful hydraulic stimulation processes. After the formation breaks down by a high enough pressure, if pumping is stopped (i.e., the pressure is removed), the formation closes itself after a brief time and the

breakdown will have little to no effect on production. That is why formation rocks are needed to be kept open. For the same reason, a proppant slurry is injected which stops the fracture faces from closing after removal of treatment pressure. The proppant can be distinguished by many of its characteristics but its properties like weight, size, and shape affect its transportability. Below are the proppants categorized.

  1.3.2.1 Proppant size. The size of the proppant is very important for several reasons. First, it should be able to flow in the fracture without premature screen-out. Typically, the fracture width should be at least three times larger than the largest diameter of a proppant particle. By changing the diameter of the proppant particle, many of its related properties can change. By increasing the diameter, the particle settling velocity increases (Palisch et al., 2008). Particle strength also decreases, which can crush the proppant after closure and decrease the efficiency of the treatment.

  In the petroleum industry, proppant size is generally measured in mesh size. Proppant size ranges from 8 to 140 mesh (105 µm – 2.38 mm). Mesh size is the number of opening across one square inch of a linear screen. It is common to use mixtures of various sizes of proppant in stimulation designs, especially for hybrid completion. But mixtures of a wide range of sizes of proppants have the potential to reduce the permeability of the proppant bed. For example, using a 100-mesh size proppant with 20/40 mesh proppant can occupy pore space in-between the proppant bed. Schmidt et al. (2014) investigated how various sizes of proppants perform when mixed together. They found that the concentration of a more conductive proppant had a significant effect on fracture conductivity. One of their conclusions was that using 40/70 sand with large size LWC (light weight ceramic) significantly improves conductivity regardless of the concentration used. Tail-in mixing

experiments in laboratories show a higher conductivity than experiments with a blended proppant.

1.3.2.2 Proppant material. Sand, ceramic, modified proppant (resin coated, light weight proppant), multipurpose proppant (traceable), and self-suspending proppant, etc. are available and used for hydraulic fracturing. Most hydraulic fracturing treatments use sand to a formation closure stress of approximately 4000-4500 psi. Beyond that formation stress, ceramic proppant is preferred.

These different proppants have their different benefits and specific applications. Sand is the cheapest as it is available in abundance, but it is not used as its raw form as mined directly. It is subjected to further optimization processes. In the United States, there are two major types of sand used as proppant (also known as frac sand or silica sand): white sand and brown sand. Most white sand is mined from geological formations found in the mid-west region of the United States. Brown sand is named due to impurities in it, which makes it cheaper and more prone to crushing even at lower stress.

Ceramic proppants are man-made and can withstand higher closure stress than their counterpart sand proppant of the same size. The materials used in manufacturing ceramic proppant are sintered bauxite, kaolin, magnesium silicate or blend of bauxite and kaolin. They have higher crush resistance even at closure stresses exceeding 8000 to 10000 psi. They are uniform and can achieve high sphericity and roundness to yield higher porosity and permeability in the proppant bed. Ceramic proppants are thermally and chemically stable compared to any other type of proppant, which increases the life of the proppant bed. But due to its complex manufacturing process, they are costlier than sand and resin-coated sand. Specific-gravity of ceramic proppant changes according to the alumina content in it.

The higher is the alumina content, the higher specific-gravity the proppant has. Table 1.1 shows distinct types of proppant according to their alumina content.

Proppant is modified to improve some of the properties of sand or ceramic proppant. Resin-coated proppant and lightweight proppant are examples of modified proppant. Sand is easily crushed under high stress after closure, creating fines. These fine sand particles flow back with the production and reduce the conductivity of the fracture.

Table 1.1 Different ceramic proppant according to alumina content (carbo-ceramics).

Ceramic proppant	Alumina content (%)	Specific-gravity
LWC	45 to 50	2.55 to 2.71
IDC	70 to 75	~3.27
HDC	80 to 85	~3.5
UHSP	Nearly 100	~3.9

The resin coating traps these formed fines and reduces the proppant flow back into the wellbore. In some cases, ceramic proppants are also resin coated for the same purpose. The main disadvantage of resin coating is low softening temperature, causing it to degrade easily. But resin coating can be cured by reacting linear resin with suitable cross-linker (curatives) to form a three-dimensional crosslink structure. The proppant can be pre-cured or cured downhole. The most commonly used resins used to coat proppants are epoxy resins, furan, polyesters, vinyl esters, and polyurethane. Lightweight proppants are manufactured to improve settling of proppant. The specific gravity of sand is approximately 2.65, and that of ceramic proppant can be as high as 3.9 according to

alumina content. Both are significantly higher than the specific gravity of slickwater. The light weight proppant is one of the alternatives to reduce settling of the proppant near the wellbore in the fracture using slick water as fracturing. It can also increase the propped length of the fracture. Walnut shells, pits, and husks were previously used as proppant in the field, but their low strength limits their application to formations with low closure stress. Proppants with specific-gravity of 0.8 to 2.59 have been used or investigated. Parker et al. (2012) have investigated the crystalline phase of a thermoplastic alloy which had excellent chemical stability, and the amorphous phase of the same for its excellent dimensional strength and heat resistance. Brannon et al. (2008) proposed deformable proppants which are resin coated nut shells, seed shells and fruit pits. The specific gravity of deformable proppant could be as low as 1.25. Research on resin-coated porous ceramic proppant was presented by Rickards et al. (2006) Resin coating prevents the fluid invasion into the porous proppant, which reduces its bulk density as low as 1.10-1.15 gm/cm^3. Figure 1.10 shows proppant performance in retaining conductivity of around 1750 mD-ft in terms of maximum stress.

Multi-functional proppants are application specific. Traceable proppants are used for post-treatment analysis and for logging purposes. Self-suspending proppants are used as alternatives to lightweight proppant to improve the settling of proppant. Self-suspending proppant is made by coating proppant with water swell able material such as a hydrogel.

1.3.2.3 Proppant shape. The ideal proppant shape should be spherical or nearly spherical and non-angular due to its optimum packing to maximize porosity and permeability of the proppant bed. Angular and pointed proppant particle can break easily compared to more spherical proppant, which leads to low conductivity. ISO 13503-

2:2006/Amd.1:2009(E) specifies the sphericity and roundness of different proppants. Ceramic and resin-coated proppant require an average roundness and sphericity of 0.7 or greater. All other proppant should have an average sphericity and roundness of 0.6 or greater. A greater sphericity and roundness with the narrow size distribution of the
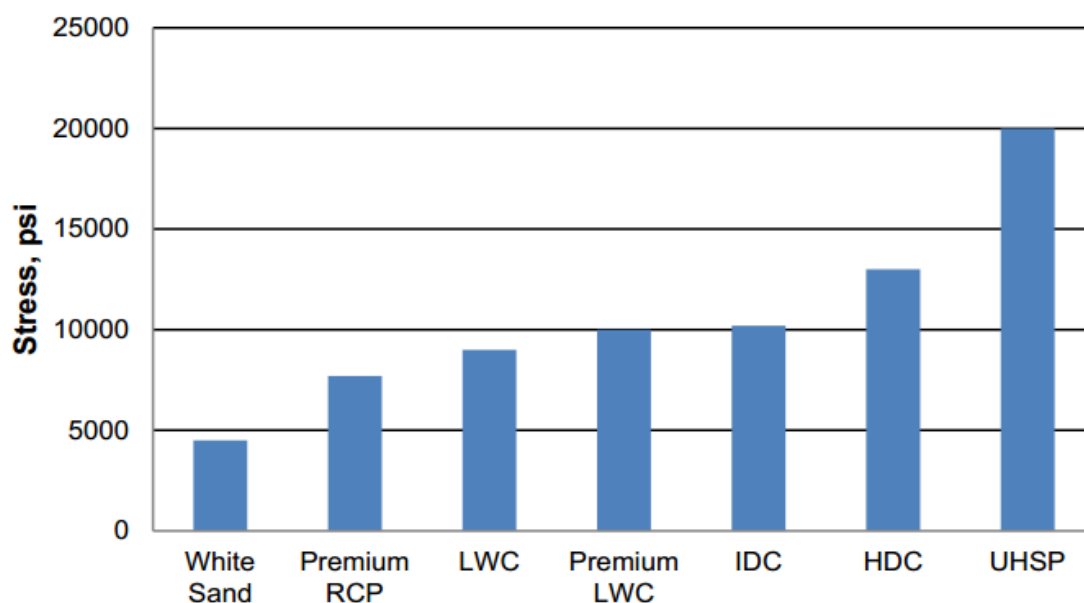
Figure 1.10 Stress at which ~1750 mD-ft is maintained by different type of the proppants (Palisch et al. 2014).

proppant offer higher conductivity for the proppant bed. Figure 1.11 shows the standard reference scale to visually estimate sphericity and roundness.

Use of elongated, rod-shaped proppant has been introduced in recent years. This development was based on the theory that the rod-based proppant packing could offer

higher porosity and conductivity. McDaniel et al. (2010) compared untapped pack porosity of spherical and rod-shaped proppant, which came to be 37% for spherical proppant to 48% that of rod-shaped proppant. Liu et al. (2015) investigated a new proposed shape of high-drag ceramic proppant. Increasing the drag force to reduce proppant-settling velocity is the concept behind the proppant studied. Figure 1.12 shows different shape of proppants which are being examined in various studies.
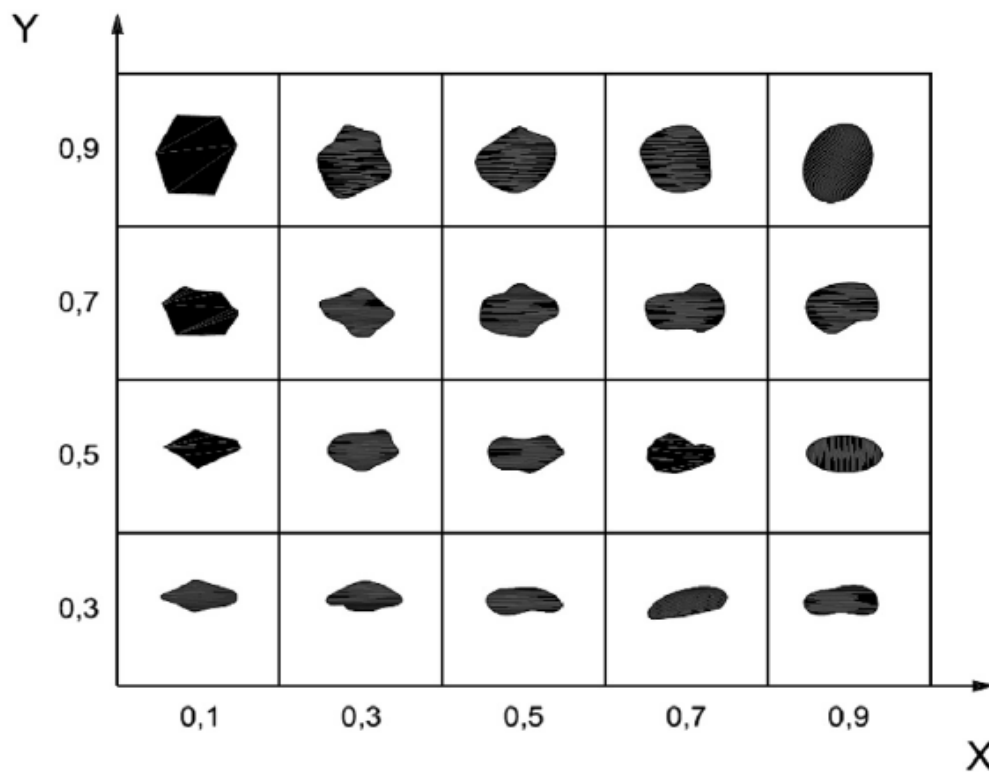
Figure 1.11 Chart for visual estimation of sphericity and roundness (X-Roundness; Y-Sphericity) (Krumbein & Schloss, 1963).

<div align="center">a)   b)</div>
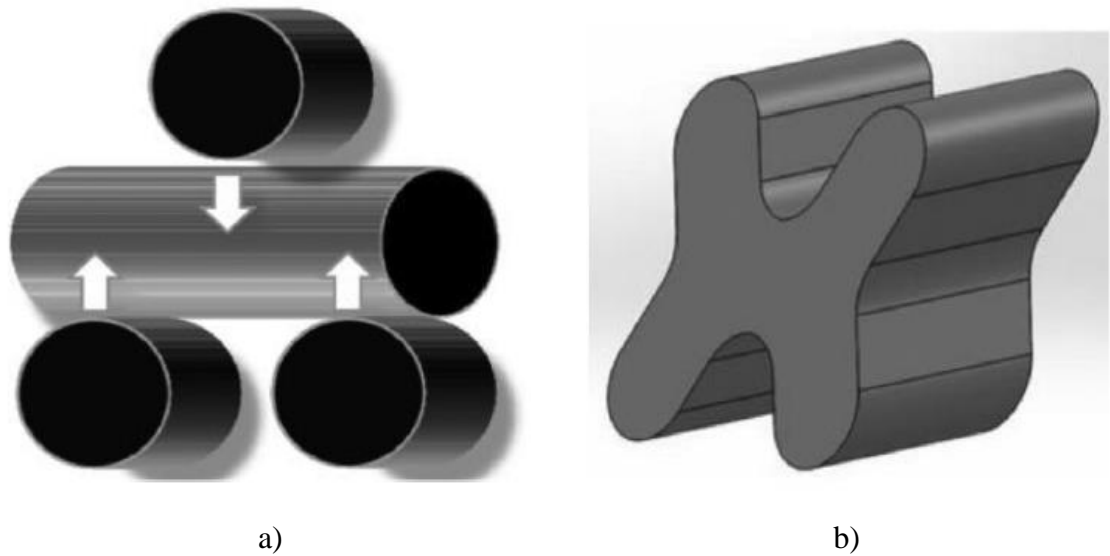
Figure 1.12 Different shapes of proppants. a) rod-shaped proppant (Edelma et al., 2013), b) high-drag ceramic proppant (Liu et al., 2015).

Many studies have been conducted to understand hydraulic fracturing, particularly with cross-linked fracturing fluids. Some of which involve the slot flow model experiments dating back as far as 1959. First of its kind was conducted by Kern et al. (1959) These studies provide a good understanding of the proppant transport in cross-linked fluids but the proppant transport is not well understood by slickwater.

1.4. OBJECTIVE OF THIS STUDY

The main objective of this study is to analyze and compare the proppant transport in hydraulic fracture of ceramic and sand proppant particles at laboratory scale. A slot-flow model was built that can accommodate variation of perforation density and position along the slot inlet, to replicate the perforation connecting the fracture to the wellbore. Proppant transportation in the slot flow model was evaluated under different conditions of proppant

type, and number of perforations and perforation placement along the fracture. Given this approach the specific objectives were

- To study the effect of varying height of single injection point on proppant transport and dune development in a fracture model.

- To study the effect of multiple injection points on proppant transportation and dune development inside a fracture, to better understand the significance of the limited entry perforation technique in proppant transport.

- To compare ceramic and sand proppant for a single injection point to study the effect of angularity on proppant transport and dune development in a fracture model.

1.5. SCOPE OF THIS STUDY

Figure 1.13 below summarizes the scope of this study. The experiments were conducted to investigate dune development with changing the perforation position using the ceramic proppant first, and then the effect of angularity of the proppant was compared by using sand proppant. The experiments were also conducted using multiple perforation with corresponding fracture condition.
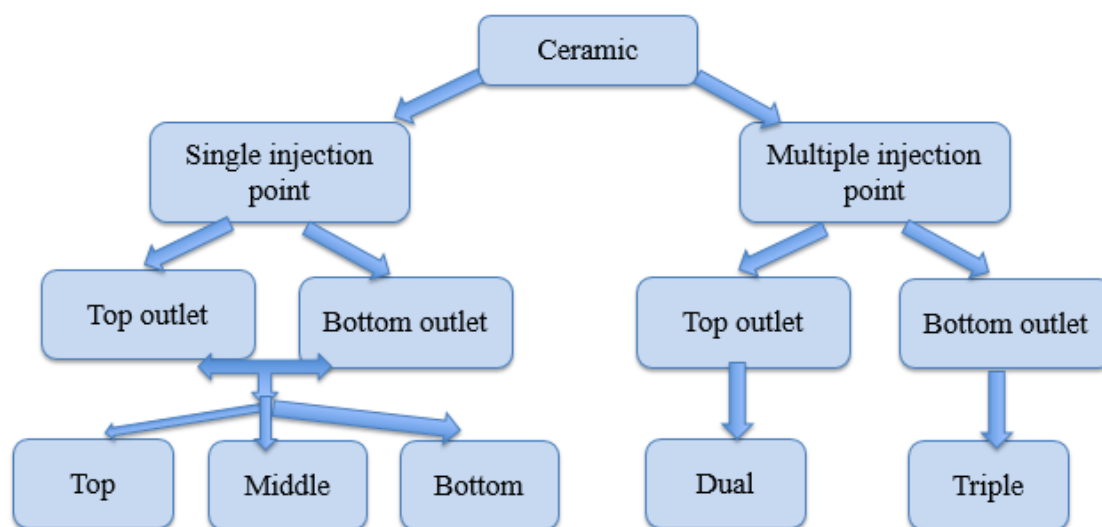
a)
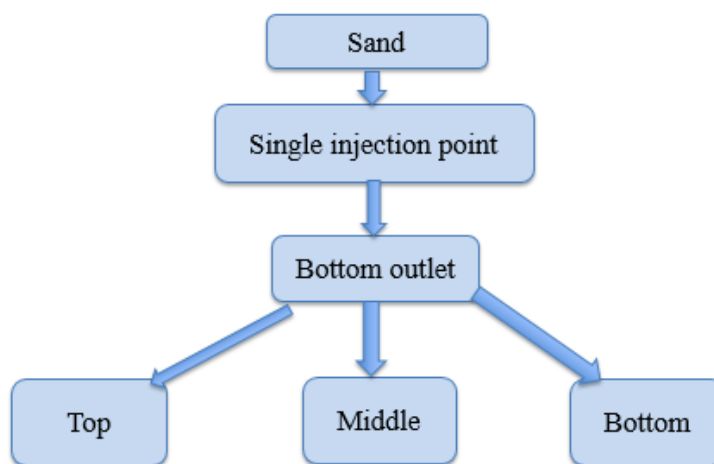
b)

Figure 1.13 The scope of this study.

2. LITERATURE REVIEW

This section discusses literature relevant to the current research. Many historical studies exist investigating proppant transport in viscous hydraulic fracturing fluid. More recent studies focus on proppant transport in slickwater. Important studies are summarized here.

Fracturing fluid imposes different forces on the proppant such as drag force and buoyance force. The drag force is induced by relative movement of proppant in the fluid phase and can be divided into two components vertical and horizontal. In Figure 2.1 below, forces acting on proppant particle in static fluid phase are shown.

In 1851, Stokes proved the free settling velocity correlation for spherical particles in an infinite Newtonian fluid column. The settling velocity for fluid with the particle Reynold's number Re < 2 is given by

$$V_s = \frac{g\left(\rho_p - \rho_f\right)d^2}{18\mu_f} \ . \tag{7}$$

McCabe and Smith (1956) showed that for the intermediate particle Reynold's number (2 < Re < 500) the settling velocity can be calculated by

$$V_s = \left[\frac{0.072\,g\left(\rho_p - \rho_f\right)d^{1.6}}{\rho^{0.4}\mu_f^{0.6}}\right]^{0.71} \ . \tag{8}$$
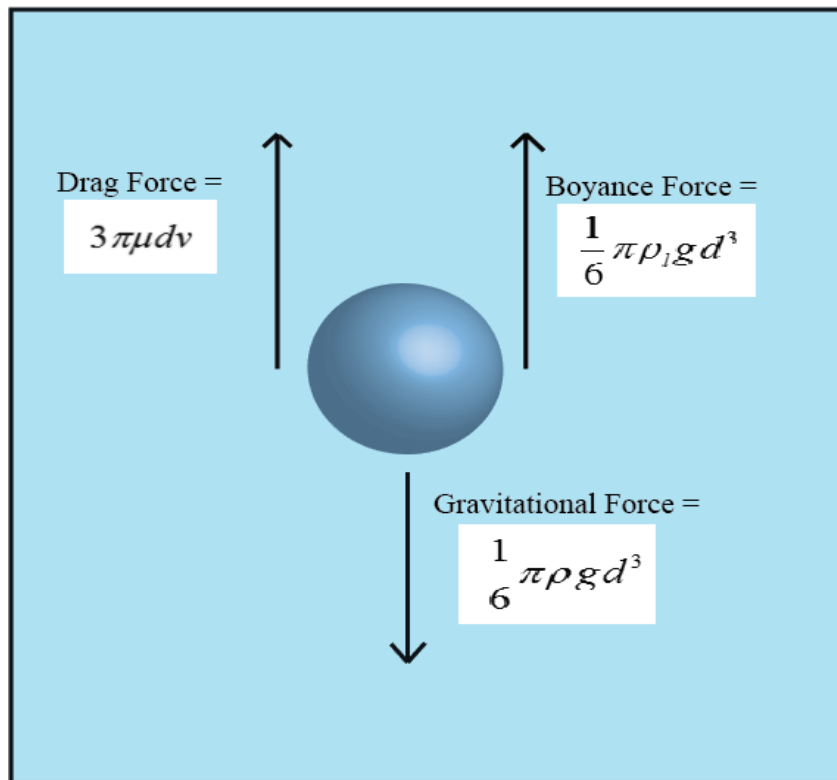
Figure 2.1 Forces acting on a particle in the fluid phase.

A particle Reynold's number greater than 500 is generally not observed in typical proppant size and density used in oil-fields. McCabe and Smith's equation is most commonly used for the settling velocity calculation in the slick water like Newtonian fluids.

When the proppant concentration is negligible or individual proppant particles are studied for settling, the above expressions are valid. But when non-negligible proppant concentration is studied, researchers must also include hindrance due to the relative movement of all proppant particles. This phenomenon is expressed by the mathematical expression of hindered velocity as the following (McGhee, 1991):

$$V_{s,hindered} = V_s \left(1 - C_v\right)^{4.65}$$ (9)

where, C_v is the volume concentration of the solid.

The above equation cannot be applied in a non-Newtonian fluid. The forces due to the fracture face should also be considered. According to different non-Newtonian fluids, changing fluid properties with changing flowrate and shear-rate must be considered in the calculation of settling velocity of the proppant. To simplify understanding of proppant transport in high viscosity fluids, Clark and Zhu (1996) defined the term N_c for power-law fluids:

$$N_c = \frac{F_H}{F_v} = 2\left(4 + \frac{2}{n}\right)^n \frac{Kq^n}{gw^{2n+1}\Delta\rho}.$$ (10)

Replacing *n* with 1 will give N_c for Newtonian fluids.

2.1. TRANSPORT MECHANISM

EDL and EDX stand for Equilibrium dune level and Equilibrium dune length respectively. These concepts were defined by Alotaibi et.al. (2015) and Dhurgham et.al. (2017).

$$EDL = \frac{average\ dune\ height}{fracture\ height} \times 100\%$$ (11)

$$EDX = \frac{average\ dune\ length}{fracture\ length} \times 100\%$$ (12)

EDL was first introduced by Alotaibi et al. (2015). During their work, they measured the height of dune at specific depths of the fracture, divided it by total fracture height, and converted it to a percentage by multiplying by 100. EDL was used and measured in the current research.

Using the results of transport mechanism study, the fracturing treatment can be optimized. Alotaibi et al. (2015) presented various transport mechanisms that occurred during their slot flow model experiment with changing EDL. The researchers used 30/70 brown sand as proppant. Figure 2.2 shows various proppant transport mechanisms observed with changing EDL while pumping the slurry.

When the pumping is stopped, the proppant, which is fluidized or rolling over the top of the dune, comes to a stop. The proppant suspended in the fluid phase settles, and the settled shape is developed, which depends on the friction coefficient of proppant. The coefficient of friction can be measured using an hourglass apparatus.

In their experiment, shown below in Figure 2.3, Mack et al. (2014) let the proppant fall slowly and freely from an orifice on a flat surface which formed a conical pile, and the angle with the horizontal surface was measured. The tangent of this angle gave the coefficient of friction for that proppant. The friction angle was less for the proppant with smooth surface.

Dhurgham et al. (2017) observed similar transport mechanisms as Alotaibi et al. (2015) with the addition of swirl and rapid suspension around 98% EDL or more. In addition to the study of the proppant transport mechanism, Dhurgham et al. (2017) also studied the effect of width heterogeneity of the fracture on proppant transport and the effect of changing leak-off pattern of the slot-flow model. From these studies, Dhurgham et al.
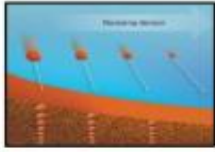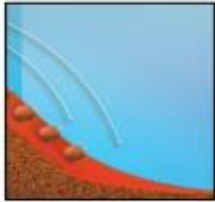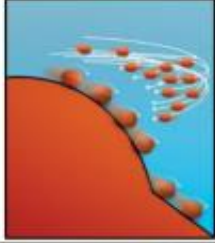
Stage	EDL, %	Dune shape	Transport mechanism	Relative proppant size range	Proppant size distribution	
					Vertically	Horizontally
1	0-10		Hindered settling	Smallest size range	Increasing	No change
2	10-75		Free settling + Rolling	Mostly mid to large size range	Layers of small and large proppant with a downward slope	
3	75-97		Rolling + free settling + Suspension	Mostly large with partially mid-size range	No certain sorting was observed	
4	97-100		Rolling + Saltation	The largest size range		

Figure 2.2 Dune development stages (Alotaibi et al., 2015).

(2017) showed that the EDL increases when the ratio of the width of inlet-side fracture to the width of tip-side fracture is increased. From the leak-off pattern experiments, they observed that existing high leak-off zone changes the shape of the dune.

Vivek et al. (2017) also conducted experiments using water as transport fluid and ceramic proppant. In their research, the results for changing flowrate agreed with the results of Sahai et al. (2014). Sahai et al. (2014) used brown sand with water as the slurry. It was observed that on increasing flowrate of the slurry injected, EDL level decreased. Vivek et
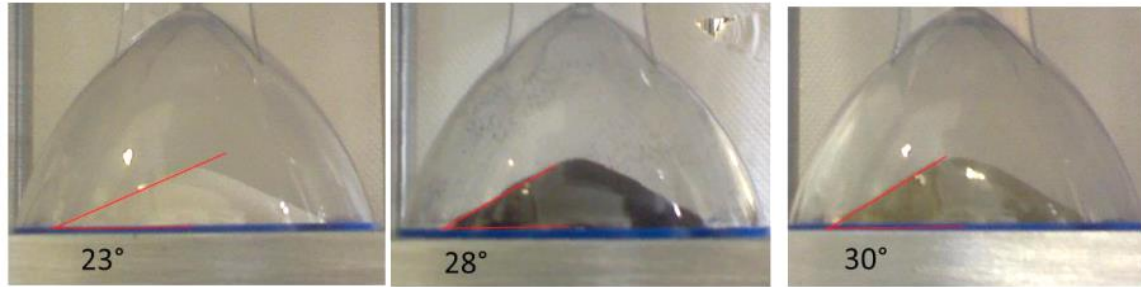
Figure 2.3 Friction coefficient of different type of proppant (Mark Mack et al., 2014).

al. (2017) observed that with increasing width of the fracture, EDL also increased at same flowrate. Vivek et al. (2017) also worked with secondary fracture and concluded that on the introduction of the heterogeneity in primary fracture, a significant effect on dune development in the secondary fracture can be observed.

Songyang et al. (2016) also studied the proppant transport in a fracture model with a secondary fracture at different inclinations to the primary fracture. In their research, they observed dropping dune height with increasing shear rate, but with increasing shear rate proppant embedment increased in the secondary fracture. They were also successful in capturing the key features of the dune using a dense discrete phase model (DDPM) in their numerical study.

Li et al. (2016) also studied the changing angle between the primary and the secondary fractures. Using slickwater as a transport fluid and 40/70 and 30/50 sand, they

observed the effect of the sand ratio of the different sizes and the angle of secondary fracture. They used Solidworks software to build a model to simulate the results.

Ngameni et al. (2017) tried to illustrate the proppant distribution among the perforation clusters in a horizontal wellbore with various sizes of the proppant. Palisch et al. (2008) showed the advantages and the disadvantages associated with the slickwater fracturing.

Many other studies have been conducted using low viscosity fracturing fluids like linear gel, water with polyacrylamide, foam-based fluids and viscoelastic surfactants. Malhotra et al. (2013) introduced alternate-slug fracturing treatment. In this method, sand-carrying water and proppant-free polyethylene oxide solution are injected alternately.

2.2. LIMITED ENTRY PERFORATION

The limited entry perforation technique was first introduced in 1960's for vertical well. But now, it is widely used in horizontal wells as well. The concept of limited entry perforation has many applications. One of such applications was introduced by Haung et al. (2017).

Haung et al. (2017) in their numerical study used a single-phase flow model and a reservoir with poroelastic behavior coupled with a conventional finite element method. In this study, the researchers compared production from three different cases of a number of shots and perforation diameter at a constant pump rate of 60 bpm. For the base case, they used 5 clusters with a total of 12 shots and perforation diameter of 0.54 in. For limited entry perforation experiments, they reduced the perforation diameter to 0.42in. and the number of shots to 6 and 3 in two different cases. Researchers observed that as the shots were

reduced, the fracture became more uniform and the width of outermost fracture became smaller. Figure 2.4 and Figure 2.5 show the fracture propagation in these three cases. It can be noted that the cluster spacing was 50 ft. They observed production improvement using limited entry perforation and a uniform pressure profile from all the fractures formed after production of three years.
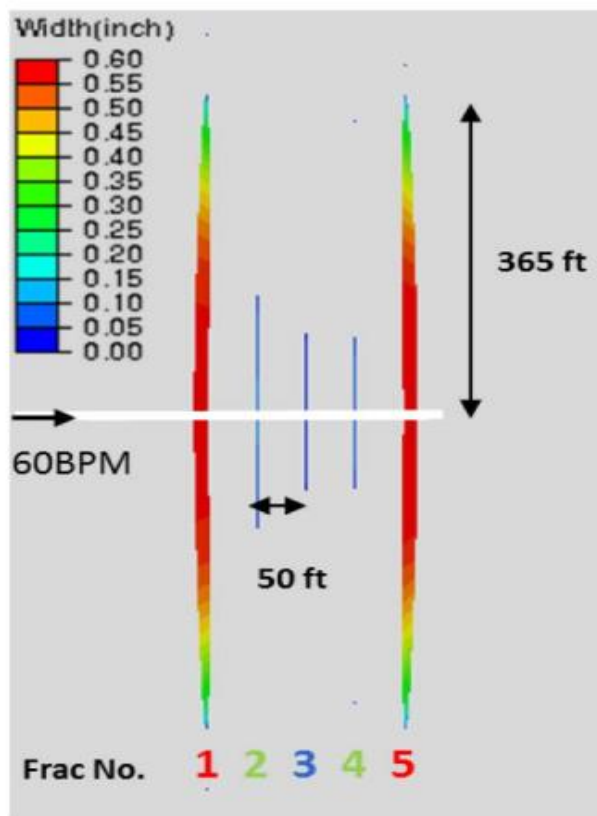
Figure 2.4 Fracture propagation in a single fracture stage with five perforation clusters (base case) (Haung et al.,2017).

In further studies, the researchers changed the cluster spacing to 100 ft. and concluded that when the cluster spacing is increased to a point the stress shadow effect is reduced so that, the application of limited entry perforation did not significantly affect production.
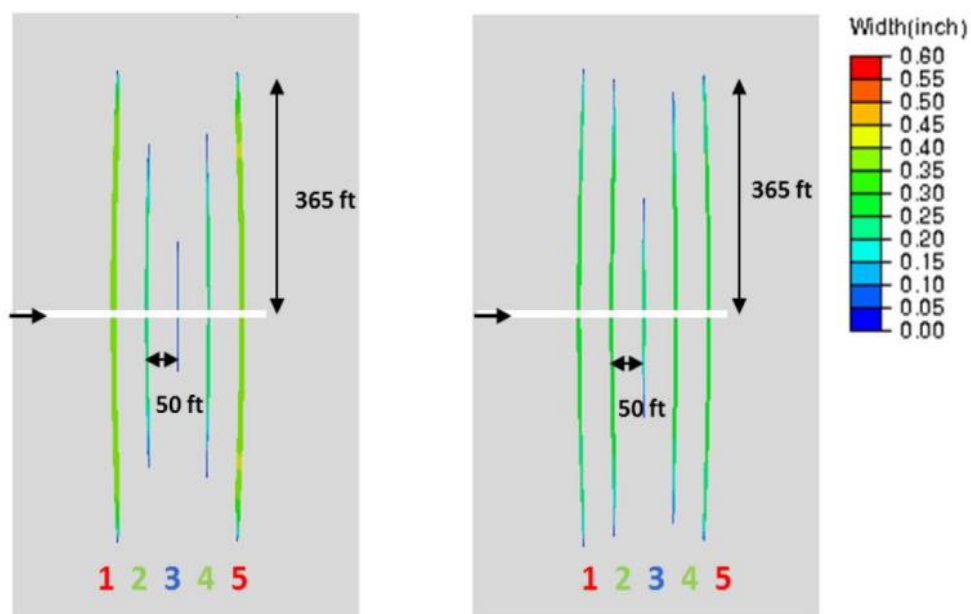
Figure 2.5 Fracture length and width distribution of proposed design (Haung et al.,2017).

3. EXPERIMENTAL METHODOLOGY

3.1. EXPERIMENTAL SETUP

For this research, an experimental apparatus was developed to study the proppant transport and placement in the fracture during a fracturing treatment. Pumping of the slurry was achieved by applying constant pressure to the specific volume of the proppant slurry with nitrogen gas. The apparatus created was a parallel plexiglas setup with three injection points on the fracture as well as two outlet points. To study the effect of perforation position relative to the evolving fracture, various combinations of proppant, injection points and outlets were used to perform experiments.

3.1.1. Experimental Apparatus. The apparatus used during the experiments consisted of the following components: two parallel Plexiglas bolted together, rubber sheet, accumulator, nitrogen gas cylinder. For analysis and recording the experimental results a camera and tripod stand was used. Figure 3.1 below is a schematic of the experimental apparatus used for this research.

3.1.1.1 Plexiglas plates. Two smooth plexiglas plates of 590 mm length and 290 mm height were used as fracture. These plates were drilled on one of the face to accommodate inlet and outlet valves. The valves were positioned at 38mm away from sides and 27 mm, 112 mm, and 197 mm from the bottom of the fracture called bottom, middle, and top inlet/outlet for the slot model respectively. The plates were bolted together to enclose the fracture vertically. To provide a width for the fracture, a rubber sheet was cut accordingly and placed between two plates, which created a fracture slot flow model with
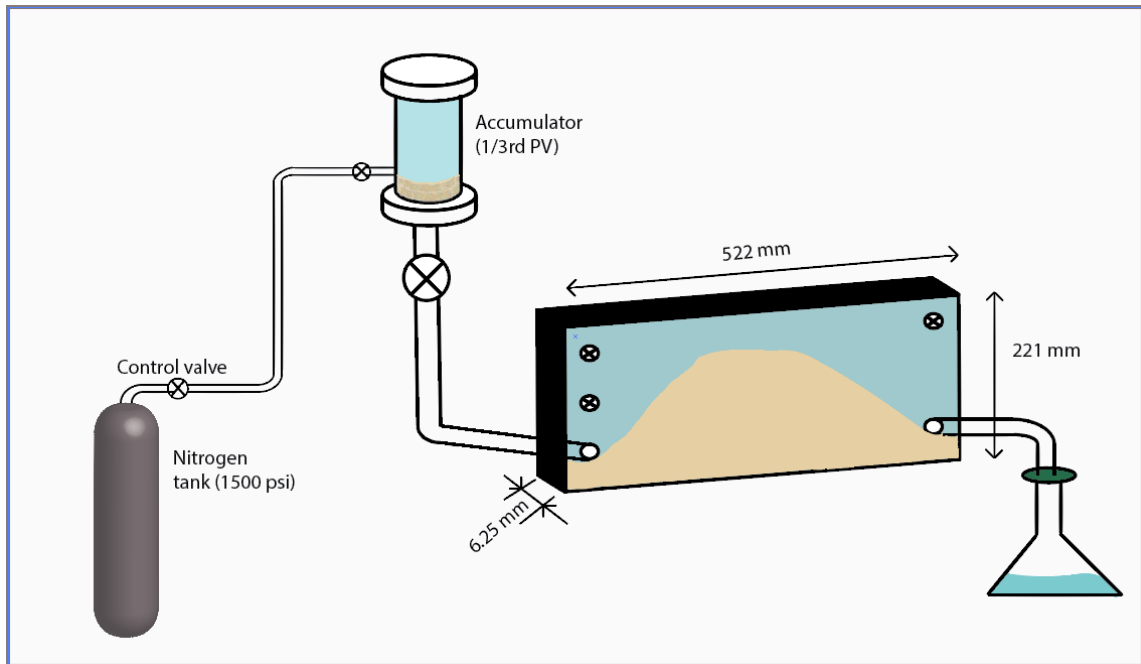
Figure 3.1 Schematic Diagram.

uniform width of 6.25mm (or 0.25inch), 522mm average length, and 221 mm average height. Figure 3.2 shows the back-face view of the fracture slot model from where all the observations were made. A wooden structure was supporting the slot model in vertical position. Water was prefilled in the slot model to replicate pad volume in a fracturing treatment. The word "inlet" is used interchangeably with "injection point" and the word "outlet" is used interchangeably with "ejection point" throughout this report.

3.1.1.2 Accumulator. The experiments were run in a step-wise manner to understand of the dune formation during various stages of the proppant injection process. A constant specific slurry volume (260 ml of 1 lbpg slurry) was injected and repeated until the equilibrium was reached. This slurry sample was kept in cylindrical accumulator, which

Outlet   Inlet

Bottom   Top   Bottom   Middle   Top
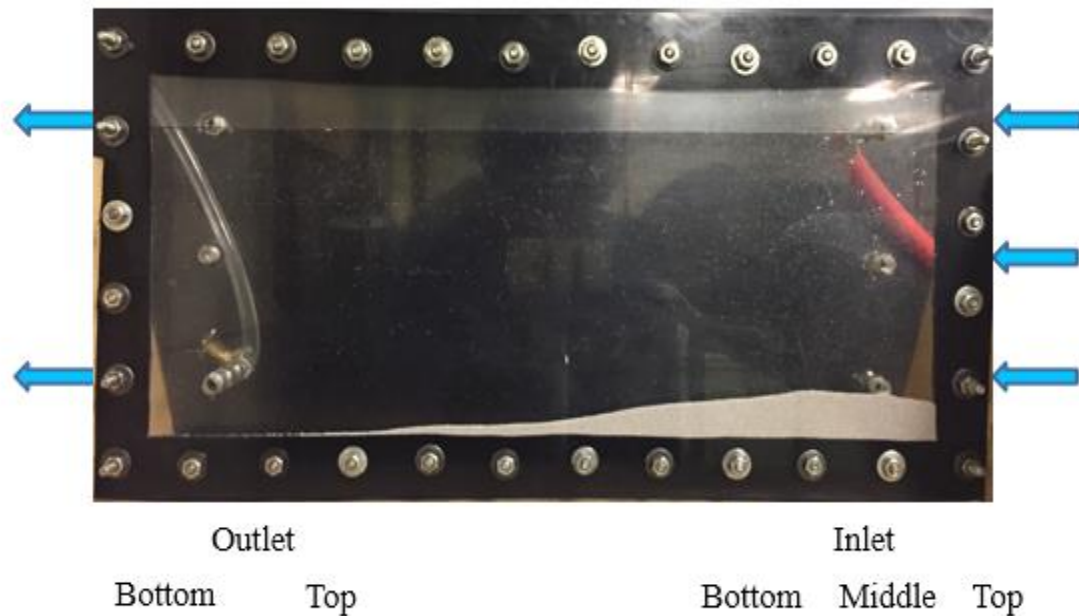
Figure 3.2 A back-face view of the fracture slot model.

had a provision that can apply nitrogen pressure to pump the slurry into the slot model. As

shown in Figure 3.3 the accumulator is connected to nitrogen cylinder. Injecting nitrogen

into the accumulator creates turbulence in the slurry, mixing the fluid and proppant.

The maximum volume of the accumulator is 345 ml. The specific slurry used was

the largest volume which could be injected without plugging the nitrogen inlet with

proppant particles. A constant pressure of 50 psi was used which created approximately

120 ml/s flowrate for the experiments.

The experimental setup could be categorized according to the number of inlets used:

- Single injection mode

- Multiple injection mode

Figure 3.3 Accumulator.

Also, the experiments could be sub-categorized according to the proppant used:

- Ceramic

- Sand

These experiments were repeated with changing configurations of inlet and outlet, which

represented different fracture condition.

3.1.1.3 Experimental parameters. The experimental parameters were kept constant such as height of accumulator compared to fracture (slot flow model), and nitrogen gas cylinder pressure. All experiments were conducted with proppant concentration of one lbpg. (Note: either ppg or lb/gal) The combinations of the inlet and outlet were changed from one experiment to another. The inlet represented the position of one perforation with respect to the fracture. Multiple inlets represented the fracture connected through more than one perforation. The top outlet represented a fracture with height growth in lower formations while bottom outlet represented a fracture growing in upper formations. Injected sand particles were used to compare dune development of angular proppant to that of more spherical proppant (ceramic). The width of the fracture was kept constant throughout all the experiments.

3.1.2. Fluid Selection. Deionized water was used for all experiments in the research and the viscosity of the fluid was not changed. Initially experiments were attempted with tap water. However, this led to charged particles that were hydrophobic which reduced repeatability of the experiments. This problem was resolved using deionized water.

A slurry of one lb/gal was prepared using deionized water and proppant. 250 ml of fluid was mixed with 30 gm of 30/50 mesh size CARBO ECONOPROP™ ceramic proppant or brown sand having same mesh size. The total slurry volume created for each injection was 260ml

3.1.3. Proppant Properties. Different properties of ceramic proppant and sand used in the study are given in Table 3.1 and Table 3.2. The brown sand used in this study had specific gravity of 2.65

Table 3.1 Basic properties of ceramic proppant used in study (Carbo ceramics 2015).

Roundness	0.9		Apparent specific gravity	2.7
Sphericity	0.9		Absolute volume (gal/lb)	0.044
Bulk density (lb/ft3)	96		Solubility in 12/3 HCl/HF acid (% weight loss)	1.7
(g/cm3)	1.56			

Table 3.2 Ceramic proppant conductivity and permeability data (Carbo ceramics 2015).

Closure Stress (psi)	Reference conductivity in mD-ft at 250^0F for $2lb/ft^2$ 30/50	Reference permeability in Darcies at 250^0F for $2lb/ft^2$ 30/50
2000	4150	220
4000	3300	180
6000	2550	140
8000	1600	90
10000	975	65

3.1.4. Experimental Configurations. This subsection describes different configurations of the experiments. The experiments were conducted with two different set of outlets for checking repeatability of the experiments. One of the reason to use top outlet was make dune development unaffected by outgoing slurry from the fracture model as well as it can represent fracture height growth in lower formations. While bottom outlet can represent height growth in upper formations.

3.1.4.1 Single perforation injection. Experiments were conducted with a single perforation in three positions- top, middle and bottom of the fracture slot inlet. The details of these experiments are described here.

Bottom injection: The bottom slot model uses a configuration with the inlet at $1/8^{th}$ fracture height or 27mm from bottom. Figure 3.4 shows this configuration.

a)

b)
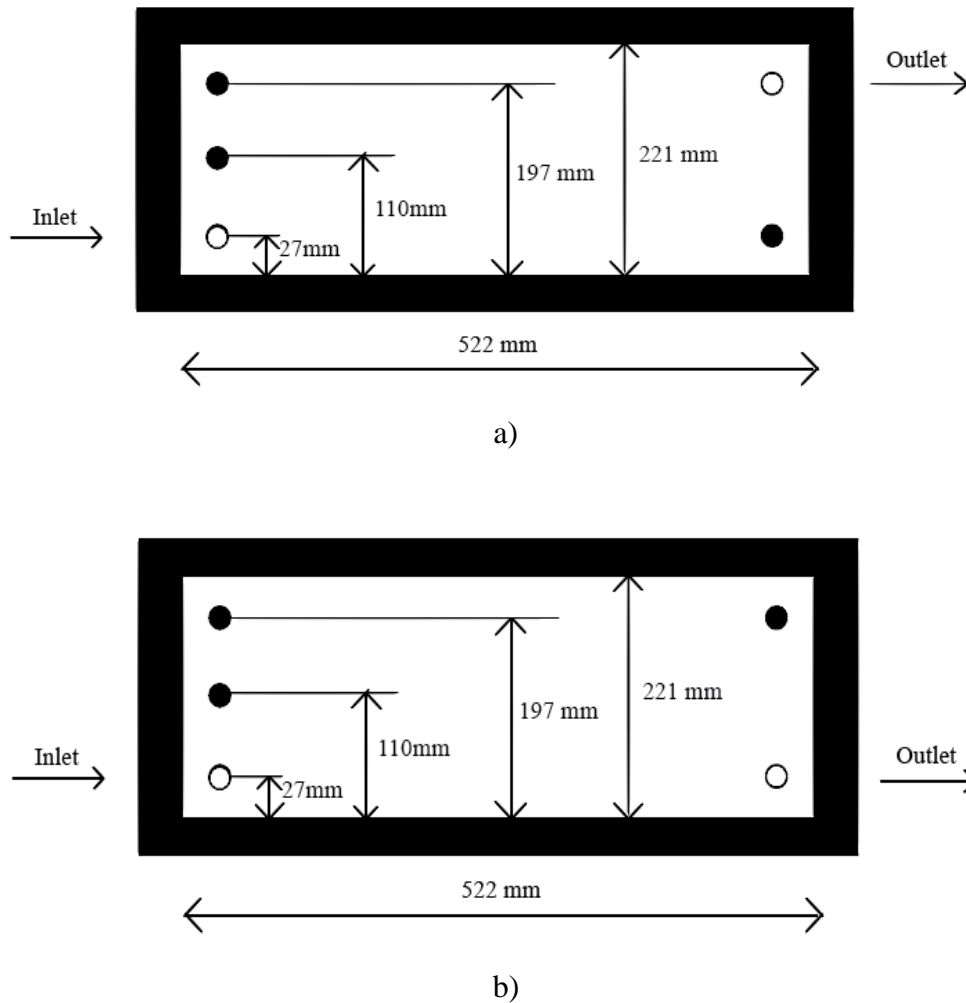
Figure 3.4 Slot configuration for bottom injection fracture with a a) top outlet b) bottom outlet.

Middle injection: The middle slot model uses a configuration with the inlet in the middle of the fracture or 110mm above the bottom of the fracture. Figure 3.5 shows single middle injection configuration.

a)

b)
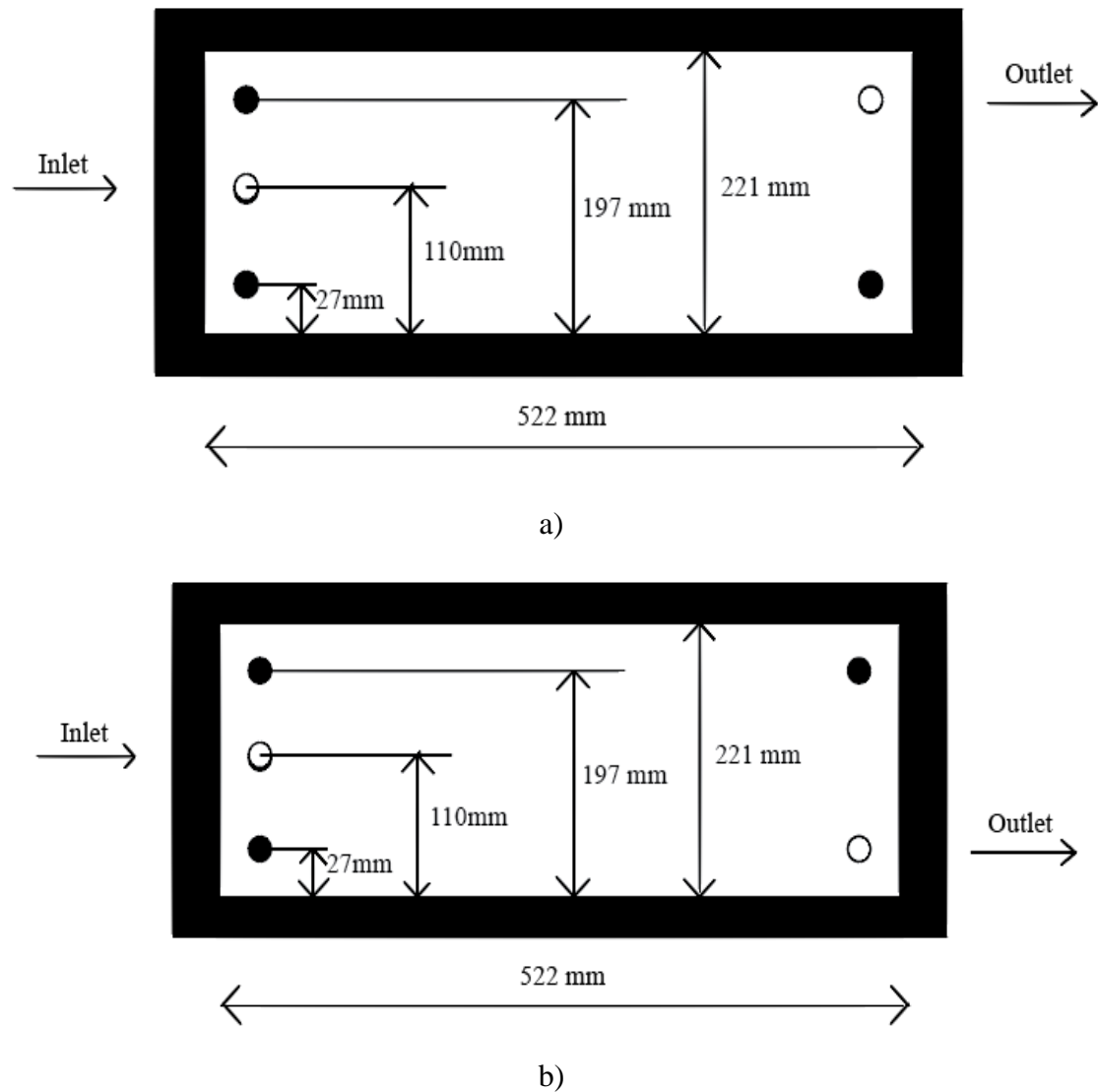
Figure 3.5 Slot configuration for middle injection fracture with a a) top outlet b) bottom outlet.

Top injection: The top slot model uses a configure with the inlet at $7/8^{th}$ of the fracture height or 197mm from bottom. Figure 3.6 shows a schematic of the experiments. Each single inlet position was studied for both a fracture with a bottom outlet and a fracture with a top outlet.

a)

b)
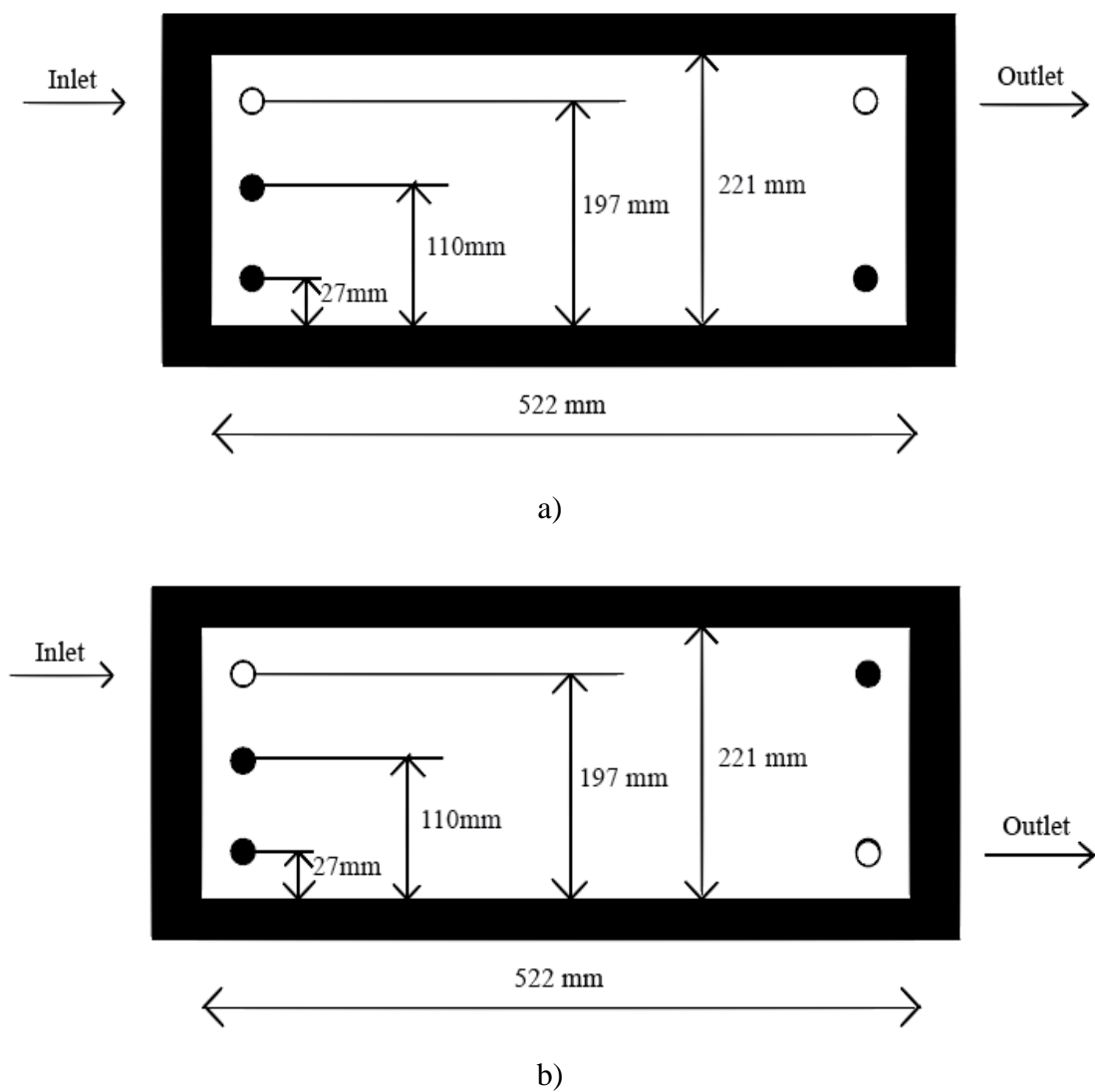
Figure 3.6 Slot configuration for top injection fracture with a a) top outlet b) bottom outlet.

3.1.4.2 Multiple perforation injection. Experiments were also conducted for multiple injection points in the fracture slot to simulate the impact of more perforations during fracturing, their impact on sand transport.

Dual injection: The dual injection model refers to the slot flow model with two inlets, one at top and the second inlet in middle, as shown in Figure 3.7. This experiment was conducted as a top outlet fracture condition.
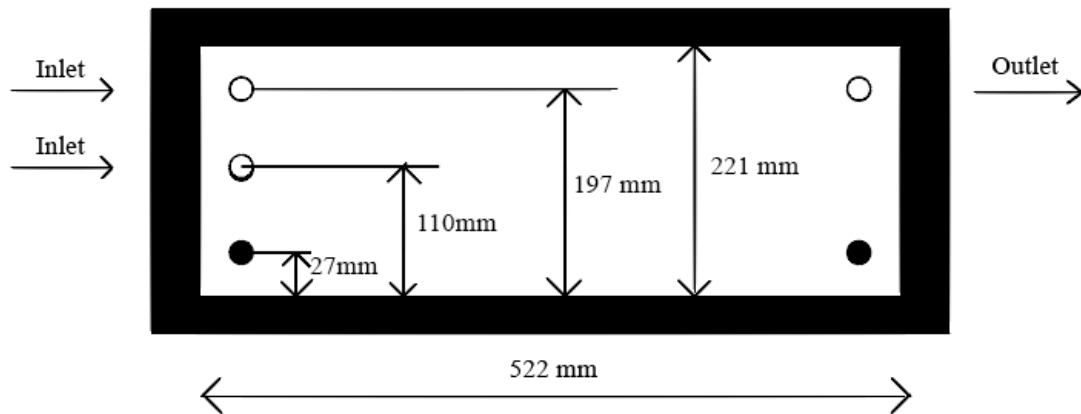
Figure 3.7 Slot configuration for dual injection (top outlet fracture).

Triple injection: The triple injection model refers to a slot flow experiment with inlets at the top, middle, and, bottom all active at the same time, as shown in Figure 3.8. This experiment was conducted as a bottom outlet fracture condition.
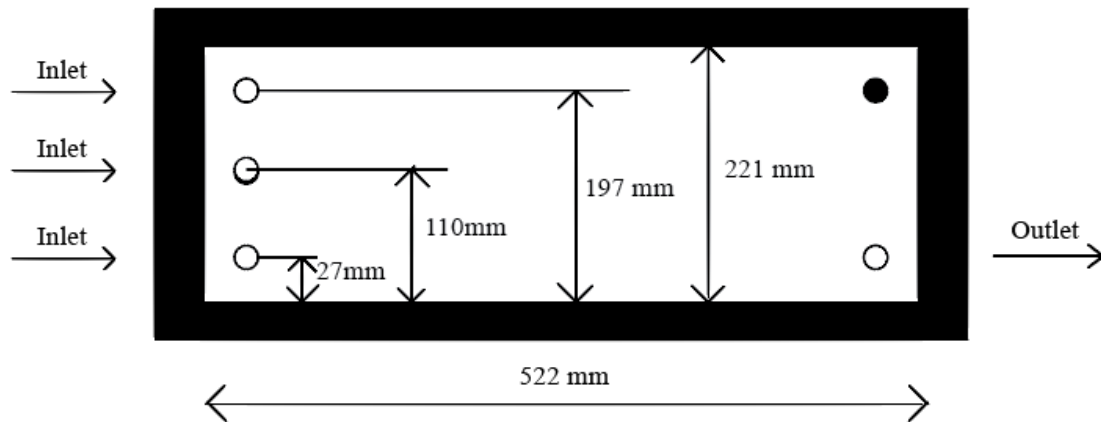
Figure 3.8 Slot configuration for triple injection (bottom outlet fracture).

3.1.4.3 Angularity effect. Experiments were conducted using brown sand to analyze the effect of angularity of the proppant particles on the dune development in the fracture. Three experiments with varying inlet at top, middle and bottom and bottom outlet fracture condition were performed for repeatability. These experiments were compared with the earlier experiments using the rounder ceramic proppant.

3.2. EXPERIMENTAL PROCEDURE

The slot flow experiments were prepared and conducted in a controlled environment. The visual data for the experiments were collected using photos and videos. Quantitative measurements were made for the proppant in dry condition. The slot model was later cleaned and prepared again for the next experiment with different conditions. The procedure is described in detail in sections 3.2.1 and 3.2.2.

3.2.1. Conducting the Experiment. The slot model is connected and arranged as shown in Figure 3.9. Then, transport fluid (water or linear gel) was used to fill the slot model which represents pad volume of the fracturing treatment. Afterwards the accumulator was filled with the slurry volume and cameras were set to record the experiment. A black steel plate was used behind the slot flow model to enhance video recordings of the experiment. The valve at the end of the accumulator was opened and at last the gas injection valve was opened to run the experiment. Care was taken to ensure no nitrogen gas was injected that could disrupt the dune with high turbulence imposed by the gas. The injection time was in range of 2.5 to 3.5 seconds. The remaining slurry volume was measured and proppant was dried and weighed. By verifying the slurry concentration, consistency and accuracy of the experiments were maintained. The photos were taken after
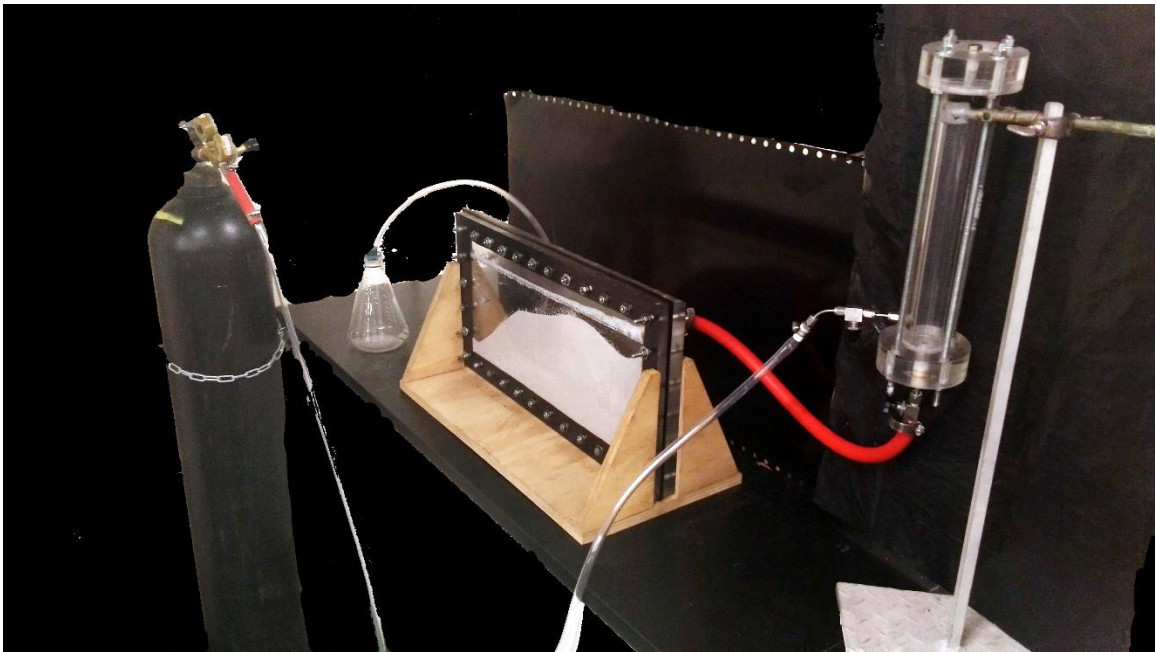
Figure 3.9 Overall experimental setup.

each injection runs. After that, the accumulator was filled again with same volume of slurry and all the equipment were rearranged. The experiment was repeated until equilibrium was reached. Equilibrium referred to the point where subsequent injection made no change in EDL, and the amount of slurry injected was the same as the amount of slurry volume collected from outlet.

3.2.2. Data Collection and Analysis. The recorded videos and photos provided the dune and flow data used in the analysis. Proppant dune height, injection time of the slurry and transport mechanism were noted from videos and photos taken during the experiments. These results were normalized to the fracture pore volume (FPV) injected. FPV can be defined as the ratio of the slurry volume injected to the total fracture volume. Slurry volume is summation of all volume of transport fluid and volume of proppant to reach EDL.

$$FPV = \frac{Slurry\ volume}{Fracture\ volume} \tag{13}$$

$$Slurry\ volume = \frac{proppant\ weight}{proppant\ density} + Transport\ fluid\ volume \tag{14}$$

Every photo was digitally measured using trail version of GetData software or using digitize2.m a MATLAB code written by A. Prasad (2001) which was originally developed by J. D. Cogdell (2000). The software inputs were photos. The X-axis and the Y-axis to form plane of reference were selected followed by selection of points of interest. For these experiments, points of interest were the point which represent proppant dune shape. Twenty-one points were taken which closely represented the dune in digital form.

Microsoft excel was used to graph and further investigate dune development patterns, proppant area coverage, and the injection mechanism with respect to FPV, EDL and EDX. From these graphs, angular analysis was undertaken. Surface area was calculated as area under the curve using trapezoidal rule.

For further investigation, the dune was horizontally divided into 3 portions: (1) Buildup dune (2) Constant dune (3) Drawdown dune. As the name suggests, the portion of dune, which has increasing slope with respect to height having angle more than 20^0 was called buildup dune. Buildup dune was found near the inlet of the fracture. The portion of dune, which was almost constant with respect to height having angle in range of -15^0 to $+5^0$ was called constant dune. EDX was measured using this portion of the fracture. The remaining portion of the dune towards the outlet of the fracture was most negative in slope.

Alternatively, manual points were selected and measurements were recorded as shown in Figure 3.10. These points were kept the same throughout the research study. The digitally recorded measurements were localized to these points as well. All the experiments were recorded from backside of the model. In Figure 3.10, point one is closest to inlet point and point twenty-one is at 515 mm depth in the fracture.

The Figure 3.11 shows how the EDL and EDX were calculated during this research. The value of *l, h, h₁, x₁* are measured using graphical representation of the dune from using MS-excel and value of EDL and EDX are measured according to the equation mentioned earlier.

So, for the case shown in Figure 3.11

$$EDL = \frac{h_1}{h} \times 100 \tag{15}$$

Point	Depth (mm)	Point	Depth (mm)
1	0	12	290
2	34	13	309
3	54	14	336
4	86	15	358
5	109	16	390
6	136	17	407
7	158	18	440
8	188	19	461
9	209	20	490
10	236	21	515
11	254		
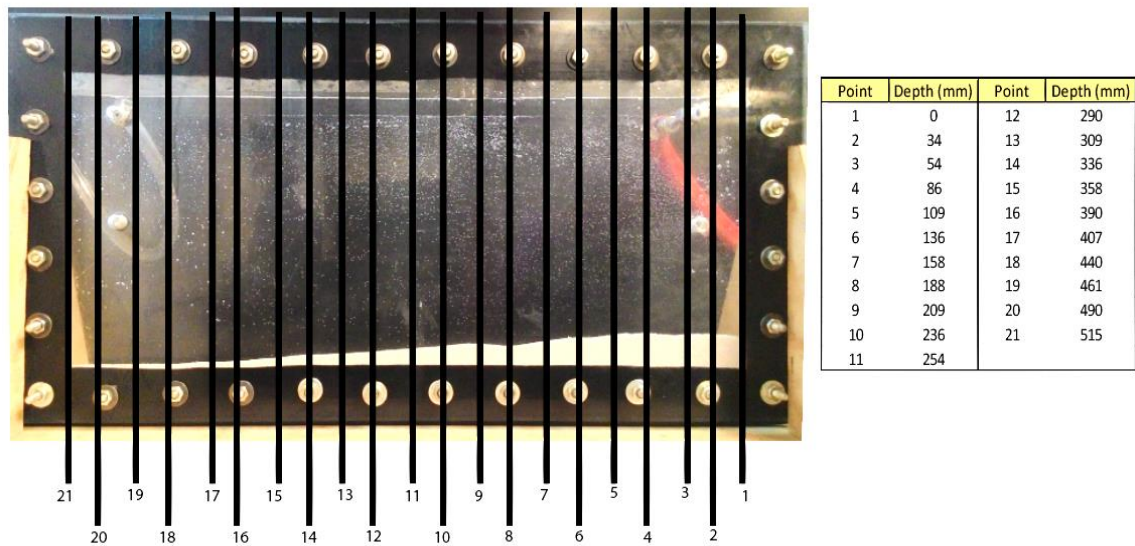
Figure 3.10 Measurement point along the depth of the fracture.

$$EDX = \frac{x_1}{l} \times 100 \qquad (16)$$

The angles of different sections were calculated as shown below in Figure 3.12 and can be given by:

$$\theta = \tan^{-1}\left(\frac{h_2}{x_2}\right). \qquad (17)$$

The negative value of angle suggest height is decreasing for the dune.

The surface area of the dune was calculated as shown in Figure 3.13. As the dune was created using points collected from digitization of photo, the dune was divided into parts. The area of the dune is summation of the areas of all these parts. This calculation is expressed as,
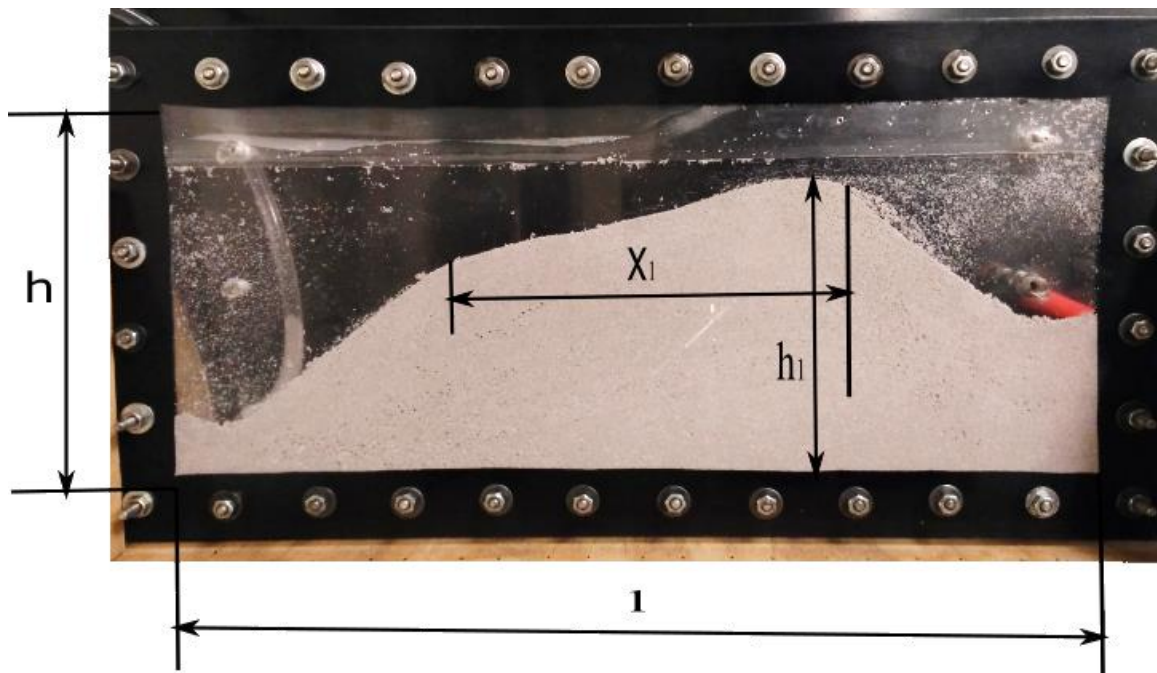
Figure 3.11 EDL and EDX calculation method illustrated.
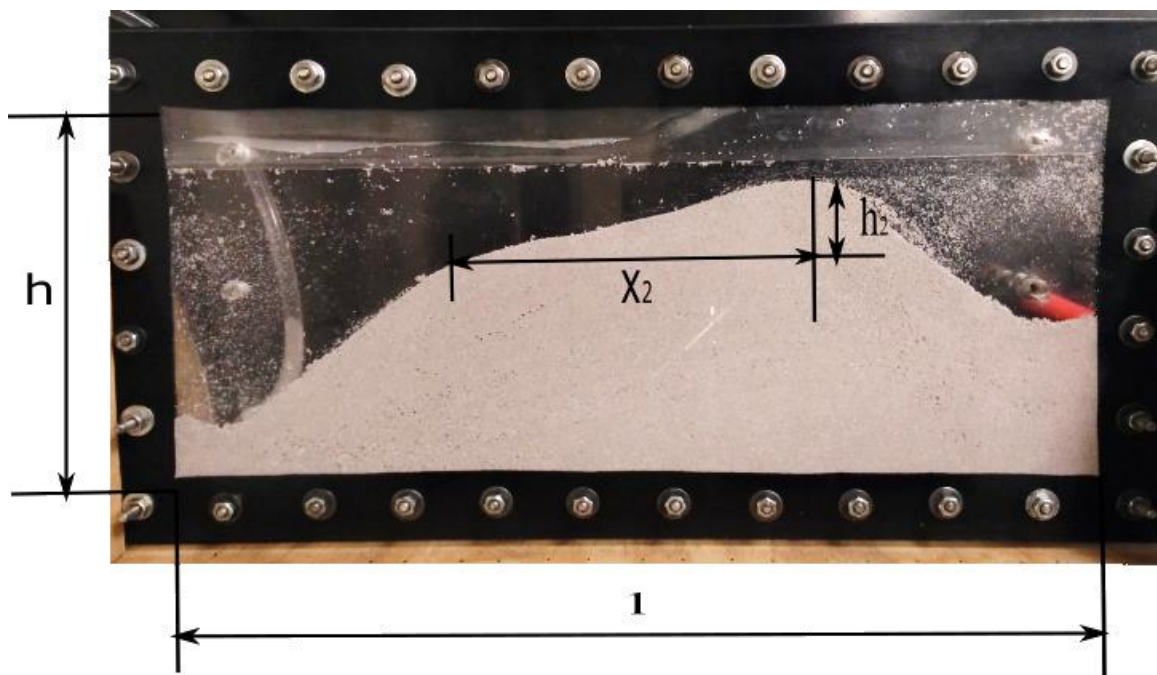
Figure 3.12 Angle calculation illustration.

$$Area\,(mm^2) = \sum_{n=0}^{19}\left((x_{n+1} - x_n)\left(\frac{y_n + y_{n+1}}{2} \right) \right) \qquad (18)$$

The surface area fraction can be given by,

$$Surface\ area\ fraction = \frac{Area\,(mm^2)}{Total\ area\,(mm^2)} = \frac{Area}{522 \times 221} \qquad (19)$$
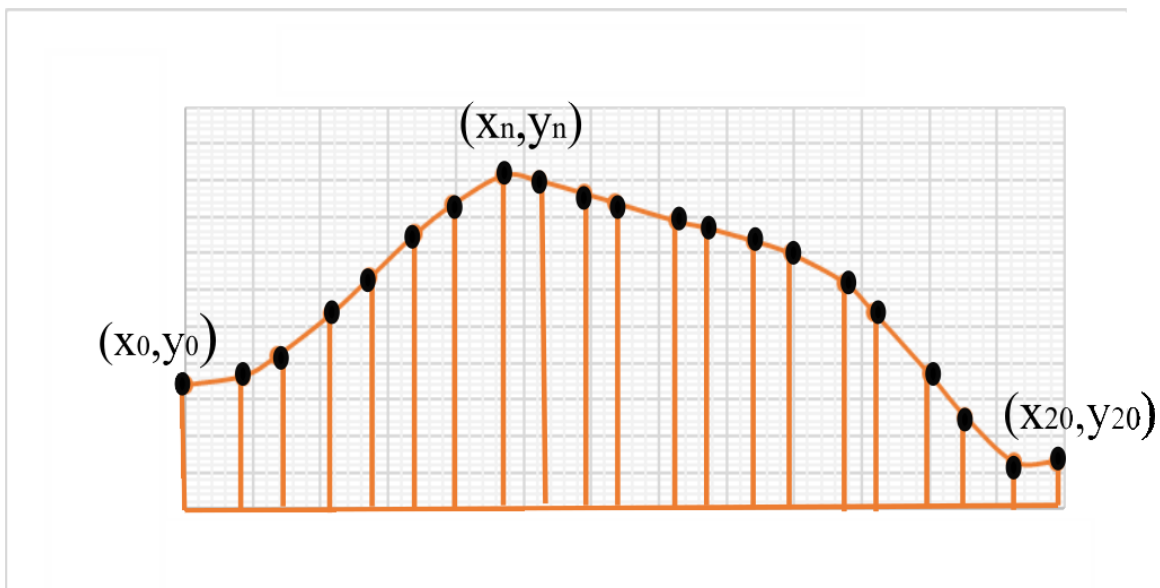
Figure 3.13 Surface area calculation from graphical dune representation.

4. EXPERIMENTAL RESULTS AND ANALYSIS

This section presents the experimental results. Eight different configurations of inlet and outlet from the slot flow model were designed and used to investigate ceramic proppant transport. Two experiments were repeated with brown sand as proppant. For every experiment, dune development was investigated. Experiments using 4 lbpg and 6 lbpg proppant concentration were conducted to check limits of the setup. The conclusion from these experiments showed that changing concentration at specific pressure changed the flowrate. In this study, flowrates are kept nearly constant by keeping proppant concentration and the nitrogen gas cylinder pressure constant.

For all the experiments a proppant weight analysis was conducted to ensure consistent flowrates and to keep the concentration of proppant slurry in the specified range. To conduct the proppant weight analysis, after each accumulator volume was injected, the remaining water volume and dry weight of proppant remaining in the accumulator was measured and compared. Measured injected concentration was maintained in the range of 0.92 to 1.10 lbpg and flowrate of the injected volume was in the range of 110 ml/s to 130 ml/s.

4.1. A NUMBER OF PERFORATION RESULTS

The experiments were conducted with different sets of changing perforation position followed by changing a number of perforation connected to the fracture model. Dune developed by these experiments are presented below.

4.1.1. Single Perforation Experiments. Three experiments were performed and repeated with changing fracture conditions, i.e. bottom outlet and top outlet fracture. All of the experiments were conducted with 50 psi nitrogen pressure to maintain an identical flowrate throughout the research. The dune formed at equilibrium was measured and graphed as discussed here.

4.1.1.1 The fracture with a top outlet. Figure 4.1, Figure 4.2, and Figure 4.3 show the experimental results for a single injection point at the bottom, middle and top of the fracture, respectively. In all cases, 30/50 mesh ceramic proppant has been used and the fracture outlet was at the top of the fracture model. The blue dots shown in Figure 4.1 to Figure 4.3 represent approximate inlet and outlet positions for the model.
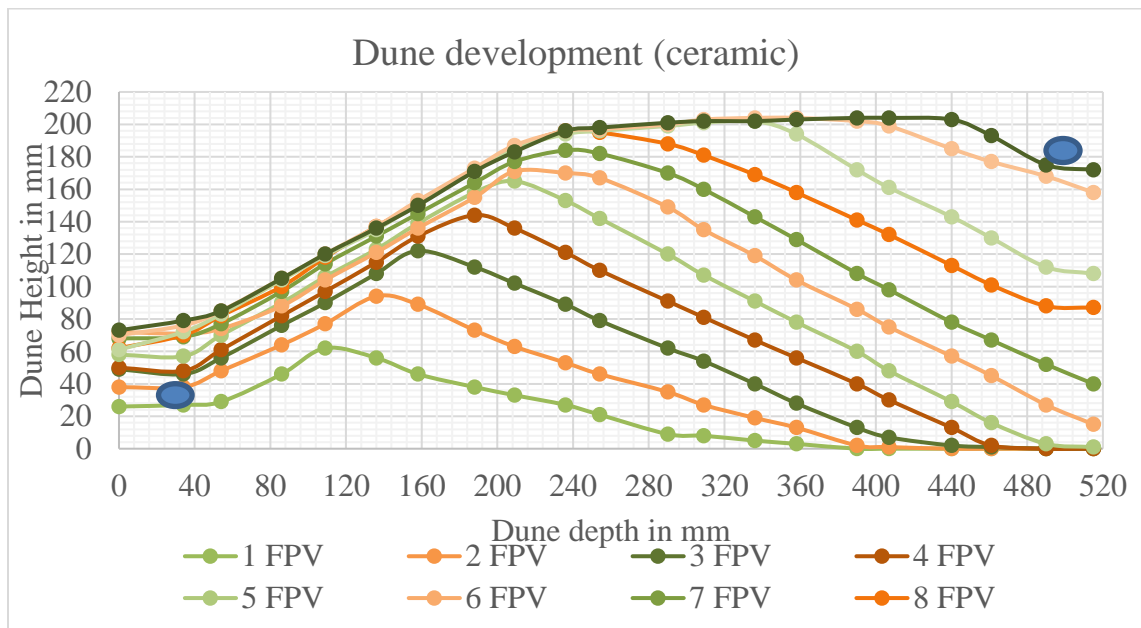
Figure 4.1 Dune development for a bottom inlet in the fracture with a top outlet.
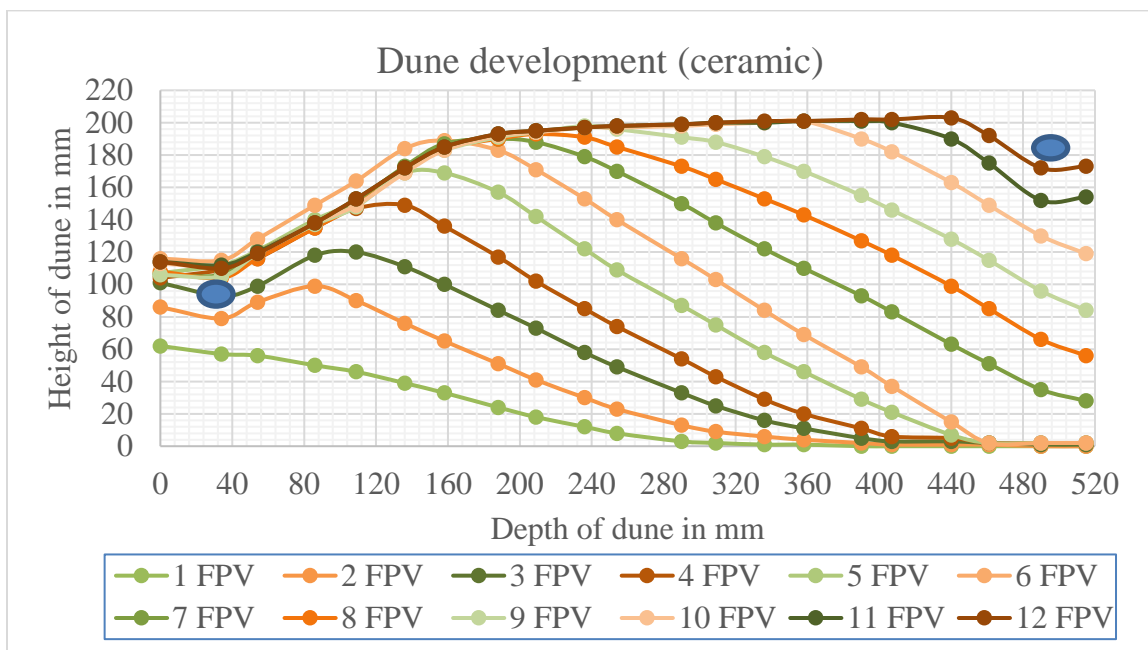
Figure 4.2 Dune development for a middle inlet in the fracture with a top outlet.
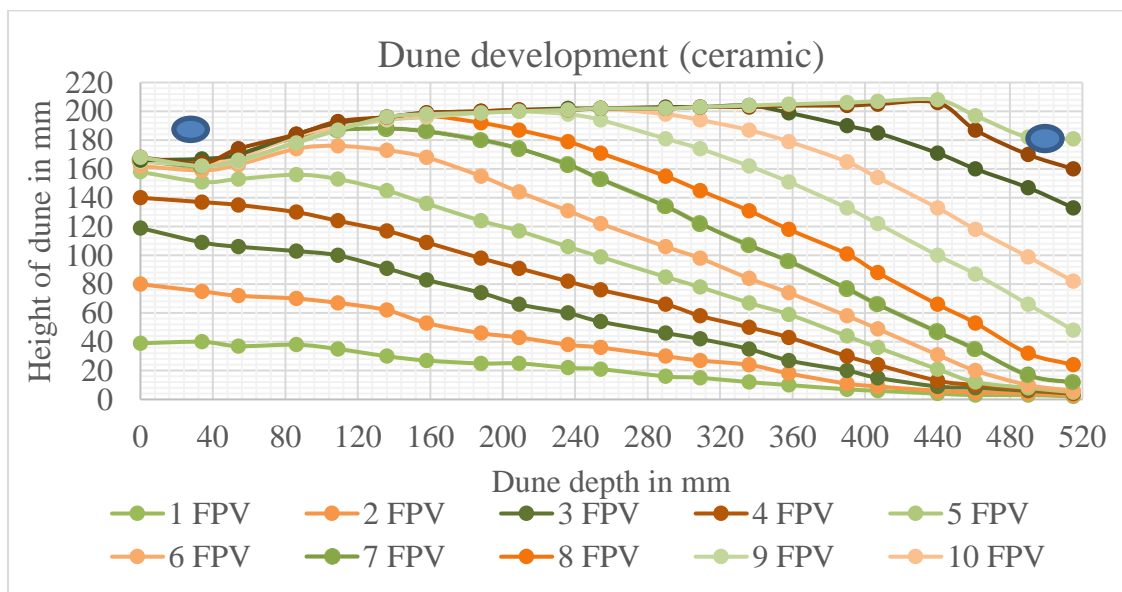
Figure 4.3 Dune development for a top inlet in the fracture with a top outlet.

4.1.1.2 The fracture with a bottom outlet. Figure 4.4, Figure 4.5, and Figure 4.6 show the experimental results for a single injection point at the bottom, middle and top of the fracture, respectively. In all cases, 30/50 mesh ceramic proppant has been used and the fracture outlet was at the bottom of the fracture models. The blue dots shown in Figure 4.4 to Figure 4.6 represent approximate inlet and outlet positions for the model.
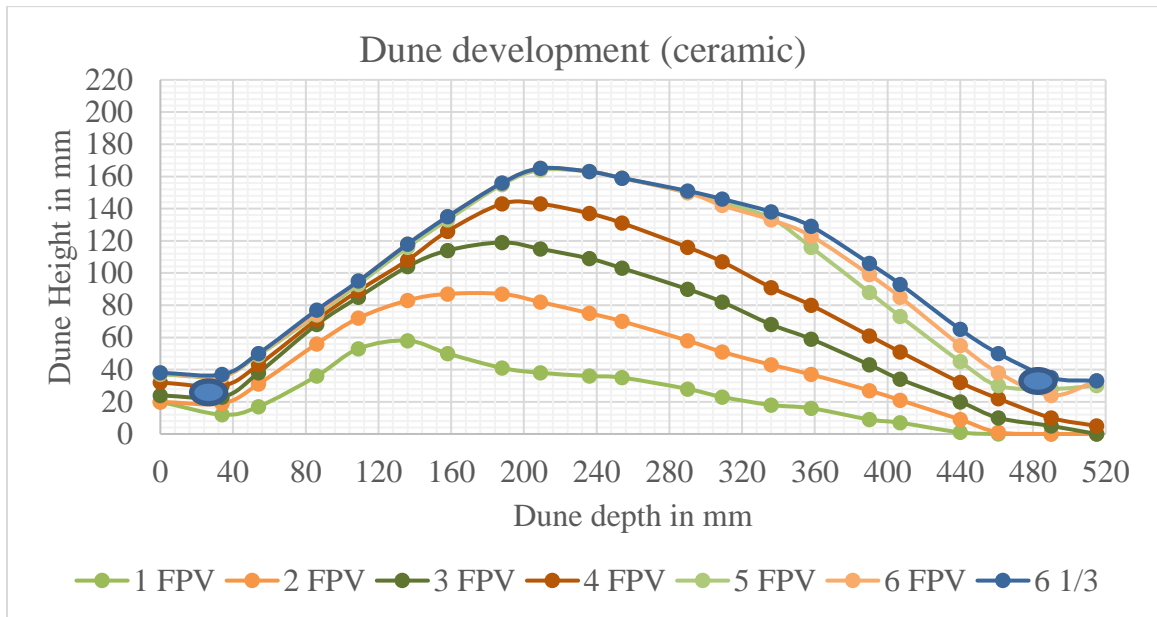
Figure 4.4 Dune development for a bottom inlet in the fracture with a bottom outlet.

Non-integral FPV represents equilibrium obtained before total Fracture pore volume, which is equal to three accumulator equivalent volume injected. So, every injected slurry volume increases the injected slurry volume by 1/3rd the fracture pore volume (FPV).
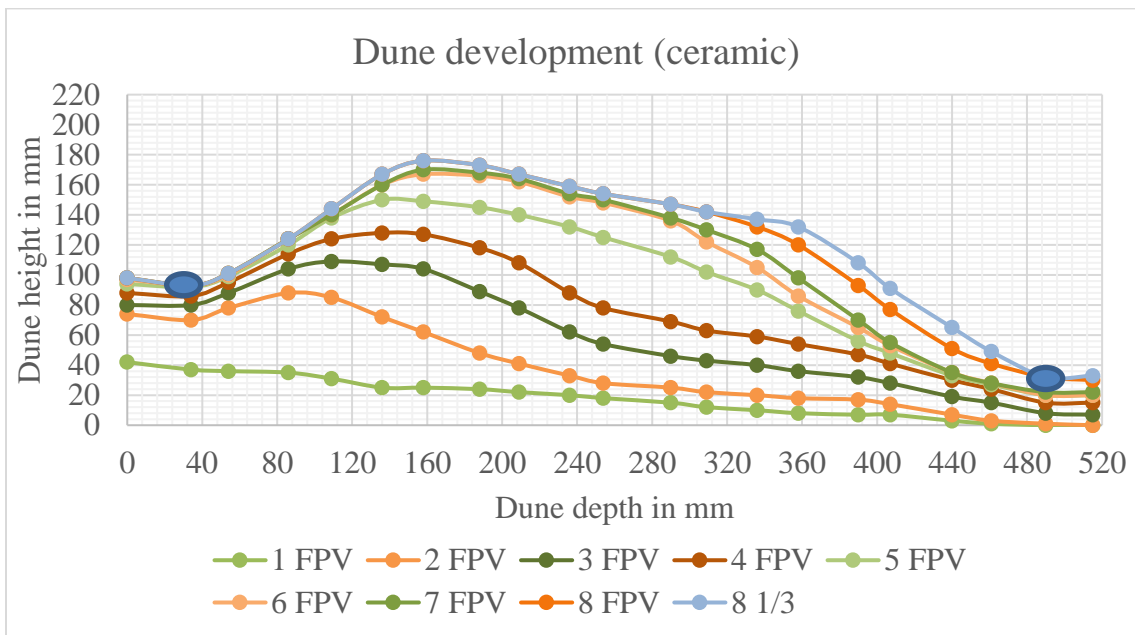
Figure 4.5 Dune development for a middle inlet in the fracture with a bottom outlet.
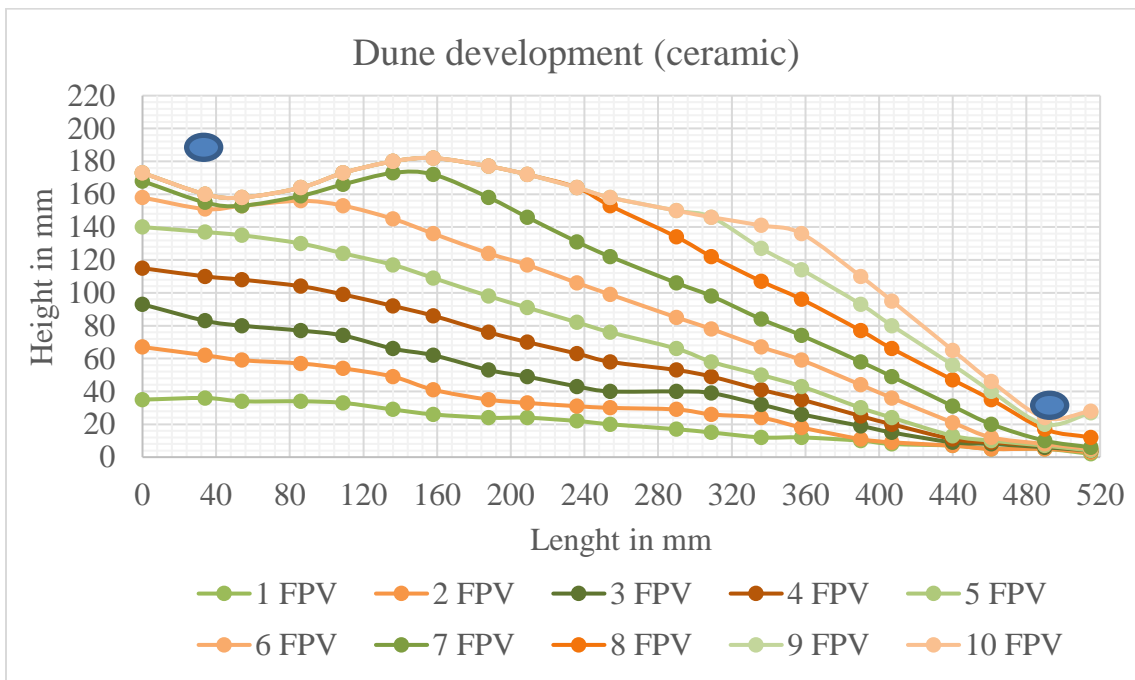
Figure 4.6 Dune development for a top inlet in the fracture with a bottom outlet.

4.1.1.3 EDL and EDX. Table 4.1 summarizes the effect of the perforation height and length on dune development obtained from the experiments. The effect is categorized in different dune measurement parameters discussed in earlier sections. In this section EDL and EDX patterns are discussed.

For the top outlet fracture condition, there is no significant change in EDL because of injection position. This may be due to the use ceramic proppant, which supported the dune growth. But there is a change in EDL and EDX in the fracture with a bottom outlet condition. A bottom injection point gives the lowest EDL and EDX, and is therefore the worst condition for proppant transport.

Table 4.1 Single Inject point heights vs EDL, EDX.

Proppant	Fracture condition	Injection Height Fraction	EDL (%)	EDX (%)
Ceramic	Top outlet	0.125 (Bottom inlet)	92.3	44.3
		0.5 (Middle Inlet)	92	52.9
		0.875 (Top Inlet)	94	63.4
Ceramic	Bottom outlet	0.125 (Bottom inlet)	74	28.5
		0.5 (Middle Inlet)	79	38.3
		0.875 (Top Inlet)	82	42.5

For all the cases, increasing height of injection from the bottom of the fracture increases EDX. A higher EDX indicates and larger amount of stable dune.

Experimental results show that the higher the perforation occurs the fracture plane, the greater the proppant settling time. Greater proppant settling time means more time for

the proppant to travel horizontally as. Figure 4.7 and Figure 4.8 show how many FPV are needed to inject for proppant to reach the end of the fracture.
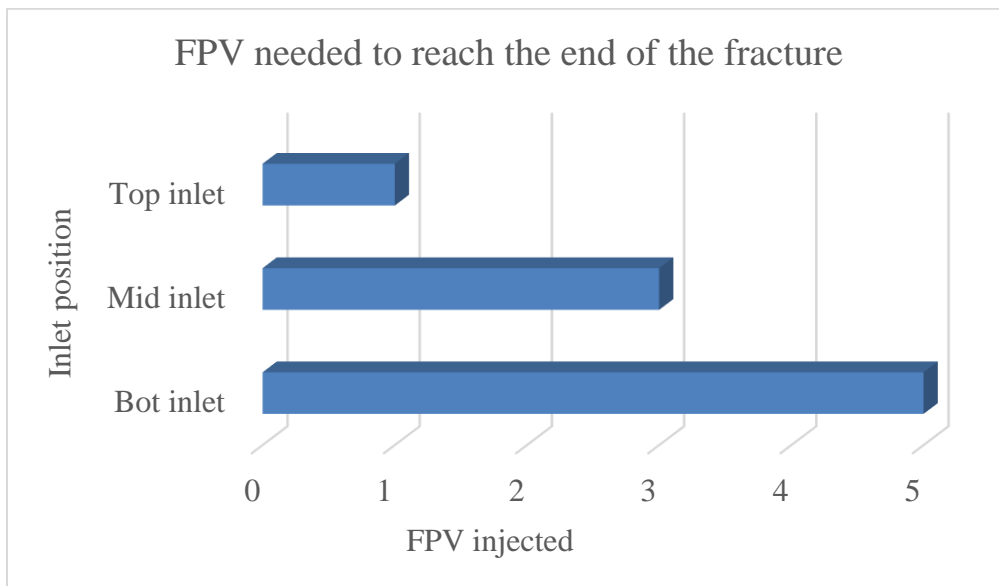
Figure 4.7 FPV needed to reach the end of the fracture for a fracture with a top outlet (ceramic).

For both the cases of the top outlet and the bottom outlet fracture condition, it can be observed that the proppant reached the end of the fracture after 1st FPV was injected from the top inlet while it took 3 FPV for the middle inlet. For top outlet fracture, it took 5 FPV for bottom inlet and for the fracture with a bottom outlet, it took 4 FPV for proppant to reach the end of the fracture model.
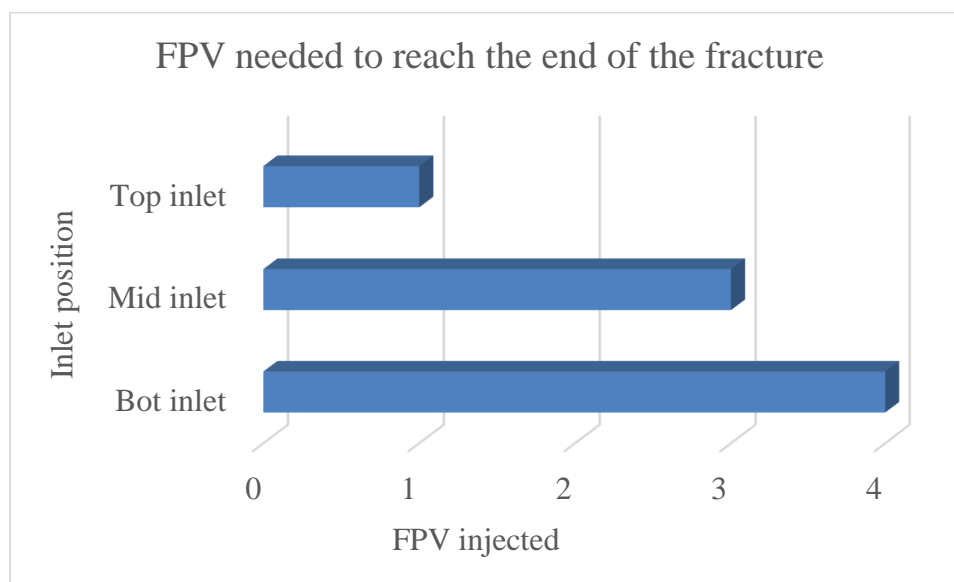
Figure 4.8 FPV needed to reach the end of the fracture for the fracture with a bottom outlet (ceramic).

4.1.1.4 Surface area. Surface area is a useful factor to measure in proppant transport. The higher the surface area covered by proppant the greater the propped fracture area and potentially fracture conductivity. Hence, propped surface of the fracture can be considered an indirect indicator of success of the fracture treatment. As the height of the single injection point increased, propped surface area of the fracture also increased. As previously discussed, the surface area was calculated using graphical dune and excel sheets data. Figure 4.9, Figure 4.10, Figure 4.11, Figure 4.12, Figure 4.13, and Figure 4.14 are the area division of equilibrium dune of the different single point injection cases.

Proppant density embedded in the dune was calculated by measuring the weight of the proppant remaining in the slot-flow model and dividing by the total proppant dune area to get proppant in lb/ft^2. For all ceramic proppant experiment it was very similar.
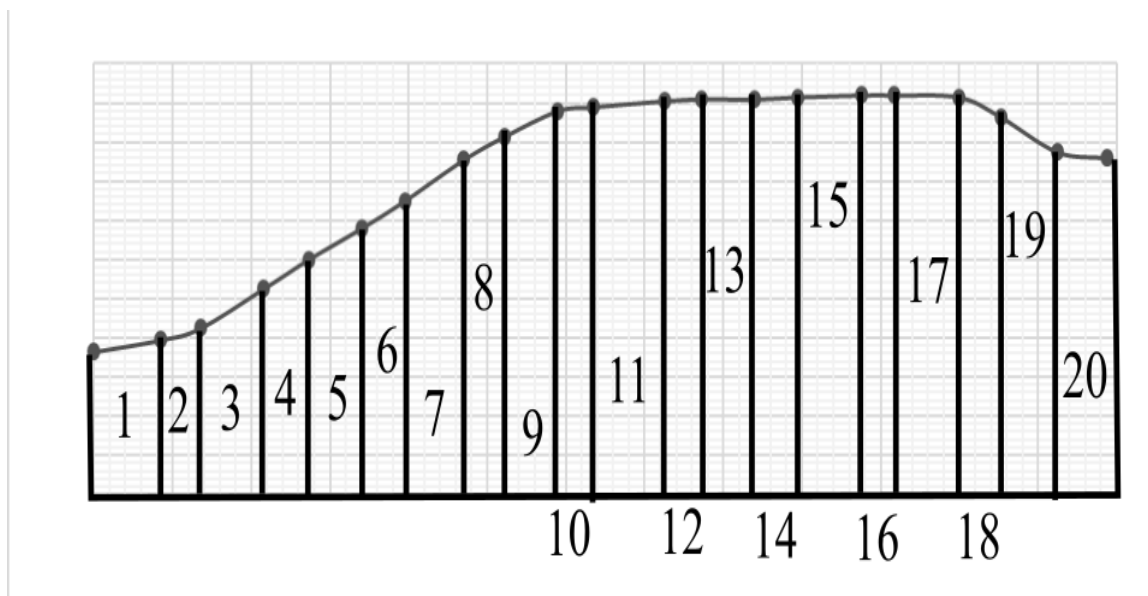
Figure 4.9 Area division of equilibrium dune for a bottom inlet in the fracture with a top outlet (ceramic).
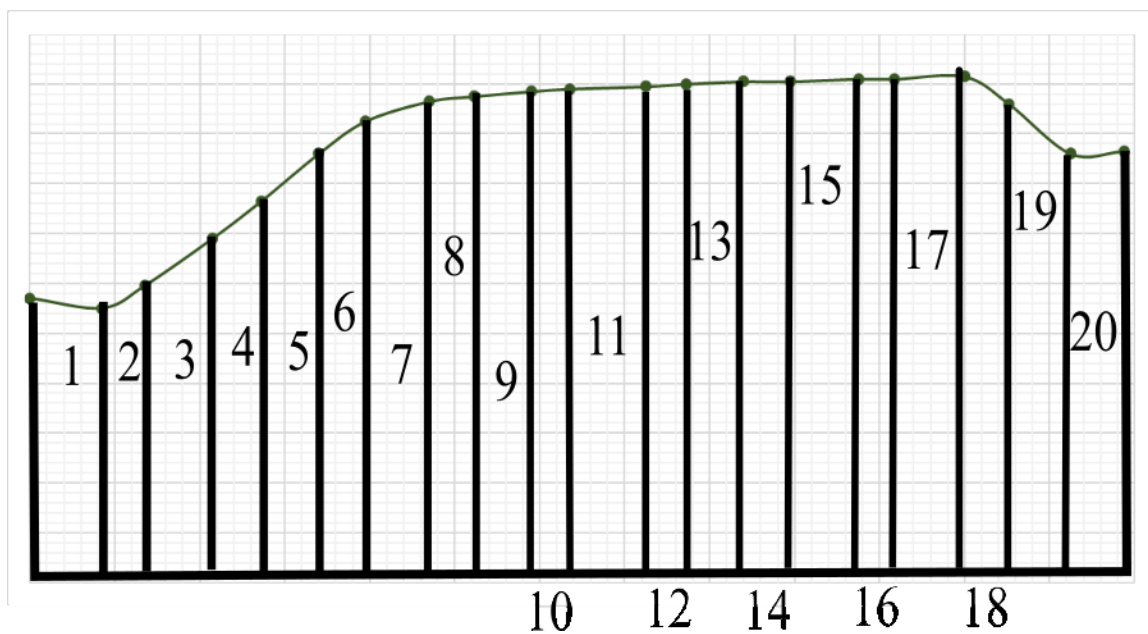
Figure 4.10 Area division of equilibrium dune for a middle inlet in the fracture with a top outlet (ceramic).
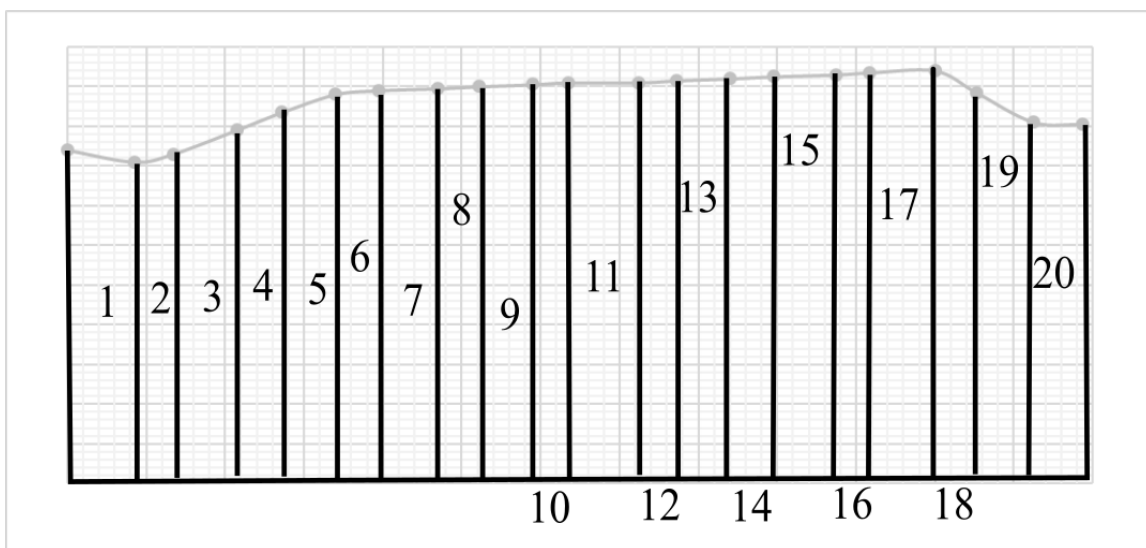
Figure 4.11 Area division of equilibrium dune for a top inlet in the fracture with a top outlet (ceramic).
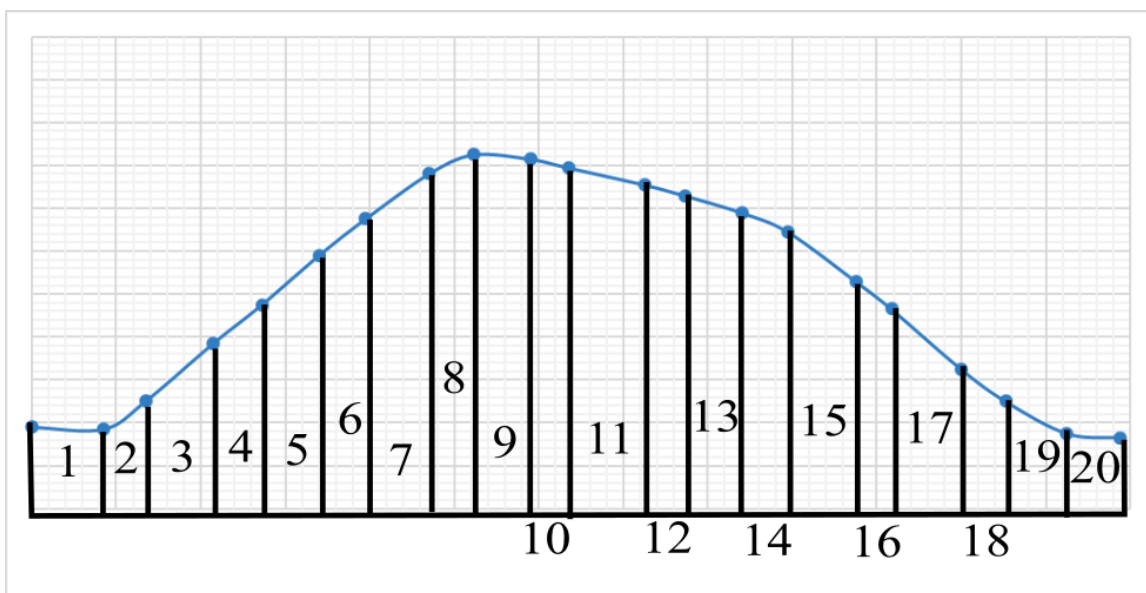
Figure 4.12 Area division of equilibrium dune for a bottom inlet in the fracture with a bottom outlet (ceramic).
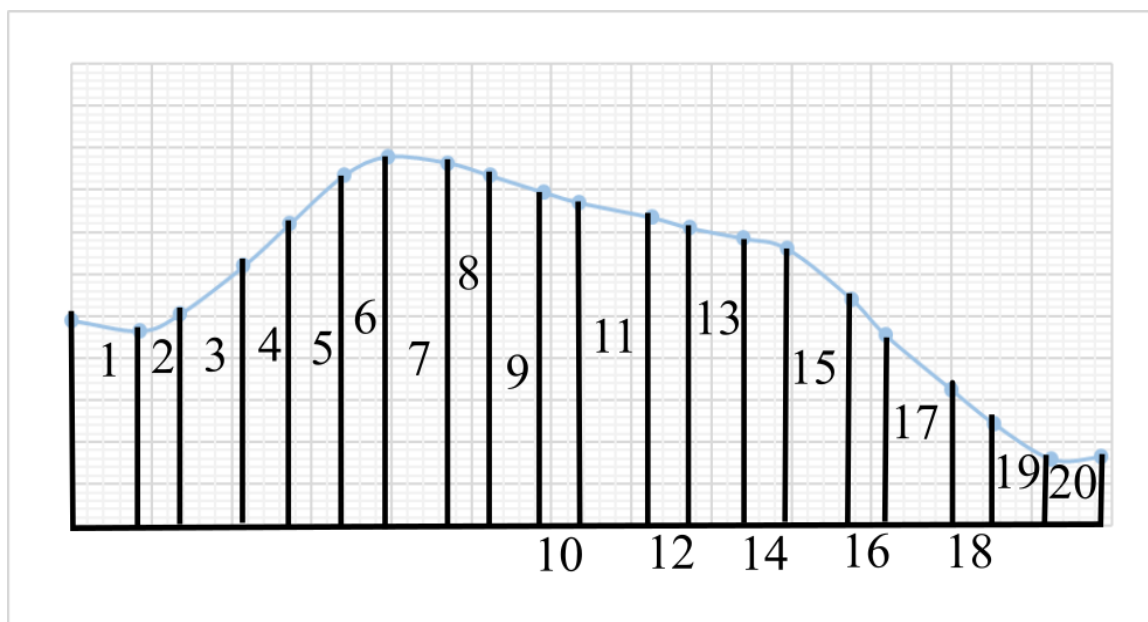
Figure 4.13 Area division of equilibrium dune for a middle inlet in the fracture with a bottom outlet (ceramic).
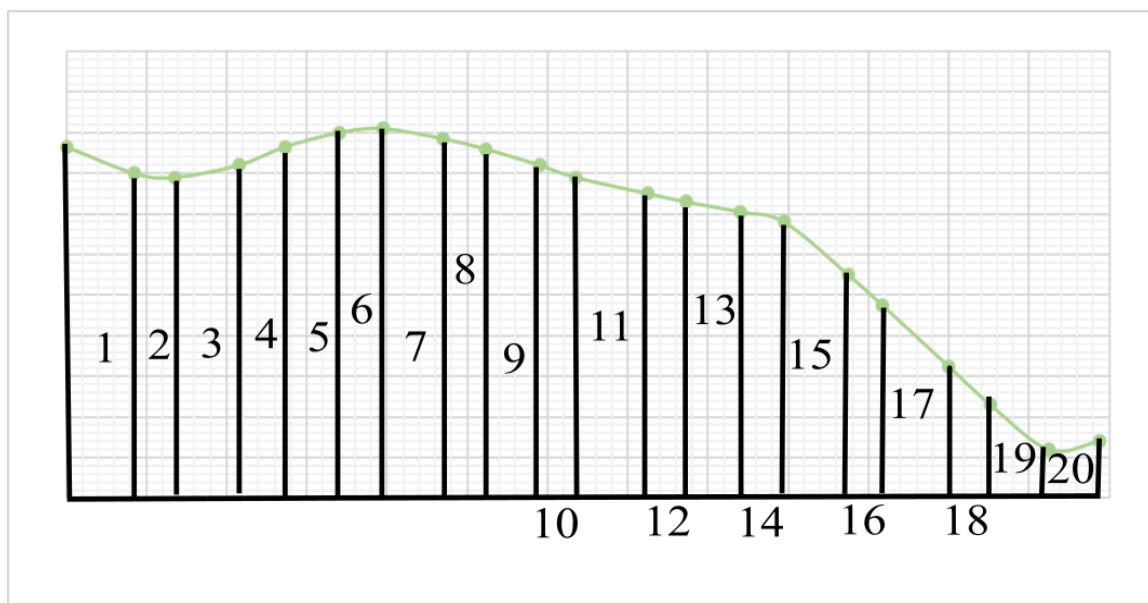
Figure 4.14 Area division of equilibrium dune for a top inlet in the fracture with a bottom outlet (ceramic).

These divided areas were calculated and summed to find total surface area of the propped fracture for each experimental case. These results are summarized in Table 4.2, and Table 4.3

Table 4.2 Summation of surface area of equilibrium dune for single perforation experiments (ceramic).

Fracture condition	Top outlet			Bottom outlet		
Inlet	Bottom	Middle	Top	Bottom	Middle	Top
Area of Part 1	2584	3808	5610	1275	3247	5661
Area of Part 2	1640	2290	3280	870	1940	3180
Area of Part 3	3040	4112	5504	2032	3600	5152
Area of Part 4	2587.5	3346.5	4197.5	1978	3082	3875.5
Area of Part 5	3456	4387.5	5170.5	2875.5	4198.5	4765.5
Area of Part 6	3146	3927	4334	2783	3773	3982
Area of Part 7	4815	5670	5955	4365	5235	5385
Area of Part 8	3717	4074	4189.5	3370.5	3570	3664.5
Area of Part 9	5116.5	5292	5413.5	4428	4401	4536
Area of Part 10	3546	3555	3627	2898	2817	2898
Area of Part 11	7182	7146	7272	5580	5418	5544
Area of Part 12	3828.5	3790.5	3847.5	2821.5	2745.5	2812
Area of Part 13	5454	5413.5	5494.5	3834	3766.5	3874.5
Area of Part 14	4455	4422	4499	2937	2959	3047
Area of Part 15	6512	6448	6576	3760	3840	3936
Area of Part 16	3468	3434	3510.5	1691.5	1691.5	1742.5
Area of Part 17	6715.5	6682.5	6847.5	2607	2574	2640
Area of Part 18	4158	4147.5	4252.5	1207.5	1197	1165.5
Area of Part 19	5336	5278	5495.5	1232.5	1174.5	1015
Area of Part 20	4337.5	4312.5	4537.5	850	812.5	650
Total Area	85094.5	91536.5	99613.5	53396	62042	69526

Table 4.3 Surface area and surface area fraction for single perforation experiments.

Proppant	Fracture condition	Injection Height Fraction	Surface Area(mm²)	Surface Area Fraction
Ceramic	Top outlet	0.125 (Bottom)	85094.5	0.74
		0.5 (Middle)	91536.5	0.79
		0.875 (Top)	99613.5	0.86
Ceramic	Bottom outlet	0.125 (Bottom)	53396	0.46
		0.5 (Middle)	62042	0.54
		0.875 (Top)	69526	0.60

The area covered by the proppant represents propped area of the fracture. For a top outlet fracture slot flow model, linear change in the propped area was observed. For bottom inlet, almost 74% of the fracture surface are is covered with proppant. When we change inlet to the middle position, propped area increases to approximately 79%. But for top inlet, it increases by more than 12% to around 86% of total fracture area compared to bottom inlet. Figure 4.15 shows the linear trend, and regression analysis yields R^2 values more than 0.99.

The surface area fraction for a bottom outlet fracture gives a linear relationship as well with increasing height of inlet from the bottom to the top of the fracture as shown in Figure 4.16. Propped area increases with increasing height of inlet from the bottom of the fracture model. From 46% propped area for the bottom inlet to almost 54% for the middle inlet and 60% of the propped area for the top inlet.
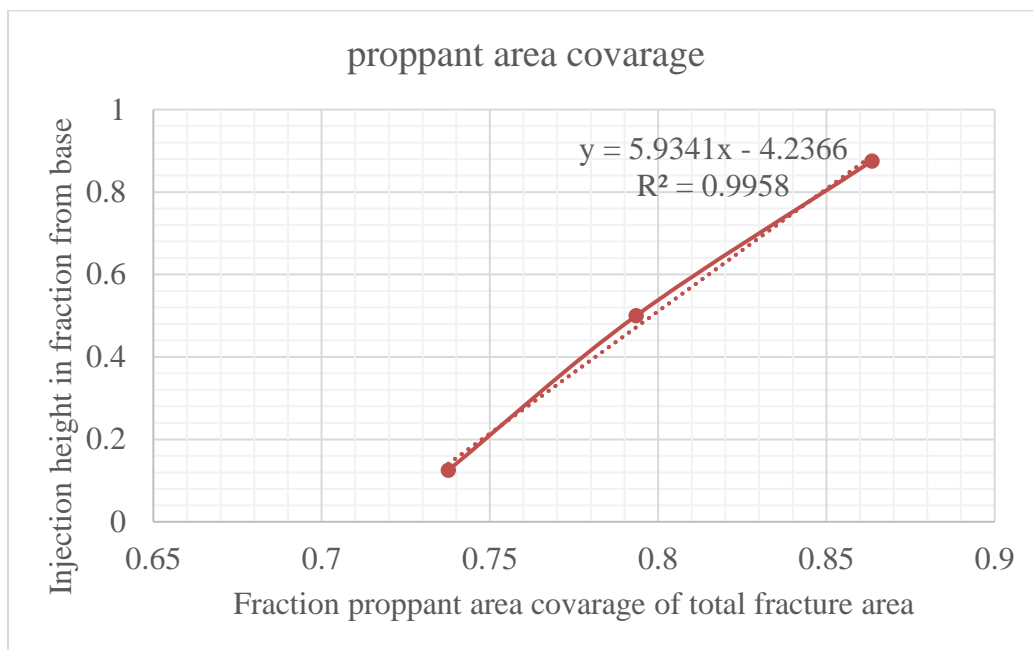
Figure 4.15 Fractional area of ceramic proppant coverage for a fracture with a top outlet.
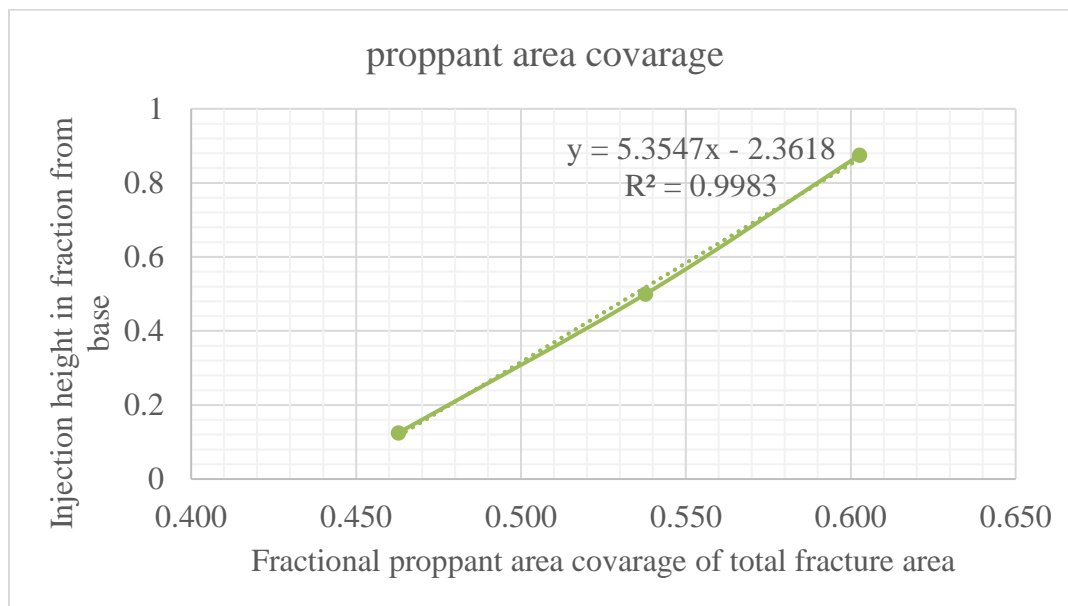
Figure 4.16 Fractional ceramic proppant area coverage for a fracture with a bottom outlet.

4.1.1.5 Dune angle comparison. Dune shape can be measured with one more factor which is the angle of the dune formed. Angle of dune was measured using excel data as shown in Figure 4.17, Figure 4.18, Figure 4.19, Figure 4.20, Figure 4.21, and Figure 4.22. The dune angles are summarized in Table 4.4 and Table 4.5
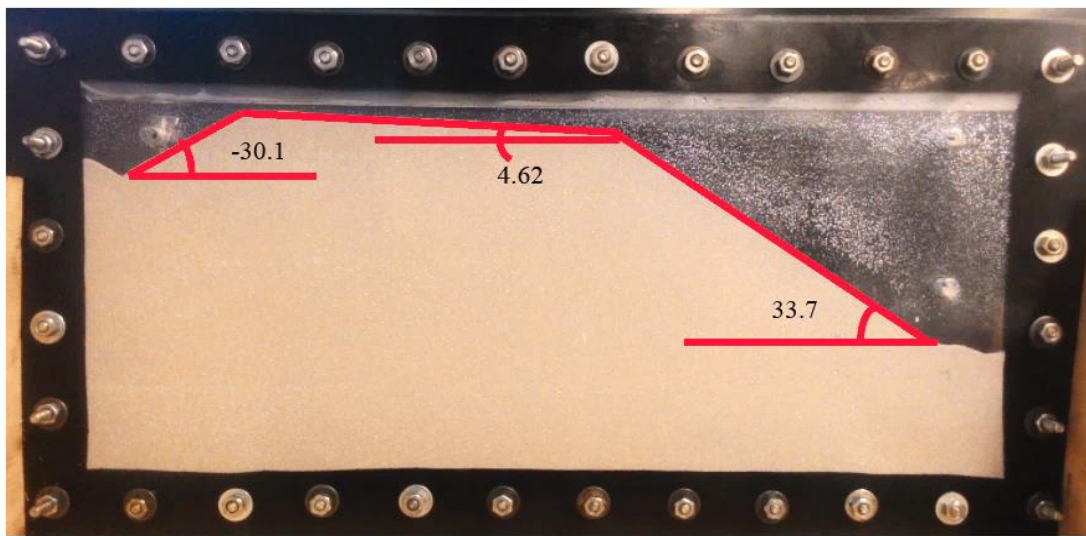
Figure 4.17 Angle measurements for the bottom inlet and a top outlet experiment (ceramic).

Table 4.4 Equilibrium dune angle measurement for the fracture with a top outlet (ceramic proppant) and a single inlet.

Characteristics	Buildup angle	Dune angle	Drawdown angle
Top inlet	22.1	2.09	-29.7
Middle inlet	29.4	2.6	-29.7
Bottom inlet	33.7	4.62	-30.1
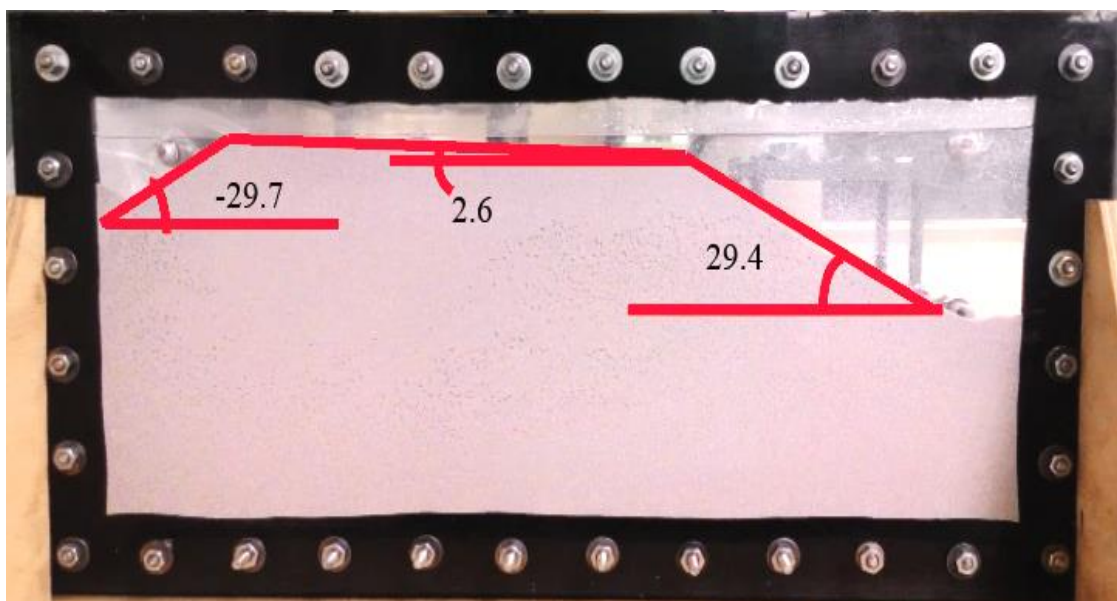
Figure 4.18 Angle measurements for the middle inlet and a top outlet experiment (ceramic).
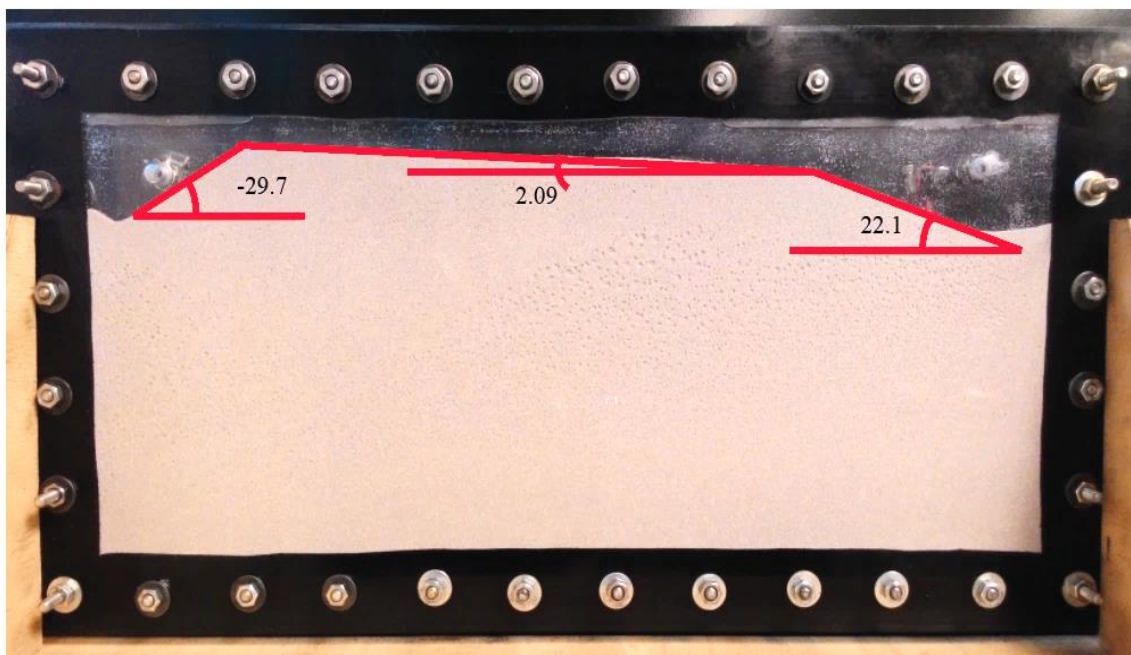
Figure 4.19 Angle measurements for the top inlet and a top outlet experiment (ceramic).
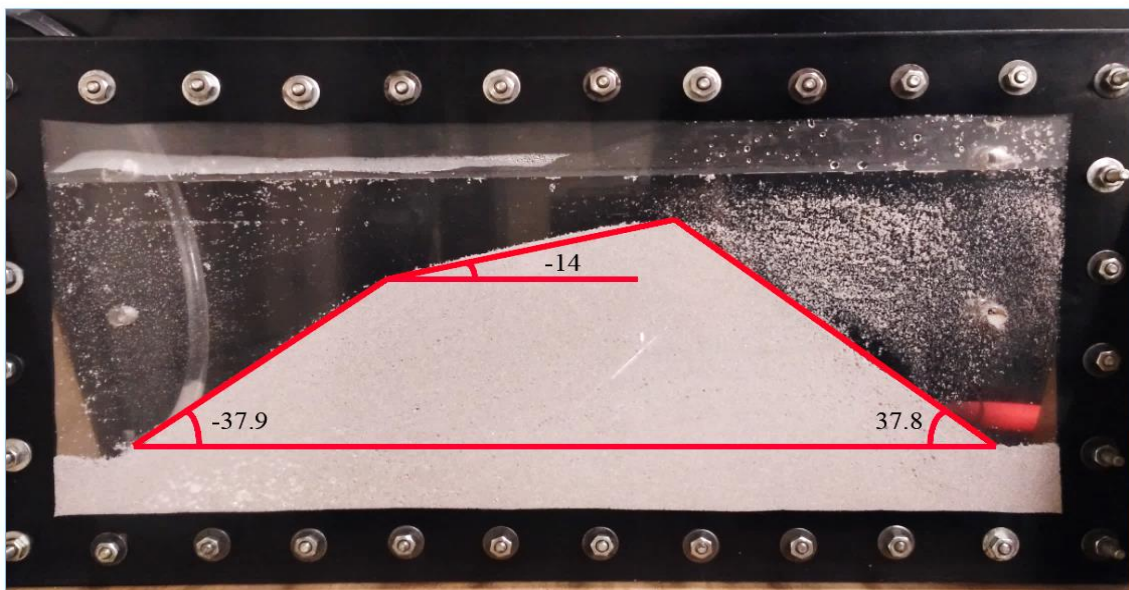
Figure 4.20 Angle measurements for the bottom inlet and a bottom outlet experiment (ceramic).
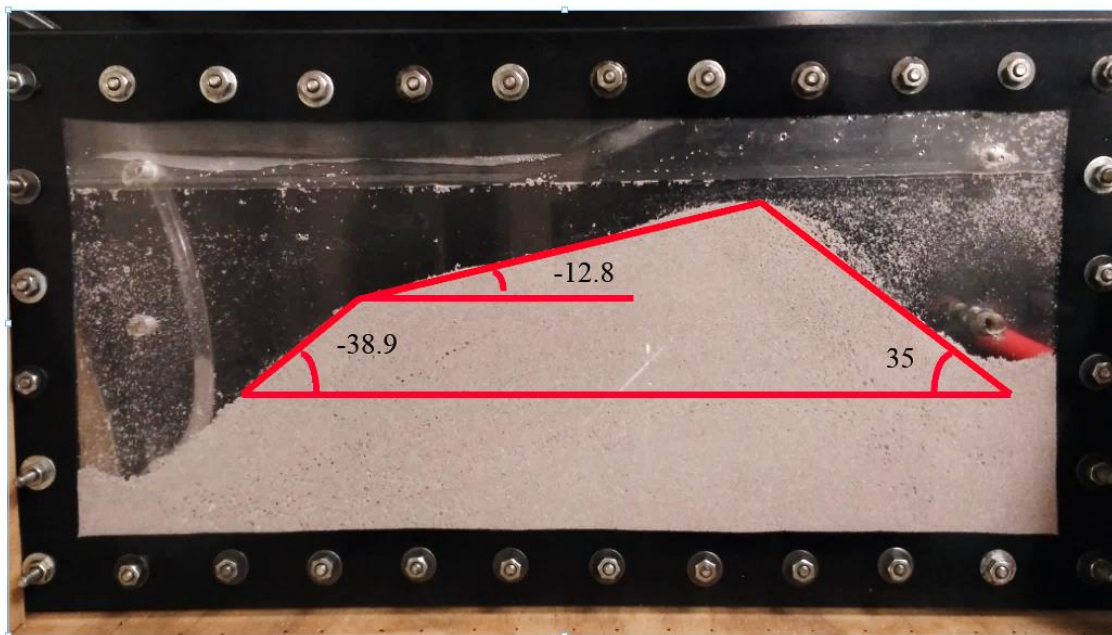
Figure 4.21 Angle measurements for the middle inlet and bottom outlet experiment (ceramic).
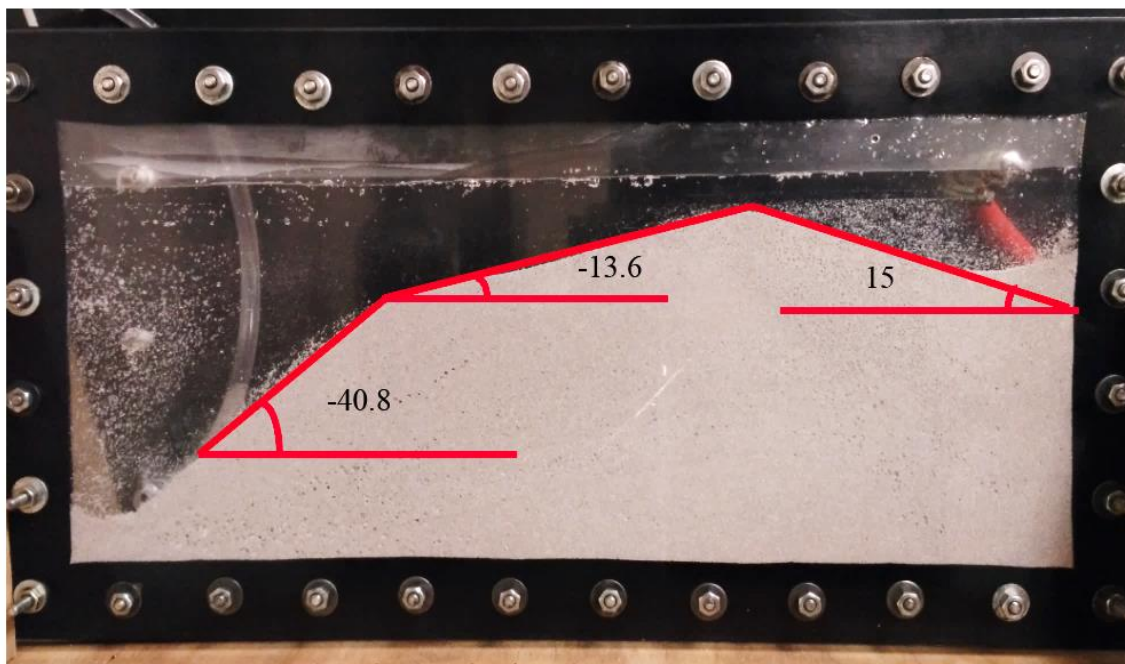
Figure 4.22 Angle measurements for the top inlet bottom outlet experiment (ceramic).

Table 4.5 Equilibrium dune angle measurement for bottom outlet fracture (ceramic proppant) with a single inlet.

Characteristics	Buildup angle	Dune angle	Drawdown angle
Top inlet	15	-13.6	-40.8
Middle inlet	35	-12.8	-38.9
Bottom inlet	37.8	-14	-37.9

According to different angles of the dune in different part of the dune, the dune was divided into distinct parts as shown in Figure 4.23 below.
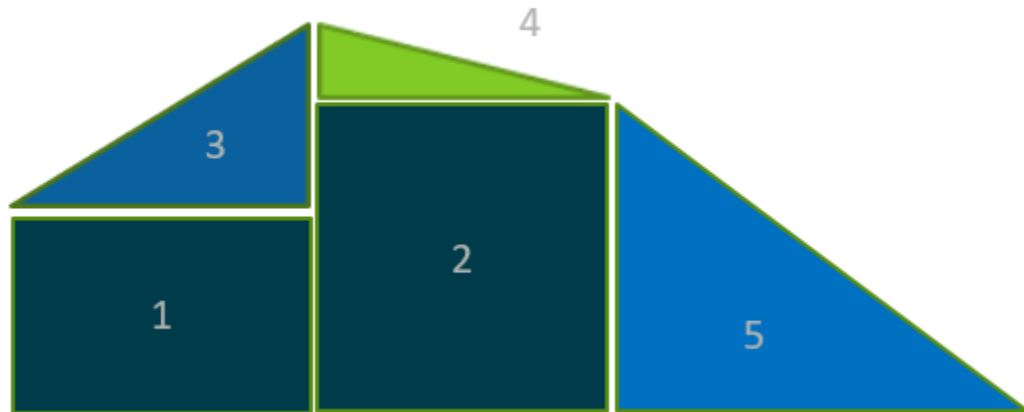
Figure 4.23 Dune divided in distinct parts.

Part one in Figure 4.23 above is formed due to the free settling of the proppant. From the experiments, it was observed that the height of this part depends on the inlet. As the height of the inlet increased, the height of part one also increased. As this part is formed by free settling of proppant, it is favorable to have this part larger.

The length of the second part of the dune represents EDX. This part of the dune is formed by saltation, rolling, suspension, and settling i.e. all of the transport mechanisms. After it is formed, proppant in this part remains unaffected form injected slurry. This part gives support to proppant dune and accounts for stable, long-term high permeability propped fracture.

The shape of part three of the dune is dependent on friction angle of the proppant. During the slurry injection, this part stays fluidized due to the turbulence of incoming slurry. When pumping is stopped, this fluidized proppant slurry settles down. This settling proppant is supported by its friction and buoyance force. For ceramic proppant, a friction

angle of 28^0 was observed in air by Mark Mack et al. (2014). From Table 4.4 it can be observed that the friction angle for ceramic proppant used in this study laid in range of 29^0 to 34^0.

In the top outlet fracture, part four of the dune was observed with positive slope in the range of 2^0 to 4^0, while the slope of the same part in propagating fracture was negative. For the bottom outlet fracture model dune angle laid in range of -12.5^0 to -16^0. This is due to active saltation of proppant dune. The slot flow model studied had fracture depth little more than twice the height. Due to this, the outlet of the fracture and low flowrate has a significant effect on the shape of the dune. The profound effect of the outlet (leak-off points) on dune shape was observed by Dhurgham et al. (2017) in their high leak-off model. These high values of dune angle reduce the area of the second part as well.

Part five of the dune is a pioneer for part two of the dune. As shown in Figure 4.24, when the dune propagates deeper in the fracture, size of part two grows. As more incoming proppant settles in this part, previously settled proppant become part of the immobile dune and increases EDX of the dune. In Figure 4.24 , the green shaded portion is part two of the dune for 7th FPV injected while at equilibrium i.e. after 8 and $1/3^{rd}$ FPV injection we can clearly see a larger size of part two.

The shape of this part depends on friction angle of proppant as well as the fluid movement after stopping pumping. If no further dune is developing i.e. in the case of a fracture with a top outlet, angle ranges -29.7^0 to -30.3^0 for ceramic proppant during this research. While for the fracture with bottom outlet, these angles were in the range of -38^0 to -41^0.
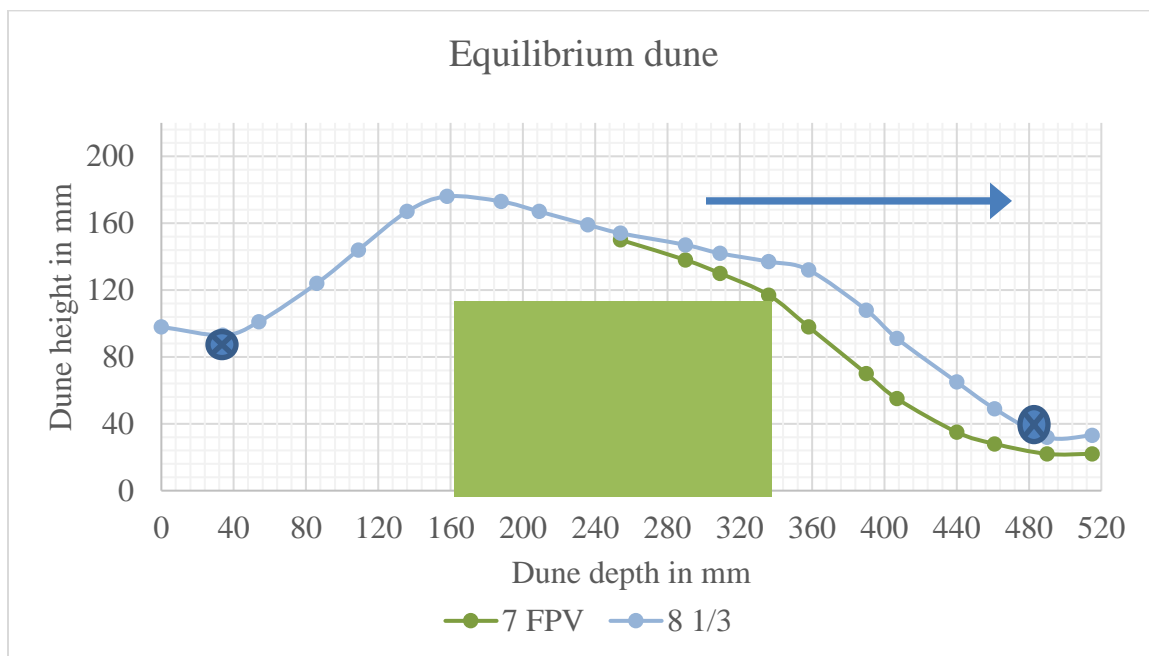
Figure 4.24 Changing dune from 7th FPV to equilibrium for middle inlet, ceramic proppant, bottom outlet.

Even after equilibrium is achieved, part three, four and five of the dune keep on changing. The shape did not change but the saltation, suspension, and rolling of the proppant change the proppant position in other words new incoming proppant replaced the existing proppant bed while keeping the shape of the dune same.

In Figure 4.25 the equilibrium dune of a fracture with a top outlet and a fracture with a bottom outlet is compared. A significant difference in EDL and EDX can be observed. The shape of the dune near the injection point is similar but the later portion of the dune is strongly driven by the location of the outlet.
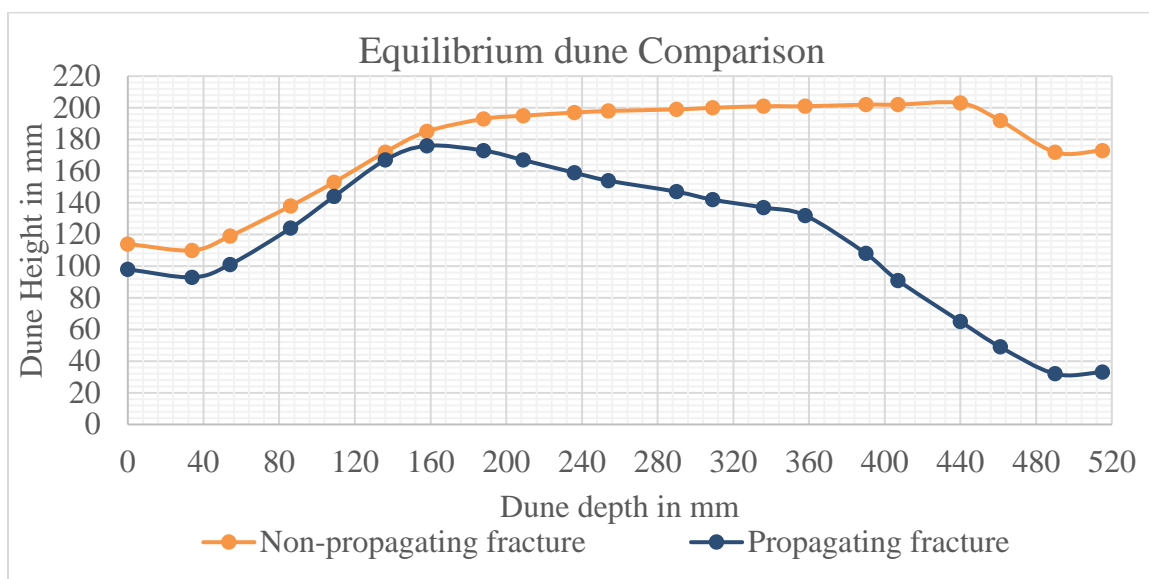
Figure 4.25 Equilibrium dune comparison for a fracture with a bottom outlet and a fracture with a top outlet (ceramic).

4.1.1.6 Single perforation experiment observations. Due to the difference in height of the perforation, proppant particles have a different time to settle in the fracture. This resulted in different shape of proppant dune. In Figure 4.26 , it can be observed that the greater settling time for the proppant helps push the proppant deeper in the fracture. Most of the proppant settles very near to the inlet for bottom injection and forms a hill like a small triangular dune. These results also indicate injecting from bottom inlet can lead to early saltation of proppant. Due to the proppant settling near the inlet, incoming slurry accumulates and may create back pressure in case of bottom inlet compared to middle and top inlet cases

As mentioned previously four main types of proppant transport mechanism include settling, rolling, suspension, and saltation. Settling of proppant applies little to no back
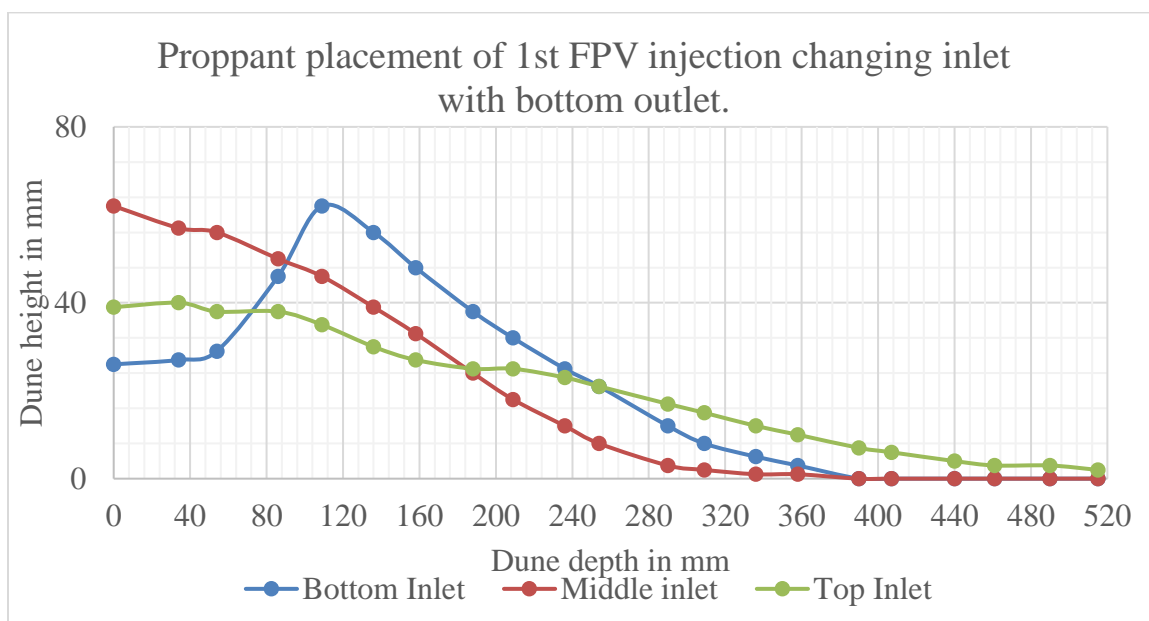
Figure 4.26 Effect of inlet height on proppant placement for first FPV (ceramic).

pressure while saltation imposes highest back pressure due to frictional drag. These results suggest active perforation higher into the fracture can start and progress proppant transport in the fracture with ease as most of the injection follows proppant settling.

4.1.1.7 Proppant passage channels. Proppant passage channels represent the area for incoming slurry above the dune and till the fracture upper boundary. Its significance for proppant transport further into the fracture is discussed in this section. The slot-flow model used in this study had the height to depth ratio of 1:2. But from field data, it is known that the fractures are generally deeper than the selected model with height to depth ratio as high as 1:20 or more.

As proppant dune rises in the fracture, area of slurry passage decreases. Due to this, proppant velocity inside fracture increases. This is favorable for proppant transport as it increases turbulence in the fluid which helps proppant in suspension for a longer time. But

for bottom inlet, increasing dune creates problems. As shown in Figure 4.27, proppant starts accumulating over the inlet and blocks the perforation which creates backpressure for the incoming slurry. When this occurs, injected proppant now travels upwards against the gravitational force to cross over proppant dune and move deeper in the fracture. Due to this movement, proppant slurry loses its kinetic energy. These two forces increase the chance of early screen-out. The red circle shows saltation form edges due to fluid present. We can observe saltation and suspension in all three cases shown below in Figure 4.27, Figure 4.28, and Figure 4.29.

Figure 4.27 Proppant movement path for bottom inlet equilibrium dune with a bottom outlet fracture condition (ceramic).

In case of the middle inlet, blocking of the inlet is reduced compared to the bottom inlet but vertical movement is still necessary for proppant to move deeper into the fracture. Compared to the bottom inlet case, the backpressure exerted on slurry is less. Figure 4.28 shows entering proppant creating turbulence at the inlet and moving towards the top of the fracture at the same time saltation and suspension occurring from top of the dune. As mentioned earlier in Table 4.1 and Table 4.3, the dune formed with middle inlet has higher EDL then the dune for the bottom inlet, as well as more proppant surface area. This creates higher velocity for proppant in the middle inlet fracture compared to the bottom inlet. So, deeper proppant penetration in the fracture can be expected compared to the bottom inlet. We can also see fluidized proppant bed throughout the proppant dune.
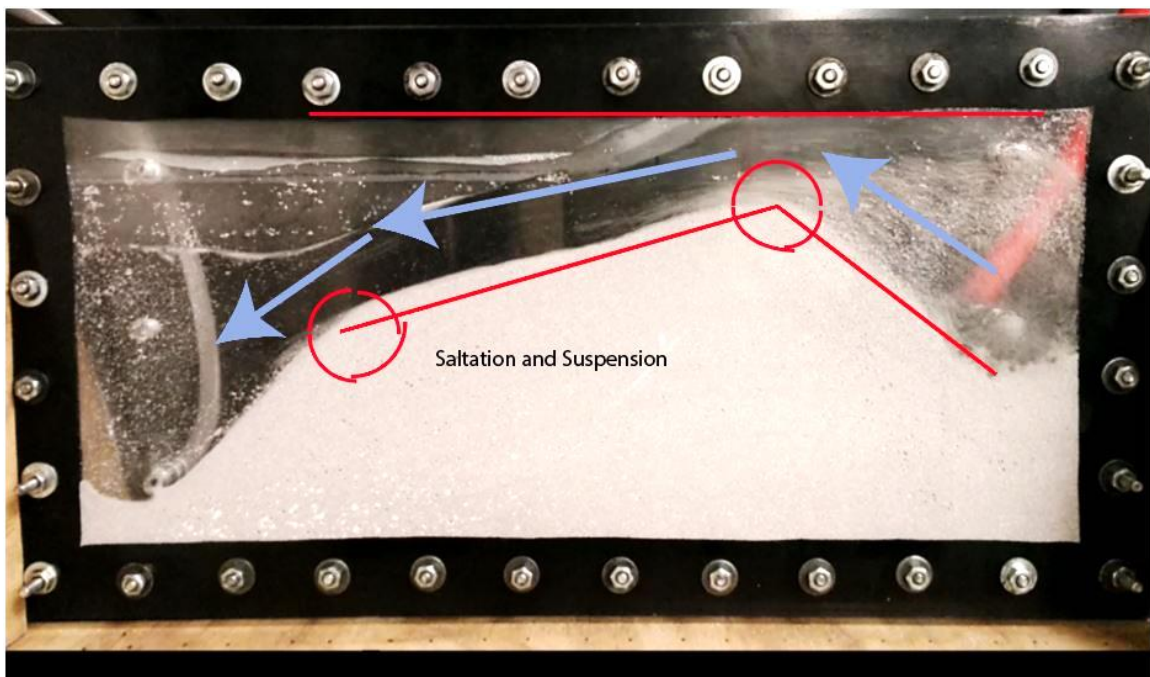
Figure 4.28 Proppant movement path for middle inlet equilibrium dune with a bottom outlet fracture condition (ceramic).

For the case of the top inlet, proppant slurry entering the fracture already is higher than dune at equilibrium. Due to this slurry entering from top inlet feels no backpressure from proppant covering the inlet as well as entering slurry doesn't have to flow up against gravitational force. Due to high EDL and more proppant placed, proppant in the fracture with top inlet has the highest velocity compared to either the middle or bottom inlet positions. Figure 4.29 shows injecting slurry from the top, its flow channel and fluidized bed due to the high-velocity slurry.

The area marked between red lines represents proppant passage channel. Smaller passage channel offers higher proppant velocity in the fracture which is favorable for deeper proppant injection
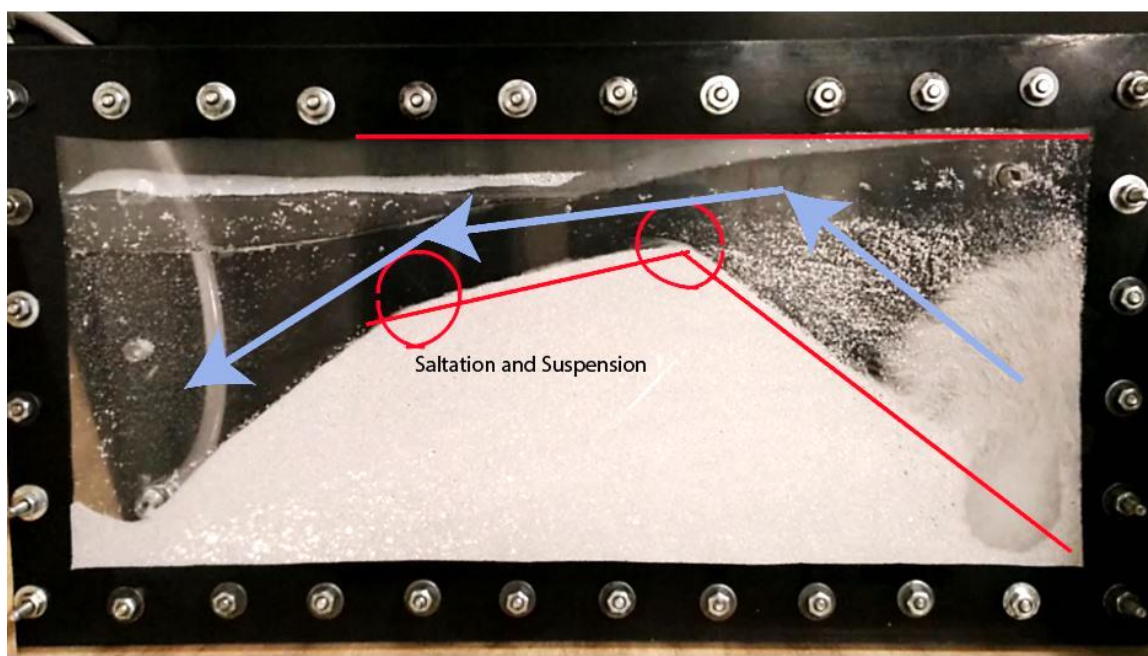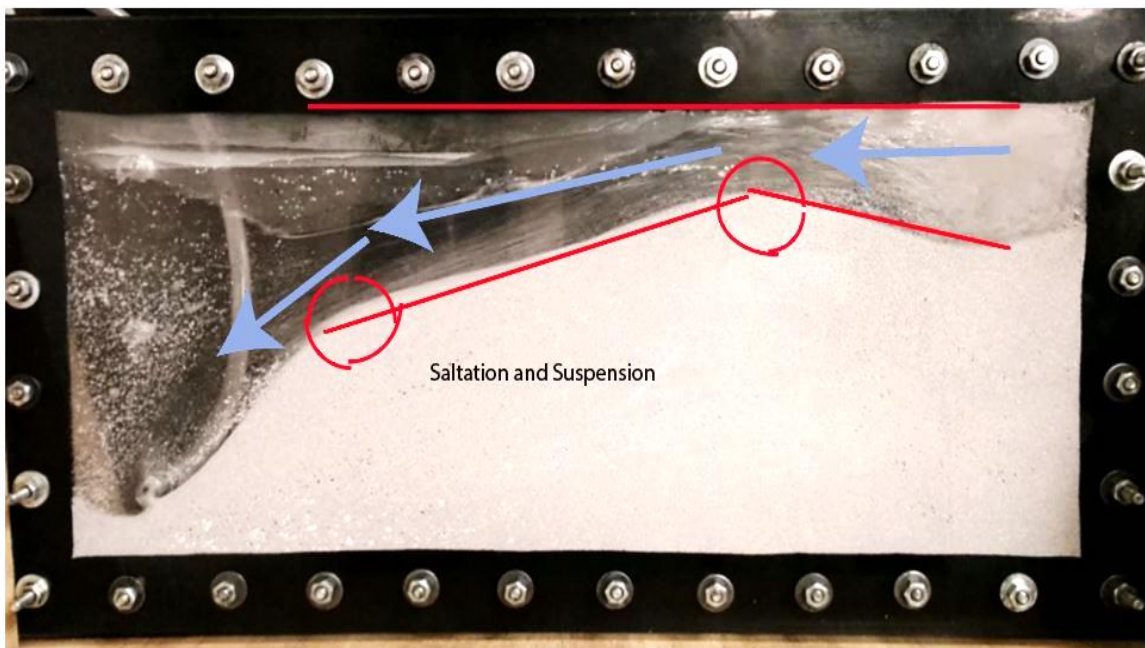

Figure 4.29 Proppant movement path for top inlet equilibrium dune with bottom outlet fracture condition (ceramic).

The areas of the proppant passage channels are given in Table 4.6. For dunes at a depth of 336mm, it can be observed that the area of proppant passage channel for top inlet is half as higher as that of bottom inlet. From flow velocity to area relation for non-compressible fluid and non-frictional flowing condition,

$$A_1 V_1 = A_2 V_2 \ .$$

(20)

It can be inferred that the injecting slurry from top inlet would have two times the velocity compared to the bottom inlet. Friction cannot be neglected for real-life calculations, but slurry entering for top inlet would still have significantly higher velocity compare to slurry entering from the bottom inlet. The proppant dune depths of 209 mm and 336 mm were selected to randomly to compare the results.

Table 4.6 Area of proppant channel of three cases of a fracture with bottom outlet till two different dune depths (ceramic).

Injection	Area of Proppant passage channel till 209 mm	Area of Proppant passage channel till 336 mm
Bottom inlet	26640 mm^2	35145.5 mm^2
Middle inlet	17543.5 mm^2	26462.5 mm^2
Top inlet	10523.5 mm^2	18926 mm^2

4.1.2. Multiple Injection Perforation. Two different experiments were performed with different fracture condition and compared with respective base cases with a single inlet. These new cases include multiple injection points with simultaneous injection. One case evaluated is when there is injection at both the top and the middle points. The other case assumes simultaneous injection through all three points. Figure 4.30 and Figure 4.31 show the dune development of these cases. Blue dots in the figures represent approximate location of inlet and outlets from the slot-flow model.

4.1.2.1 Dual injection. The model was constructed as shown in earlier section with a top outlet fracture condition and experiment was conducted with the same amount of pressure for nitrogen cylinder to achieve similar flowrate as that of the earlier experiments with single perforation. Figure 4.30 shows dune after different injected FPV for dual injection model.

4.1.2.2 Triple injection. This model was constructed as shown earlier with three inlet points for injection. The same amount of pressure was used in the nitrogen cylinder to achieve a similar flowrate as that of the single point injection experiments. Figure 4.31 shows dune after different injected FPV for triple injection point model. Table 4.7 lists the EDL and EDX data gathered as shown in earlier section for both of the cases of multiple injection models.

FPV needed for proppant to reach the end of the fracture is considerably high because of reduced effective flowrate in the fracture that is due to gravity separation of water and proppant slurry in the injection pipes. As observed during the experiments most of the proppant slurry injected from lower active inlet while a small amount of separated
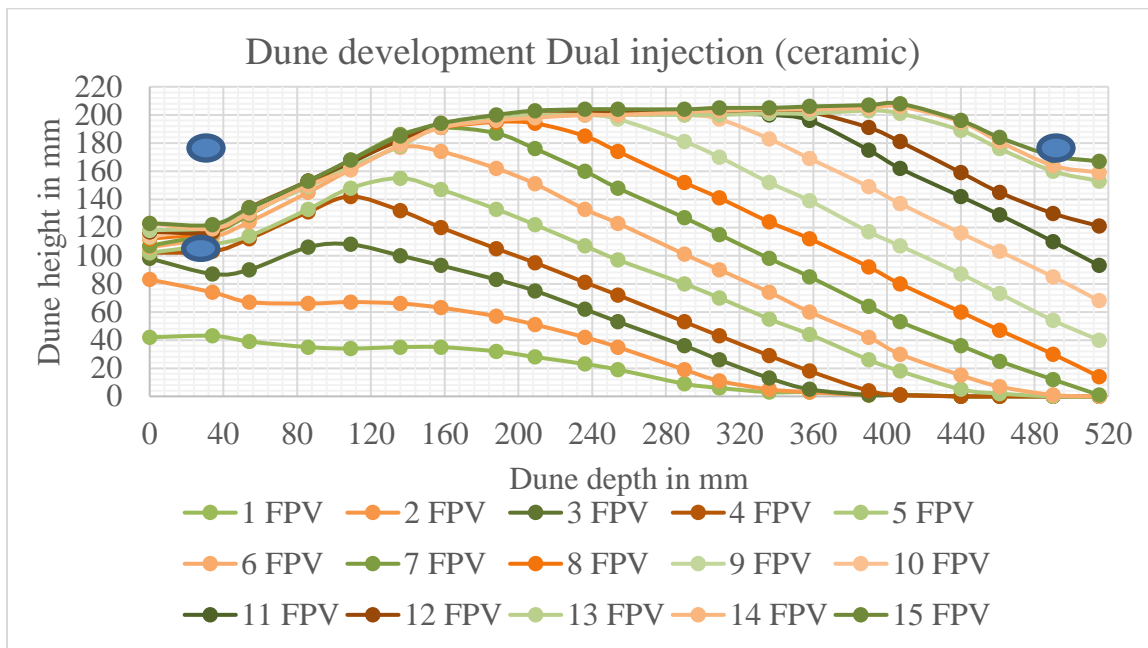
Figure 4.30 Dune development for dual (top + middle) inlet in a fracture with a top outlet (ceramic).
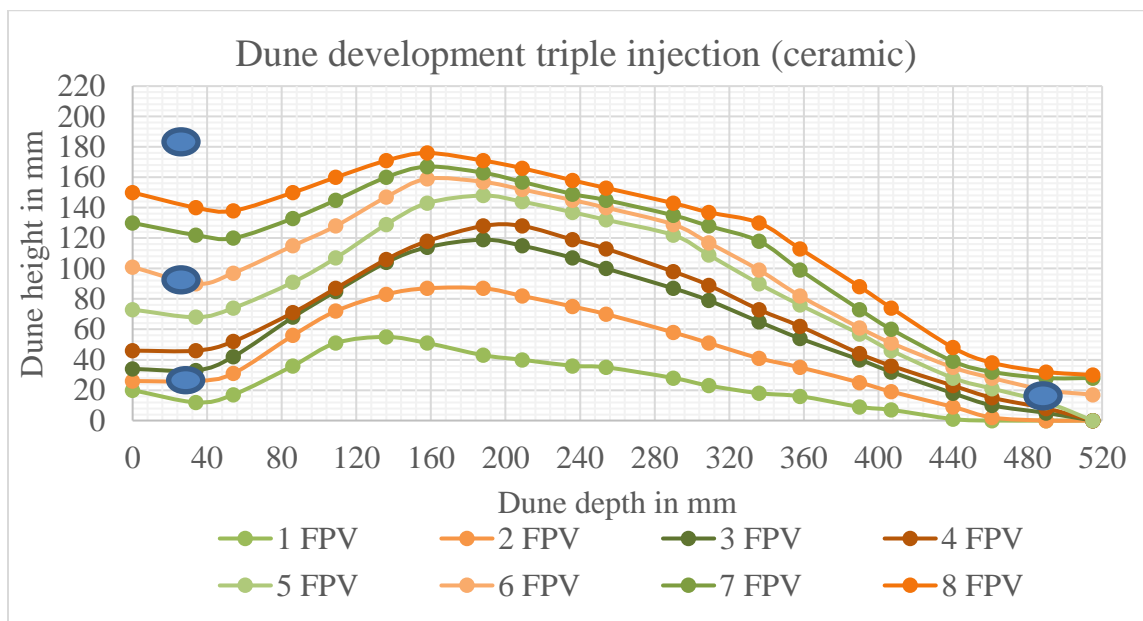
Figure 4.31 Dune development for triple (top + middle + bottom) inlet in a fracture with a bottom outlet (ceramic).

water entered the fracture from remaining inlets. For the dual inlet model, it took 7 FPV for proppant to reach the end of the fracture and for triple inlet model, it took 6 FPV to reach the end of the fracture. Which is compared to different single injection models in Figure 4.32, and Figure 4.33.
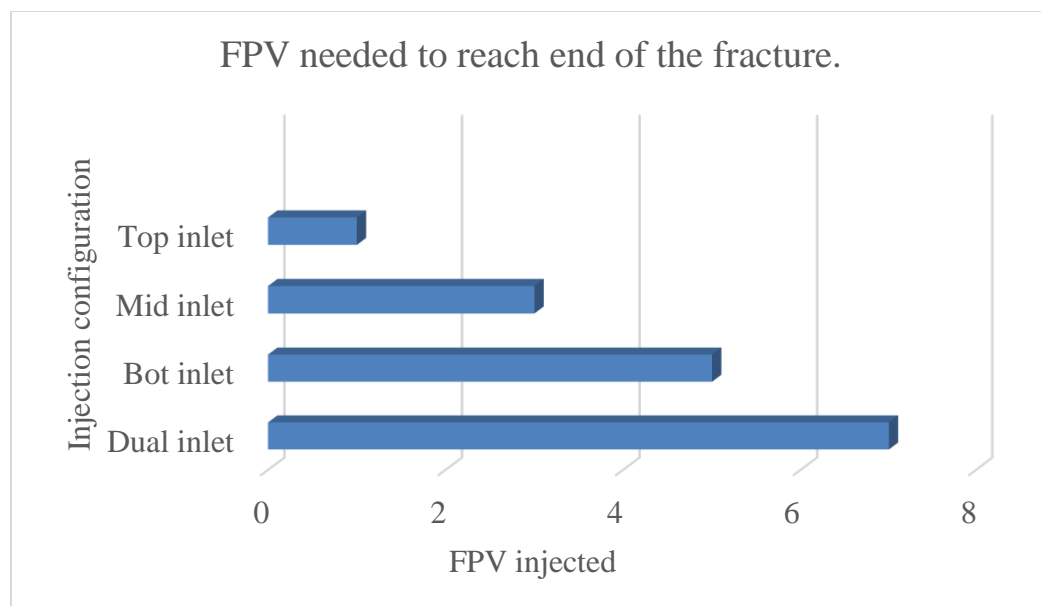
Figure 4.32 FPV needed to reach the end of the fracture for a fracture with a top outlet (ceramic).

4.1.2.3 EDL and EDX. Table 4.7 shows EDL and EDX data for multiple injection experiments. From these data, we can observe that EDL and EDX of multiple injection dunes resemble the single injection model with middle inlet experiment of similar fracture condition.
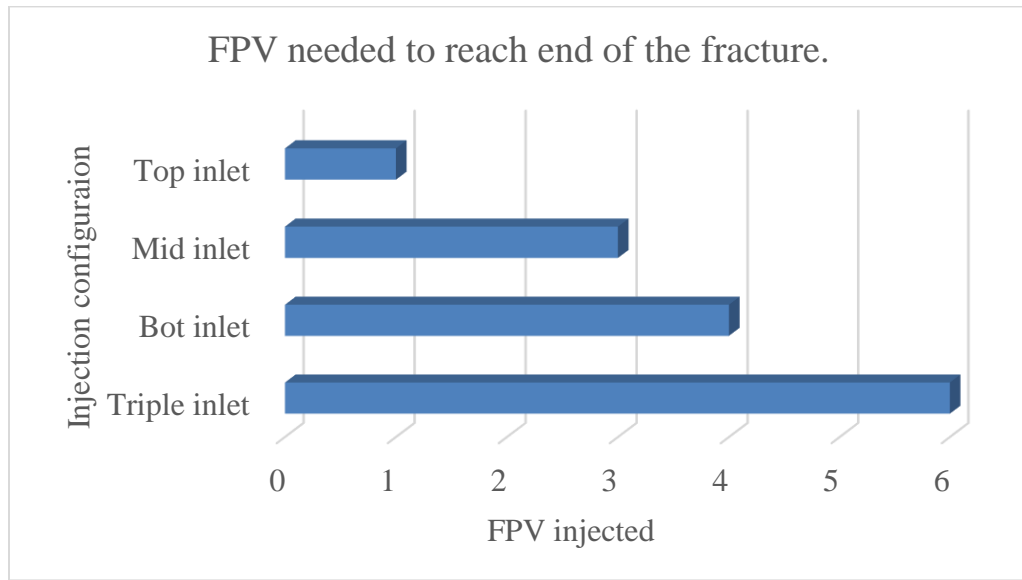
Figure 4.33 FPV needed to reach the end of the fracture for a fracture with a bottom outlet (ceramic).

Table 4.7 EDL and EDX for multiple injection fracture model (ceramic).

Proppant	Fracture condition	Injection perforation position	EDL (%)	EDX (%)
Ceramic	Top outlet	Dual (Top + Middle)	94	47.7
Ceramic	Bottom outlet	Triple (Top + Middle + Bottom)	79.6	37.9

4.1.2.4 Surface area. The surface area of these two dunes was also measured with the technique shown previously. The graphical dune was divided into small parts and area of these small parts were calculated and summed up to find overall area. The dune was divided into small parts as shown in Figure 4.34, and Figure 4.35.

The area of these parts is summarized in Table 4.8 and total area, and area fraction covered by proppant are given in Table 4.9. It can be observed that the total surface area covered by proppant is higher than that of single perforation with the bottom and middle inlet but less than top injection with same fracture condition.
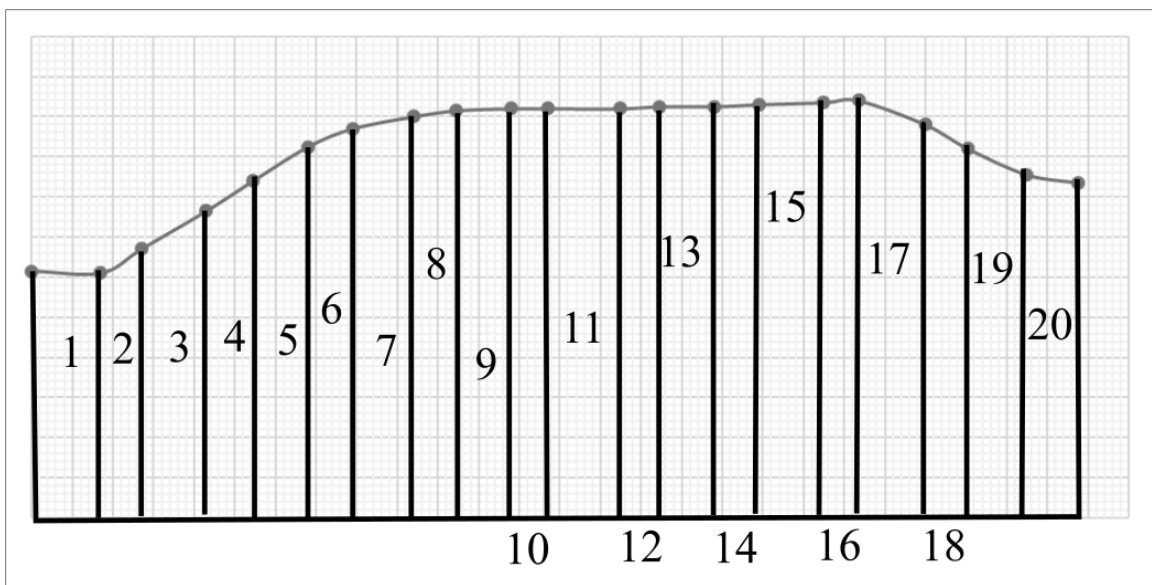
Figure 4.34 Area division of equilibrium dune for a middle inlet in the fracture with a top outlet (ceramic).

4.1.2.5 Dune angle comparison. Angles of various parts of the dune were measured using excel as previously described. The angles determined from the experiments are shown in Figure 4.36, Figure 4.37, and summarized in Table 4.10
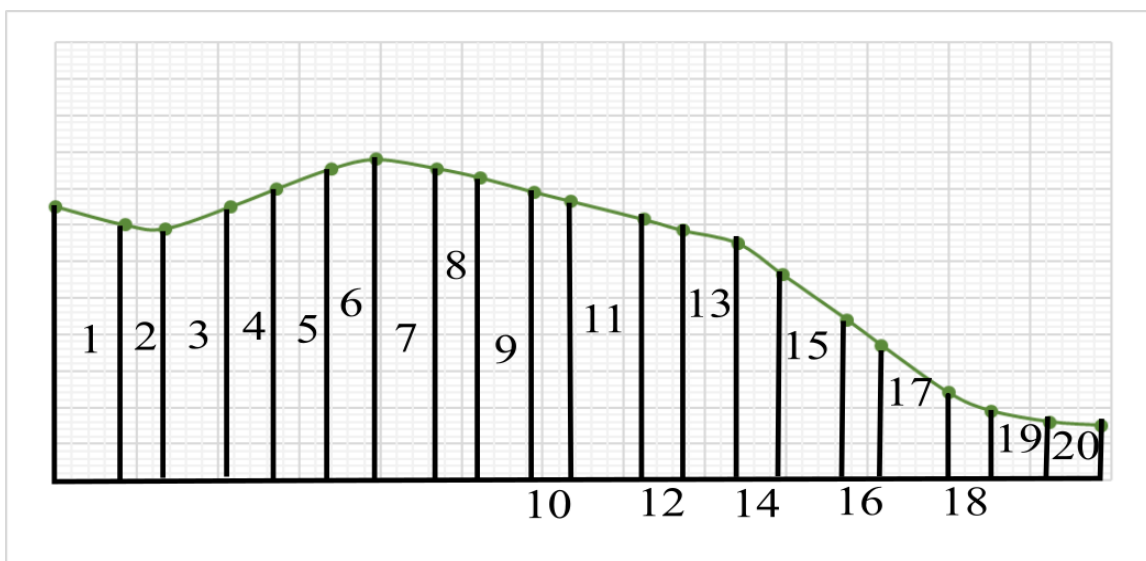
Figure 4.35 Area division of equilibrium dune for a bottom inlet in the fracture with a bottom outlet (ceramic).

Table 4.8 Part-vice area of equilibrium dune for multiple perforation (ceramic).

Fracture condition	Dual injection with top outlet fracture model	Triple injection with bottom outlet fracture model
Area of Part 1	4165	4930
Area of Part 2	2560	2800
Area of Part 3	4592	4640
Area of Part 4	3691.5	3588
Area of Part 5	4765.5	4482
Area of Part 6	4169	3817
Area of Part 7	5910	5205
Area of Part 8	4231.5	3538.5
Area of Part 9	5494.5	4374
Area of Part 10	3672	2808
Area of Part 11	7344	5364
Area of Part 12	3885.5	2688.5
Area of Part 13	5535	3672
Area of Part 14	4521	2871
Area of Part 15	6608	3712
Area of Part 16	3527.5	1623.5
Area of Part 17	6666	2442

Table 4.8 Part-vice area of equilibrium dune for multiple perforation (ceramic). (cont.)

Fracture condition	Dual injection with top outlet fracture model	Triple injection with bottom outlet fracture model
Area of Part 18	3990	1113
Area of Part 19	5147.5	1116.5
Area of Part 20	4225	775

Table 4.9 Surface area embedded by proppant dune for multiple inlets (ceramic).

Proppant	Fracture condition	Injection perforation position	Surface area(mm^2)	Surface area fraction
Ceramic	Top outlet	Dual (Top + Middle)	94700	0.82
Ceramic	Bottom outlet	Triple (Top + Middle + Bottom)	65560	0.57
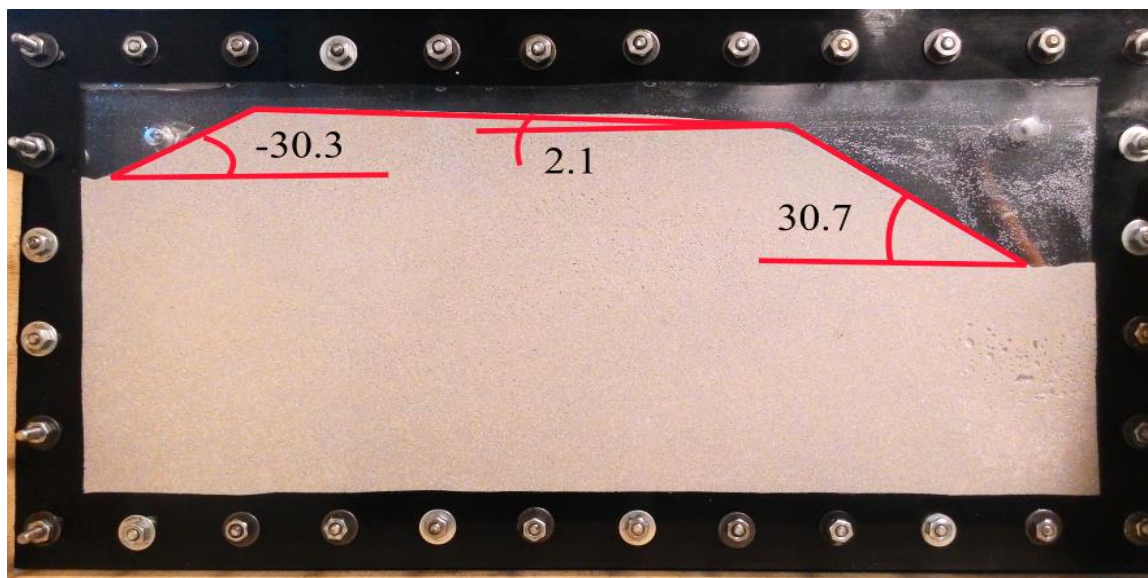
Figure 4.36 Angle measurements for dual inlet and a top outlet fracture model (ceramic).

Table 4.10 Multiple injection equilibrium dune angle measurements (ceramic).

Characteristics	Buildup angle	Dune angle	Drawdown angle
Dual inlet	30.7	2.1	-30.3
Triple inlet	20.5	-15.8	-38.5
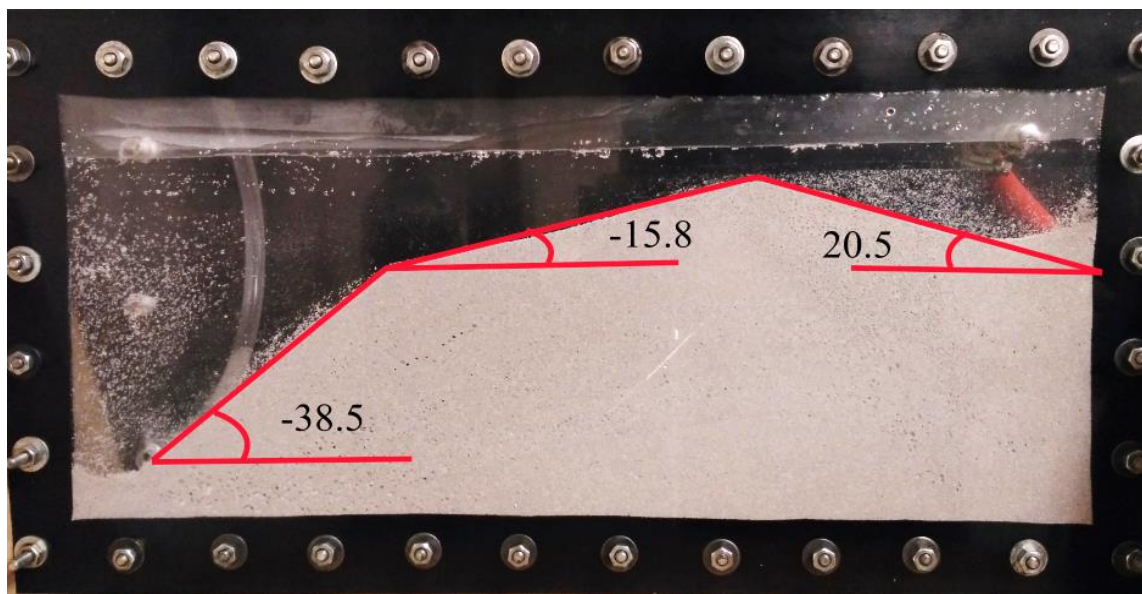
Figure 4.37 Angle measurements for triple inlet and a bottom outlet fracture model (ceramic).

4.1.2.6 Multiple perforation experiment observations. The effect of gravity separation was observed during the experiments, which changed apparent proppant concentration and proppant particle velocity of the injected slurry. In the dual injection point case, the middle inlet resulted in higher proppant concentration injected with lower effective flowrate. The propped surface area of the model was increased compared to the

single middle injection experiment. So, it can be inferred that the dune development depends on proppant particle velocity or particle Reynold's number rather than simply on injection flowrate.

A similar observation was made for triple injection. Initially, most of the proppant slurry was injected from the bottom inlet and a small amount of water was injected from the middle and the top inlet. But due to low apparent flowrate, proppant gradually blocked bottom inlet and slurry started flowing from middle inlet as well. After 7th FPV injected bottom inlet was completely blocked and bottom inlet didn't interact with fracture anymore. Figure 4.38 b) shows 8th FPV injection with completely covered bottom inlet with proppant and 5th FPV injection of dual inlet is shown in Figure 4.38 Figure 4.38a).
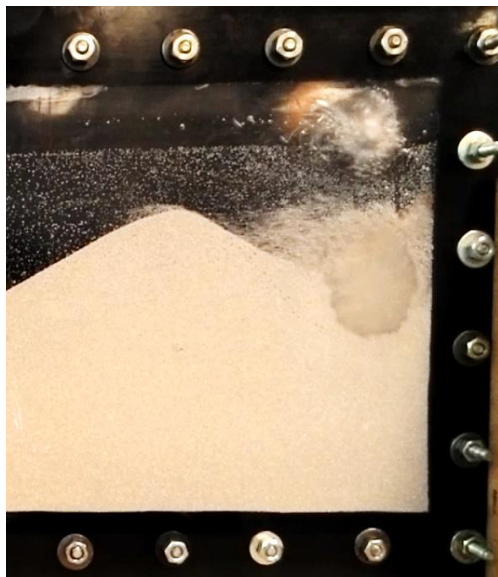
a)   b)

Figure 4.38 Still photos a) Dual inlet 5th FPV injection b) Triple inlet 7th FPV injection.

4.1.3. Dune Comparison. When the multiple injection point data were compared to single injection, it can be observed that results from the multipoint dunes are closest to the dune formed with middle inlet with similar fracture condition but with a higher surface area. EDL is almost same but EDX was observed to be dropping slightly for multiple injection models when compared with middle inlet model.

Figure 4.39 and Figure 4.40 shows the comparison for equilibrium dune of different experiments with the similar fracture end-side condition, i.e. a top outlet or a bottom outlet fracture. As it can be observed that the shape of the overall dune is dependent on inlet height and also on the outlet position. The shape of the dune with same fracture condition looks slightly similar with a slight change in maximum height (i.e. EDL) and stable dune length (i.e. EDX).
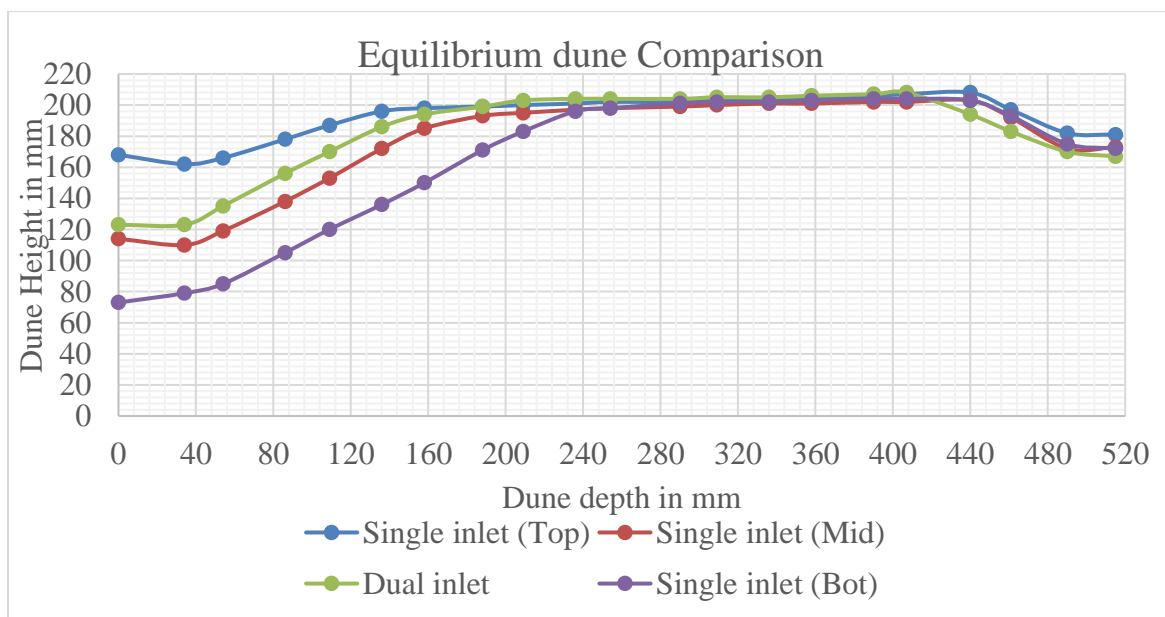
Figure 4.39 Equilibrium dune comparison for a fracture with a top outlet (ceramic).

4.2. ANGULARITY RESULTS

This effect of proppant angularity was studied by the comparing dune development of ceramic proppant with sand proppant in a fracture with bottom outlet condition. Sand proppant is typically more angular as it is obtained from mining sand deposits, whereas ceramic proppant is manufactured and typically more rounded. Figure 4.41 shows a magnified photo of ceramic proppant and sand used during this study.
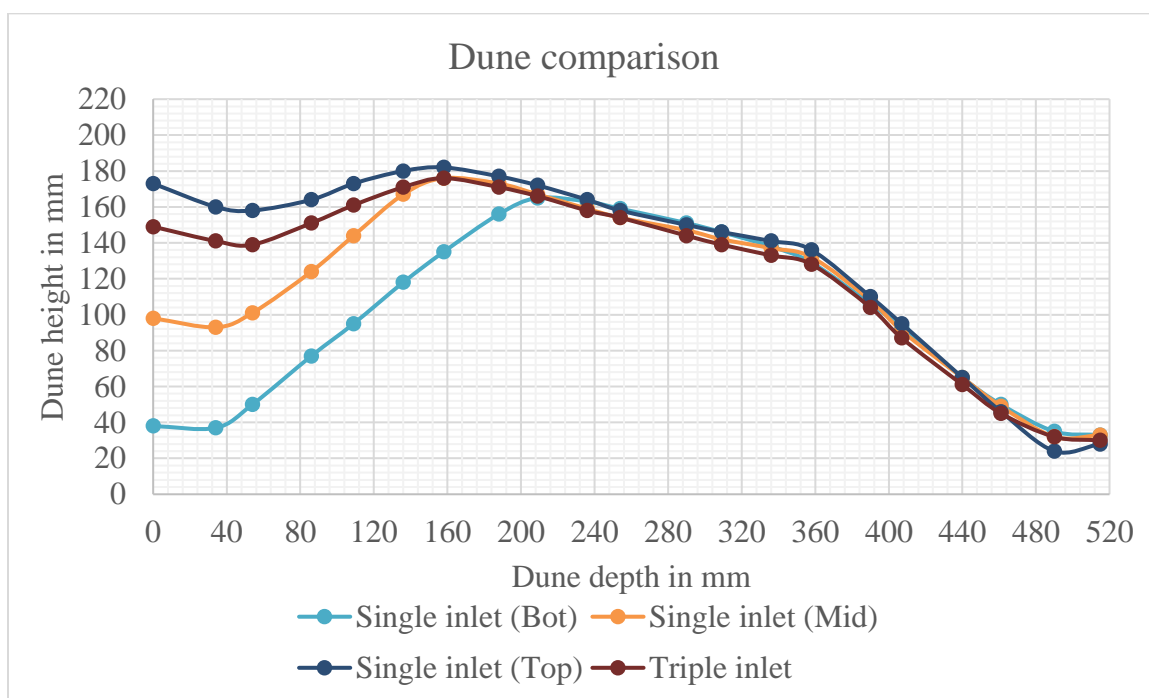
Figure 4.40 Equilibrium dune comparison for a fracture with a bottom outlet (ceramic).

4.2.1. Sand Results. In this section, results for the experiments conducted using sand proppant are presented in similar manner as earlier sections.

a)   b)
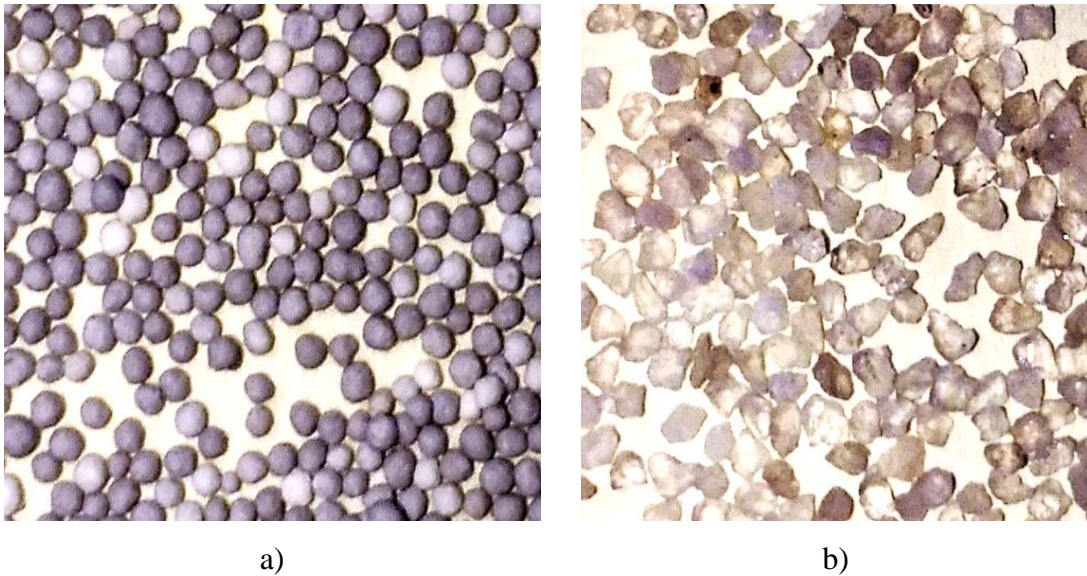
Figure 4.41 A magnified view of proppant particles a) ceramic b) brown sand.

4.2.1.1 Sand dune. Single point injection experiments for top, middle, and bottom injection points were repeated using sand, as proppant. Figure 4.42 show graphical results for a single bottom injection point. Graphs of the dunes were drawn and analyzed for these experiments as described previously, to understand dune development when injecting sand.

4.2.1.2 EDL and EDX. Table 4.11 summarizes EDL and EDX for single injection points using sand as proppant. A high EDL was observed compared to ceramic to a fracture with a bottom outlet condition. EDL was observed increasing slightly with increasing height of perforation while EDX increased 10% between the bottom and middle injection points. There was no change in EDX observed for the middle and the top injection experiments.
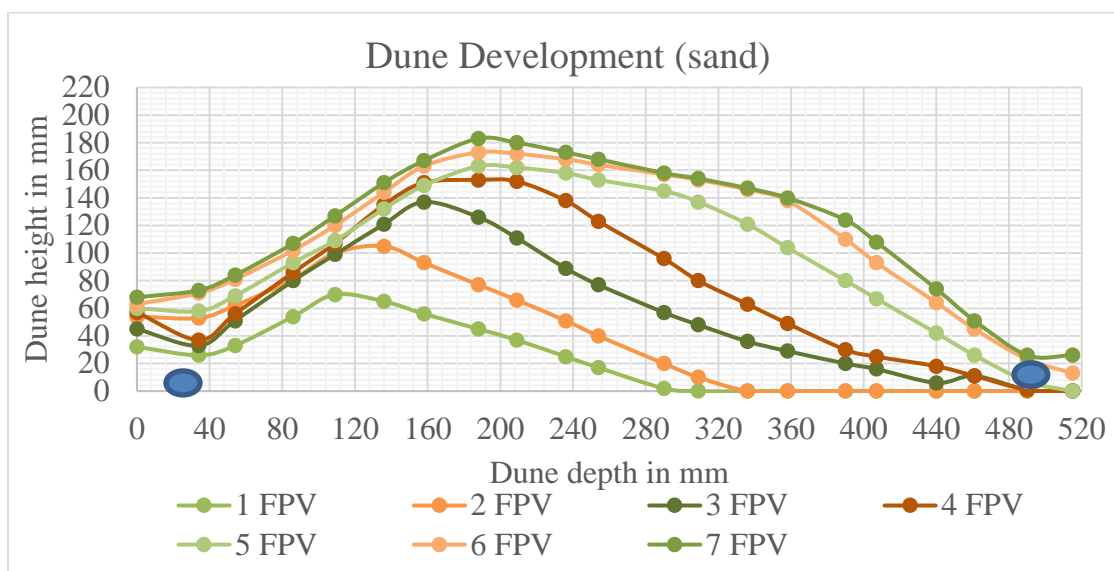
Figure 4.42 Dune development for bottom inlet in the fracture with a bottom outlet (sand).

Table 4.11 EDL and EDX for the fracture with bottom outlet and sand proppant.

Proppant	Fracture condition	Injection Height Fraction	EDL (%)	EDX (%)
Sand	Bottom outlet	0.125 (Bottom inlet)	82.8	38.7
		0.5 (Middle inlet)	85.5	48.7
		0.875 (Top inlet)	88.2	48.7

4.2.1.3 Surface area. The fracture surface area of propped fracture created with sand is shown in Table 4.13. Due to sand's angularity (shown in Figure 4.41), sand resists rolling more compare than ceramic proppant while flowing. Sand has a greater coefficient of friction due to its angularity as well. High angular dune with more sand retained in the fracture model was observed. The propped fracture surface area was calculated using

method mentioned earlier. The equilibrium dune was divided into twenty parts as shown below in Figure 4.43, Figure 4.44, and Figure 4.45 and measured using trapezoidal area calculation. The measured areas are listed in Table 4.12.

Figure 4.46 shows a graph of these results. A linear trend was observed for the increase in the surface area of settled sand proppant, similar to results obtained for ceramic proppant in the experiments. Sand covered fracture surface area increased from about 53% to about 59% when changing inlet from bottom to middle. Another 5% increase was also observed for top inlet compared to the middle inlet in proppant dune surface area. The linear trend regression analysis indicated R^2 more than 0.99 as shown in Figure 4.46.
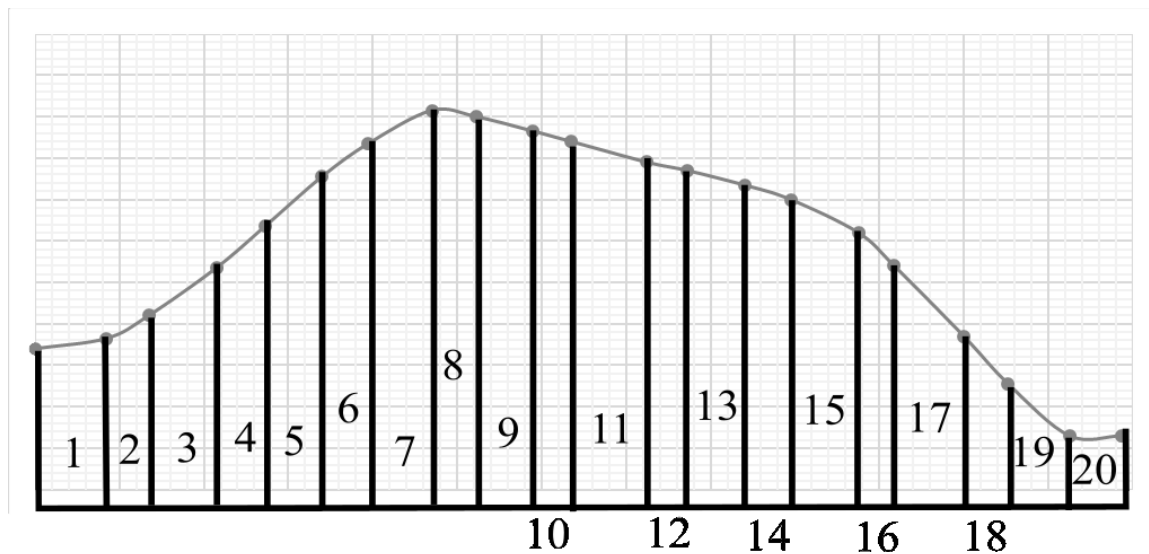
Figure 4.43 Area division of equilibrium dune for a bottom inlet in the fracture with a bottom outlet (sand).
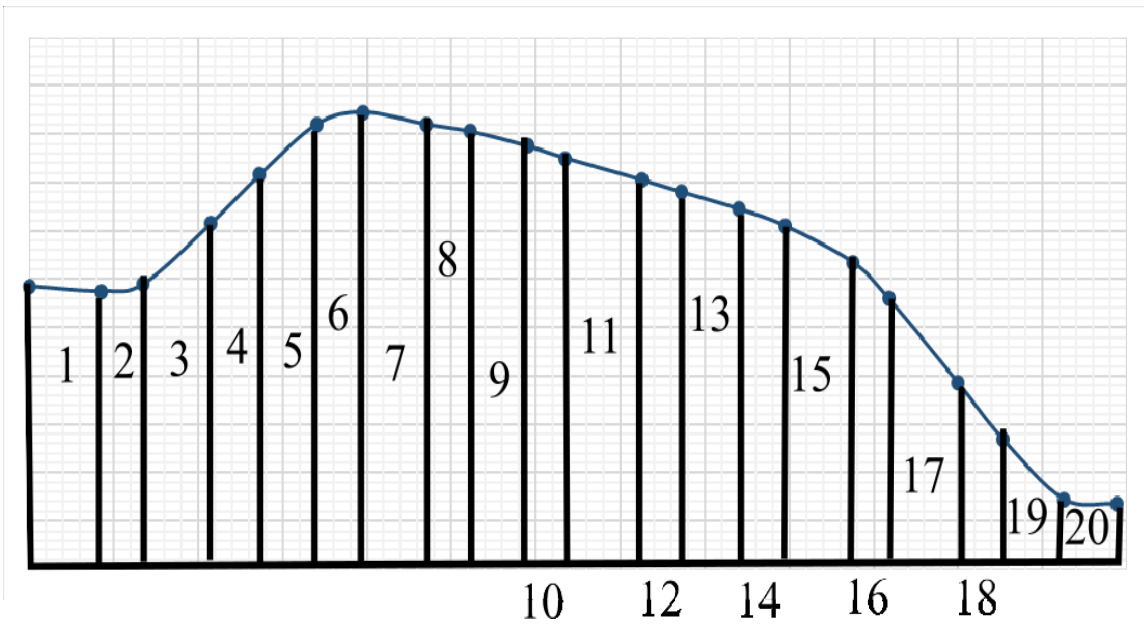
Figure 4.44 Area division of equilibrium dune for a bottom inlet in the fracture with a bottom outlet (sand).
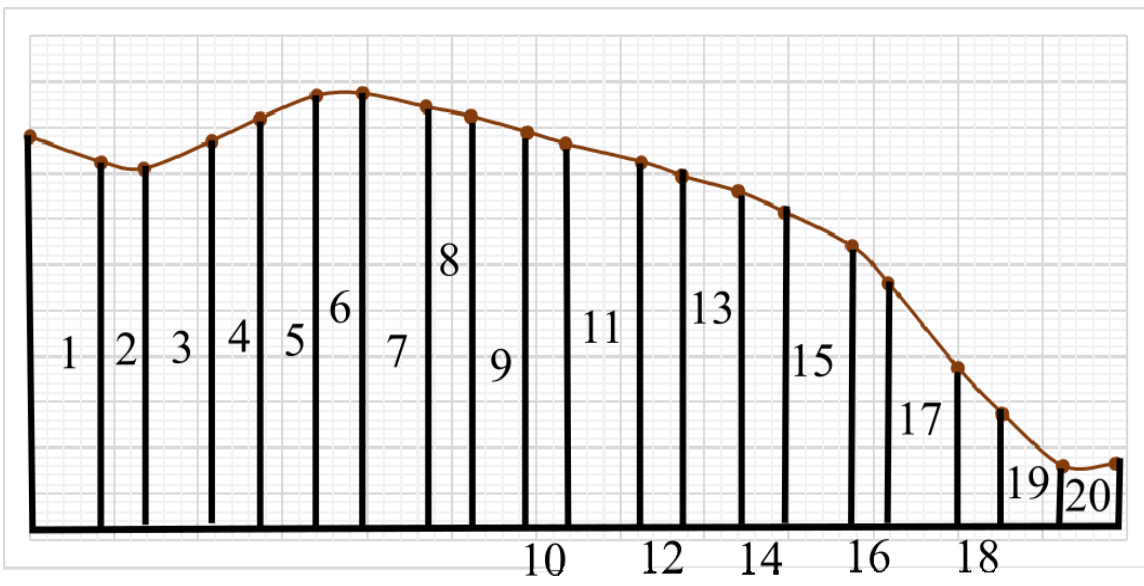
Figure 4.45 Area division of equilibrium dune for a bottom inlet in the fracture with a bottom outlet with a bottom outlet (sand).

Table 4.12 Part-vice area of equilibrium dune for single perforation experiments (sand).

Fracture condition	Fracture with bottom outlet		
Inlet	Bottom	Middle	Top
Area of Part 1	2397	3944	5797
Area of Part 2	1570	2330	3270
Area of Part 3	3056	4176	5376
Area of Part 4	2691	3519	4117
Area of Part 5	3753	4684.5	5103
Area of Part 6	3498	4103	4279
Area of Part 7	5250	5595	5760
Area of Part 8	3811.5	3832.5	3927
Area of Part 9	4765.5	4806	4900.5
Area of Part 10	3069	3105	3159
Area of Part 11	5868	5958	6084
Area of Part 12	2964	3011.5	3078
Area of Part 13	4063.5	4117.5	4198.5
Area of Part 14	3157	3201	3245
Area of Part 15	4224	4304	4336
Area of Part 16	1972	2031.5	2040
Area of Part 17	3003	3118.5	3085.5
Area of Part 18	1312.5	1375.5	1365
Area of Part 19	1116.5	1203.5	1261.5
Area of Part 20	650	700	812.5

Table 4.13 Surface area and surface area fraction for sand proppant in fracture with bottom outlet.

Proppant	Fracture condition	Injection Height Fraction	Surface Area(mm^2)	Surface Area Fraction
Sand	bottom outlet	0.25	62191.5	0.54
		0.5	69116	0.60
		0.75	75194.5	0.65
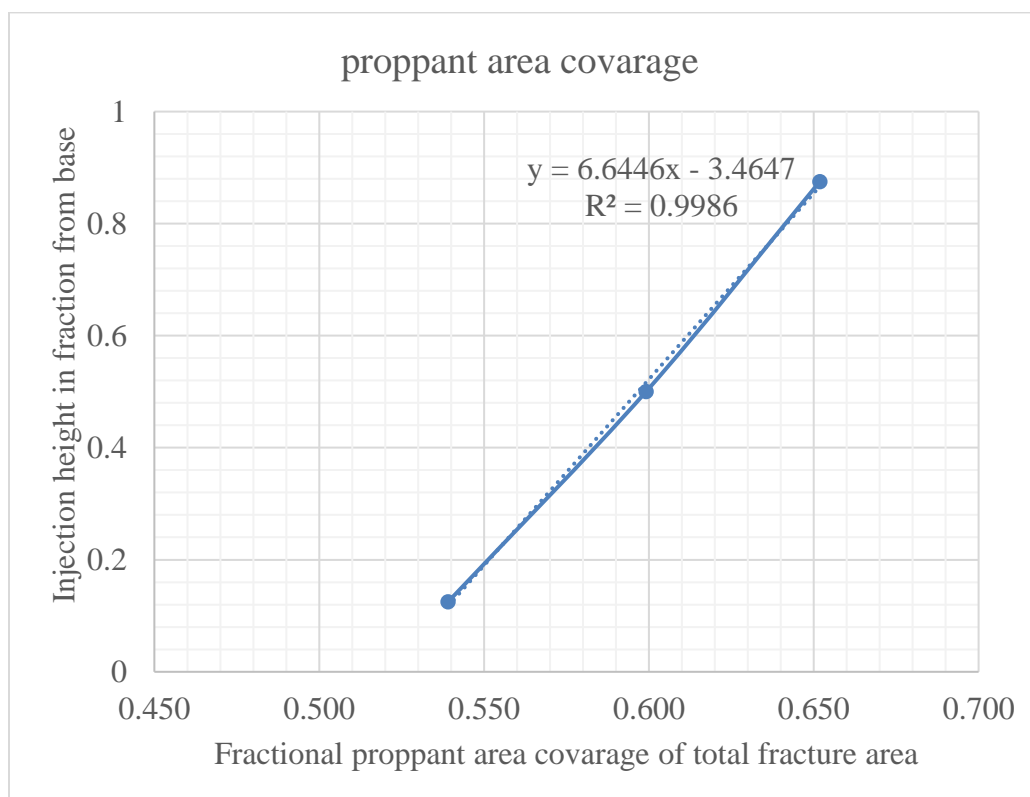
Figure 4.46 Fractional sand proppant area coverage for the fracture with bottom outlet.

4.2.1.4 Dune angle comparison. Angles of various parts of the dune were noted using the graphical representation of the equilibrium dune as mentioned in the earlier section. For the sand proppant particles, friction angle is higher than ceramic and so does the coefficient of friction. So, the buildup angle of part three of the dune was observed higher than that of ceramic proppant around 40^0. Table 4.14 shows angular analysis of dune developed by sand with changing inlet in a fracture with bottom outlet condition.
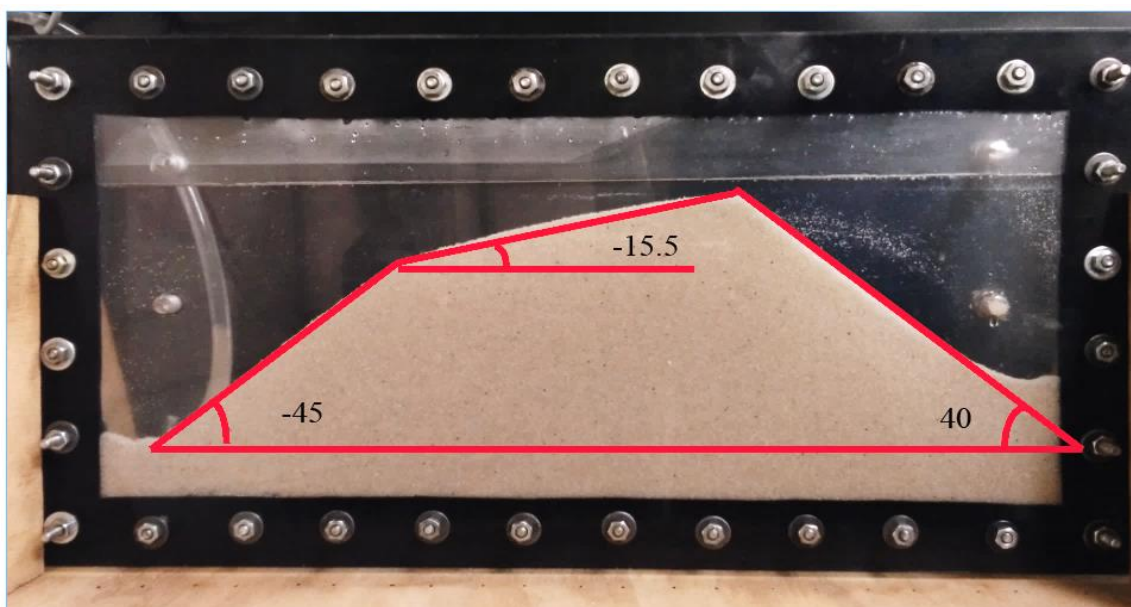
Figure 4.47 Angle measurement for bottom inlet and bottom outlet fracture model (sand proppant).

4.2.2. Ceramic Proppant Results. In this section the results for ceramic proppant are summarized in a fracture with bottom outlet and compared with the sand proppant results explained in the previous section. Table 4.15 summarizes the ceramic proppant results.

Table 4.14 Buildup, drawdown, and dune angle for dune in a fracture with bottom outlet (sand proppant).

Characteristics	Buildup angle	Dune angle	Drawdown angle
Top inlet	20.6	-14.3	-39.7
Middle inlet	39.4	-14.3	-38.4
Bottom inlet	40.0	-15.5	-45.0

Table 4.15 Ceramic Proppant results in terms of EDL, EDX, dune angles and propped surface area fraction.

Characteristics	Buildup angle	Dune angle	Drawdown angle	EDL (%)	EDX (%)	Surface Area Fraction
Top inlet	15	-13.6	-40.8	74	28.54	0.46
Middle inlet	35	-12.8	-38.9	79	38.31	0.54
Bottom inlet	37.8	-14	-37.9	82	42.53	0.60

4.2.3. Dune Comparison. The comparison of different experiment with similar inlet and outlet configuration are compared in this section. The dune formed with sand is also compared with a previous study conducted by Sahai et al. (2014)

4.2.3.1 Dune comparison with ceramic proppant. The dune formed during sand slurry is compared with the dune formed with ceramic proppant slurry injection experiments to analyze effect of angularity of proppant particles on dune development.

Figure 4.48 shows a comparison between equilibrium dune formed for the fracture with bottom outlet from bottom inlet for sand and ceramic proppant. Due to increased friction, dune height is higher and angles were steeper. But creates larger dune both in height as well as length. In other words, higher EDL and EDX were observed compared to ceramic proppant dune. The propped surface area of the fracture was also increased when compared to their counterpart dunes with ceramic proppant. Even though higher dune creates smaller area for incoming slurry, energy loss in vertical proppant movement and

frictional loss due to saltation and reduced rolling movement decreases the proppant velocity in the fracture. In turn, chances of early screen out are increased.

Similar observation for EDL, EDX and proppant-settled surface area fraction can be seen in Figure 4.49 and Figure 4.50 for middle and top inlet experiments.

Table 4.16 lists and compares this values of EDL, EDX and surface area fraction of proppant dune. The quantitative angles of the dune i.e. buildup angle, dune angles and drawdown angles are listed and compared with ceramic proppant dune results in Table 4.17. Higher dune angle and buildup angle were observed for sand as proppant, while drawdown angles were almost similar between the two proppants
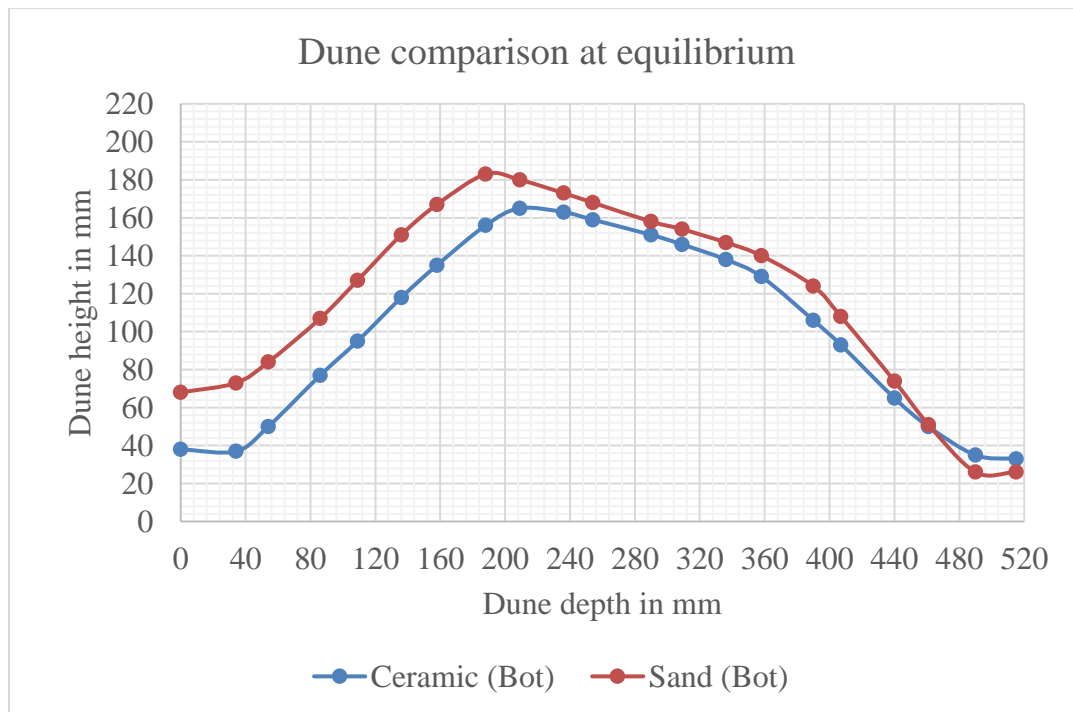

Figure 4.48 Equilibrium dune comparison for ceramic and sand with bottom outlet and bottom inlet.
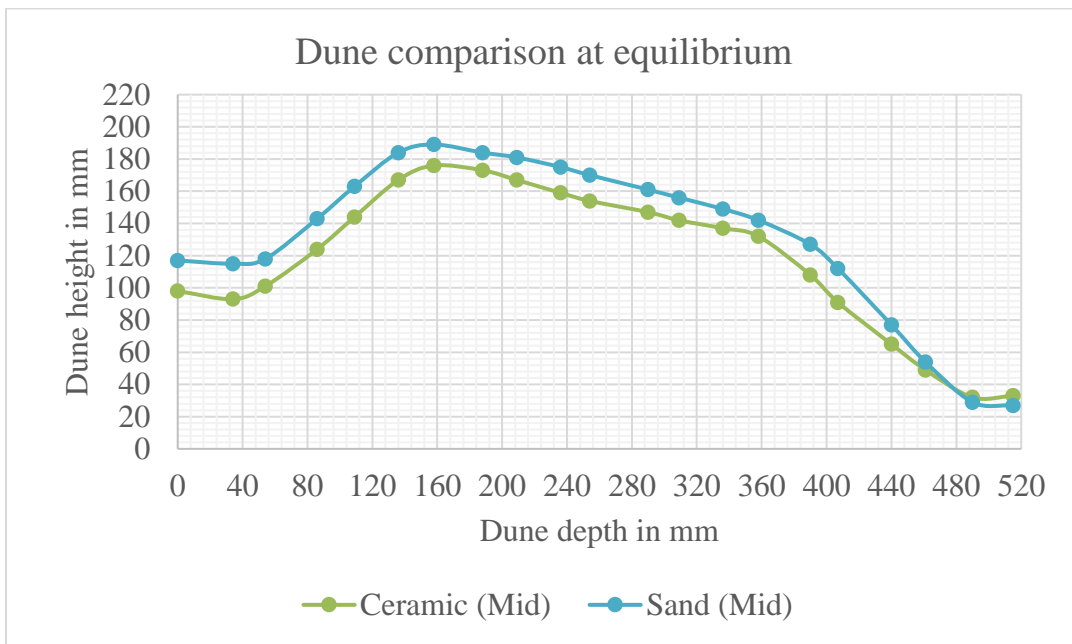
Figure 4.49 Equilibrium dune comparison for ceramic and sand with bottom outlet and middle inlet.
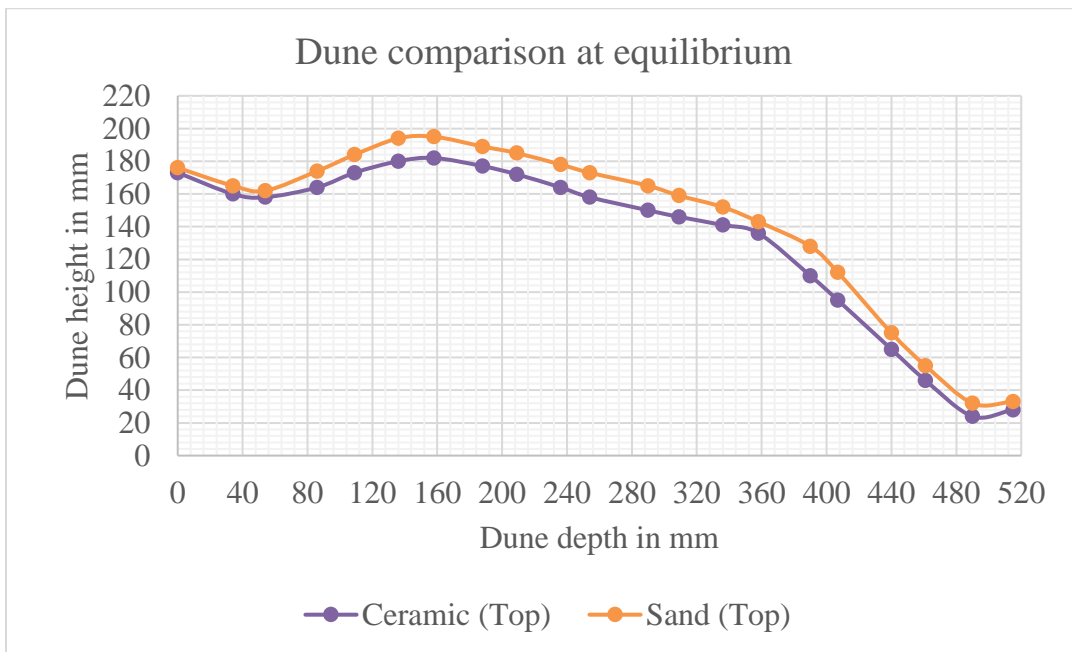
Figure 4.50 Equilibrium dune comparison for ceramic and sand with bottom outlet and top inlet.

Table 4.16 EDL, EDX and surface area fraction comparison between sand and ceramic proppant dune.

Characteristic	EDL (%)		EDX (%)		Surface Area Fraction	
Proppant	Ceramic	Sand	Ceramic	Sand	Ceramic	Sand
Bottom inlet	74	82.8	28.54	38.7	0.46	0.54
Middle inlet	79	85.5	38.31	48.7	0.54	0.6
Top inlet	82	88.2	42.53	48.7	0.60	0.65

Table 4.17 Angle comparison between sand and ceramic proppant dune.

Characteristics	Buildup angle		Dune angle		Drawdown angle	
Proppant	Ceramic	Sand	Ceramic	Sand	Ceramic	Sand
Top inlet	15	20.6	-13.6	-14.3	-40.8	-39.7
Middle inlet	35	39.4	-12.8	-14.3	-38.9	-38.4
Bottom inlet	37.8	40	-14	-15.5	-37.9	-45

Figure 4.51 shows a comparison between dune formed after 3 FPV were injected for the fracture with bottom outlet from the bottom inlet for sand and ceramic particle. It can be observed that due to high fraction angle, sand dune was taller and sharper compared ceramic dune which is shorter and smoother of two.

4.2.3.2 Dune comparison with other experiments. Data from these experiments is compared with the work of Sahai et al. (2014). Sahai conducted experiment using sand and had dune buildup angle of around 45.5^0, dune angle of -1^0, and drawdown angle of
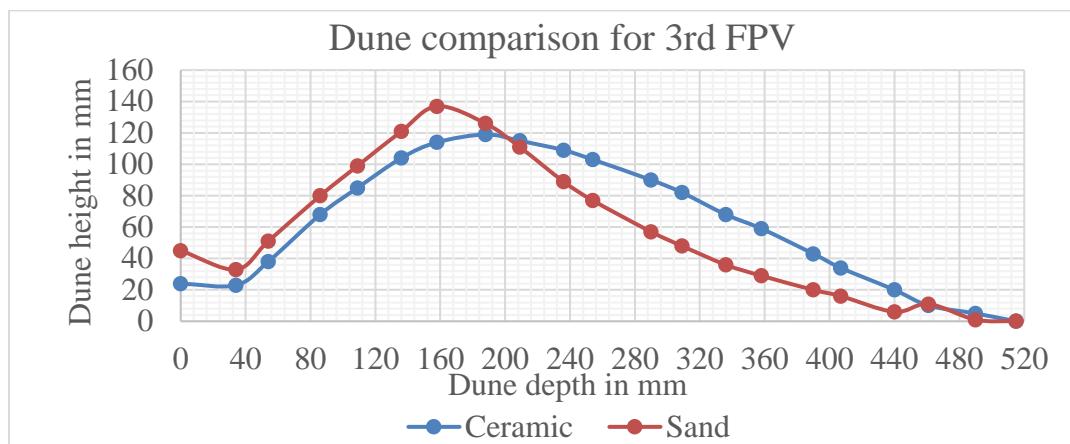
Figure 4.51 Dune comparison after 3rd FPV for ceramic and sand with bottom outlet and bottom inlet.

-40^0. These values were estimated from experimental images presented for brown sand. While during this research buildup angle was observed around 40^0, dune angle was observed in the range of -14.3^0 to -15.5^0 and drawdown angle was around -40^0 for experiments conducted using sand. Figure 4.52 shows sand dune developed by Sahai et al. (2014) in their base case of single slot experiment after 75 minutes of injection. The model was considerably large and flowrate of 25 gal/min was chosen for their experiment.

To compare Sahai's experiment with this research, dimensions were altered to a comparable value. Figure 4.53 shows comparison between the dune created during this research and Sahai's experimental work with brown sand. It can be observed that ceramic proppant dune has low buildup angle compared to sand. The dune angle is different due to the bottom outlet being to close the dune and which changes the shape of the dune.

Figure 4.52 Constructed graphical representation of the dune in single slot scenario for sand slurry injection after 75 minutes (Sahai et al., 2014).
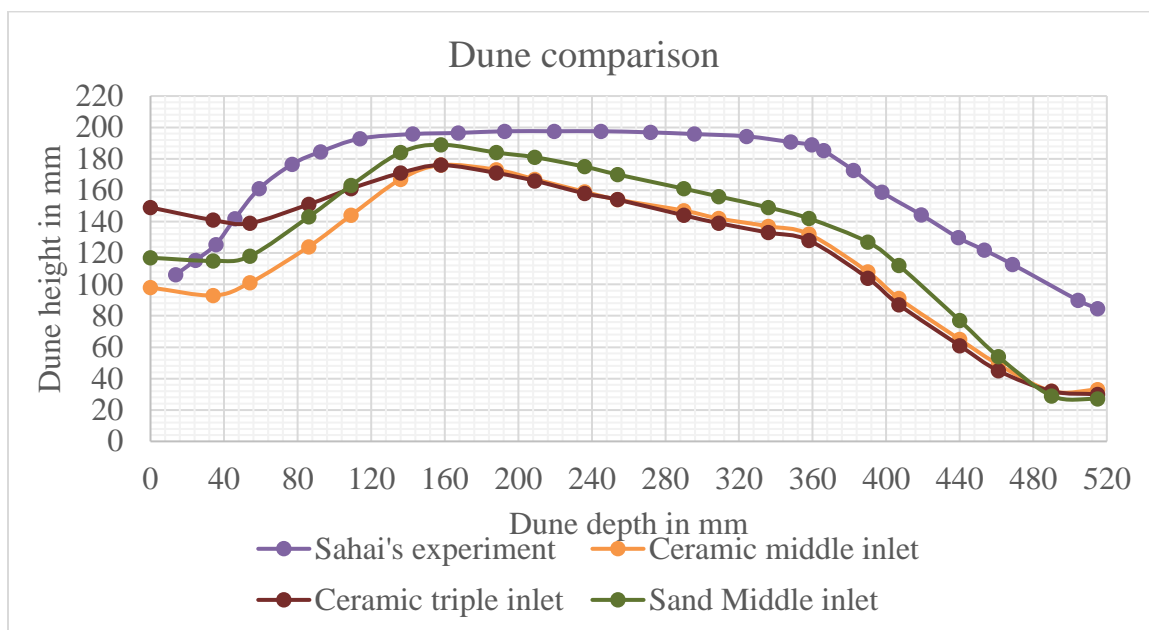
Figure 4.53 Dune comparison between Sahai's experiment and this research.

5. CONCLUSIONS AND FUTURE WORK

5.1. DISCUSSION

This work presents a comparison of single point injection with bottom outlet and top outlet, using either ceramic proppant or sand. The results indicate that if a single injection, or limited number of injection points are connected to a 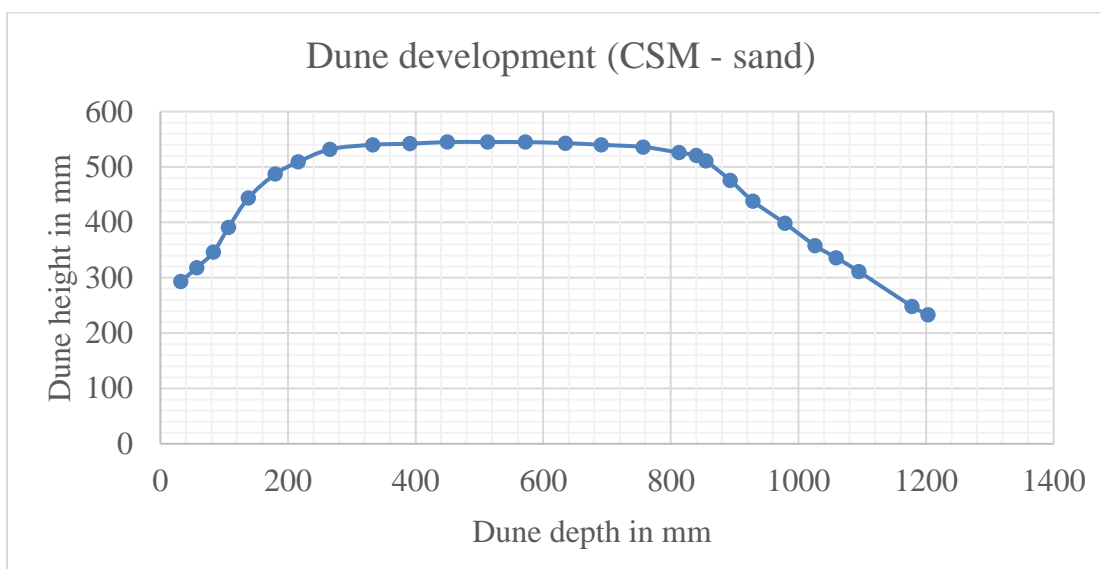planar fracture, proppant placement will be enhanced if the fracture grows uniformly upward and downward, or if there is more downward growth than upward growth (Figure 5.1 and Figure 5.2). These situations lead to the perforation(s) in the middle or toward the top of the fracture, which results in the best proppant placement.

Results of this work also demonstrate that for similar injection situations, proppant dune height (EDL) may be slightly better than ceramic proppant, but EDX is similar. Fracture conductivity was not estimated from the experiments in this study, and it is possible that ceramic proppant would yield higher conductivity even with lower surface area fractions compared to sand. This is due to the more rounded shape or ceramic proppant, which increases propped fracture conductivity.

5.2. CONCLUSIONS

After conducting this research study, following conclusions can be made:

- The perforation height, the proppant angularity, and the multiple active perforations has a significant effect on the proppant transportation.

- At a constant slurry flowrate, the proppant bed area increases with the increase in perforation height.

Figure 5.1 Horizontal well with different well trajectories that mimic height of perforation in horizontal well.
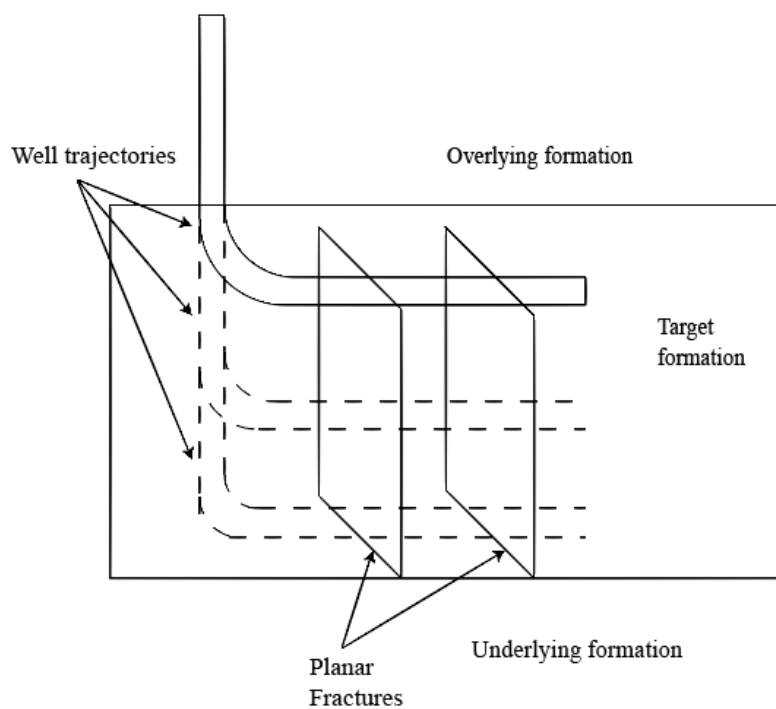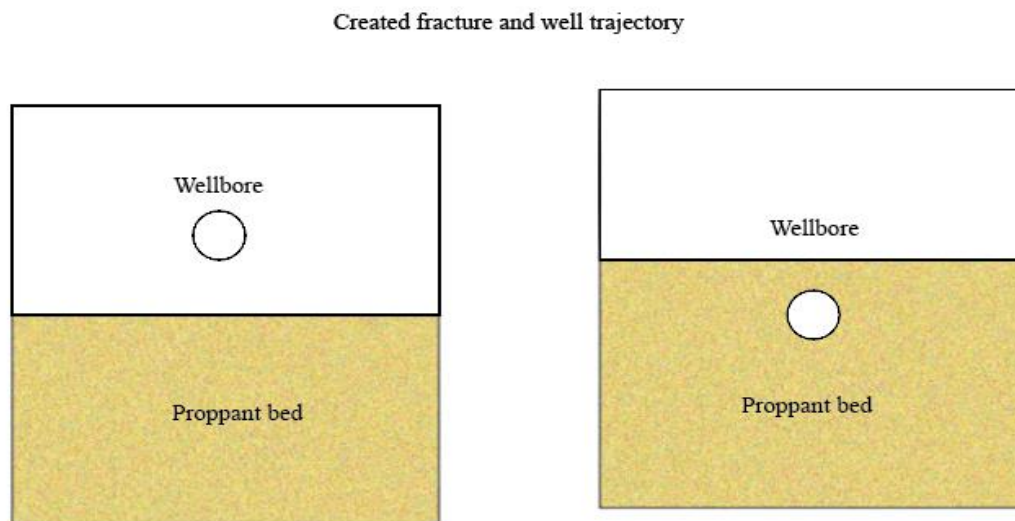

Figure 5.2 Undesired height growth versus desired treatment result.

- On increasing the number of perforations, the proppant velocity in the fracture decreases, which is due to the increase in apparent flowrate of injected slurry compared to single perforation.

- In the vertical wells, the bottom most unblocked perforation is active while the perforations above it have a little to no proppant slurry injected from the other perforations at low flowrates.

- The shape of the dune is dependent on the friction angle of proppant. Proppant with smooth surface i.e. high sphericity and roundness creates low angle dune and provide favorable passage for incoming slurry.

- The proppant passage channels' area decreases with the increase in perforation height, which provide a high velocity passage for the incoming proppant slurry and promotes the deeper proppant injections in the fracture.

- In a model with top outlet, end of the fracture wall contains the proppant dune and increased dune levels are observed.

- The dune shape analysis can be used to mathematically estimate the dune shape with higher accuracy.

5.3. FUTURE WORK

In this research work, fracture depth to height ratio was taken around 2:1 while from the field data most of the fracture have higher ratio for fracture depth to fracture height, in some cases as high as 20:1. So longer slot flow model which can accommodate height variation of perforation should be studied.

During this study for bottom outlet, it was observed drawdown angle of around 40^0s for ceramic proppant which is higher than its friction angle. The effect of outlet was believed to the reason as also seen by Dhurgham et al. (2017) in their research. A longer slot flow model can mitigate this effect and accurate shape of the dune can be identified.

To estimate shape of dune more experiments using different flow rate, viscosity, temperature of fluid and different proppants should be conducted. It can help in understanding whether the stimulation process was successful or not, and what can be done to improve.

Proppant packing density should be studied as well to compare sand and ceramic proppant. Because of high sphericity, the ceramic proppant is believed to be better at solid packing creating better permeability in the proppant dune.

APPENDIX

MEASUREMENT AND DIGITIZATION

For measurement of dune shape and for different analysis, trial version of digitization software called GetData was used. Photos taken after each FPV injected were subjected to measurement. The x and y axis were plotted on the photo according to its inclination to define plan of the measurement. Than software was given reference length for calculation. Now software was ready for output. Now several points were selected that can closely represent the proppant dune and software gave output of their position. These points were used in excel to represent the dune as graph and different analysis were done on this data. For accuracy, few points on dune was physically measured with measuring tape. Figure below shows software interface.

BIBLIOGRAPHY

Abass, H. H., Brumley, J. L., & Venditto, J. J. (1994, January 1). Oriented Perforations - A Rock Mechanics View. Society of Petroleum Engineers. doi:10.2118/28555-MS.

Alotaibi, M. A., & Miskimins, J. L. Slickwater Proppant Transport in Complex Fractures: New Experimental Findings & Scalable Correlation. doi:10.2118/174828-MS.

Britt, L. K., & Schoeffler, J. (2009, January 1). The Geomechanics Of A Shale Play: What Makes A Shale Prospective. Society of Petroleum Engineers. doi:10.2118/125525-MS.

Clark, P. E. (2006, January 1). Transport of Proppant in Hydraulic Fractures. Society of Petroleum Engineers. doi:10.2118/103167-MS.

Clark, P. E., & Zhu, Q. (1996, January 1). Convective Transport of Propping Agents During Hydraulic Fracturing. Society of Petroleum Engineers. doi:10.2118/37358-MS.

Crump, J. B., & Conway, M. W. (1988, August 1). Effects of Perforation-Entry Friction on Bottomhole Treating Analysis. Society of Petroleum Engineers. doi:10.2118/15474-PA.

Economides, M. J. and Nolte, K. G., 2000d. Reservoir Stimulation, 3rd ed. John Wiley & Sons, Chichester, England, Ch. 6, p. 37.

Edelman, J., Maghrabia, K., Semary, M., Mathur, A. K., Zaki, A. S., & Bernechea, J. M. Rod-Shaped Proppant Provides Superior Proppant Flowback Control in the Egyptian Eastern Desert. doi: 10.2118/164014-MS.

Gidley, J.L., Holditch, S.A., Nierode, D.E. et al. 1989. An Overview of Hydraulic Fracturing. In Recent Advances in Hydraulic Fracturing, 12. Chap. 1, 1-38. Richardson, Texas: Monograph Series, SPE.

Huang, J., Datta-Gupta, A., & Augustine, J. R. (2017, March 27). Optimization of Hydraulic Fracture Development and Well Performance Using Limited Entry Perforations. Society of Petroleum Engineers. doi:10.2118/185093-MS.

http://www.corelab.com/owen/tcp-htdblast.

https://www.eia.gov/.

http://www.ogj.com/articles/print/vol-110/issue-5/drilling-production/improved-gas-recovery-2-conclusion-productivity-increase.html.

H.D. Brannon, A.R. Rickards, C.J. Stephenson, R.L. Maharidge, Method of Stimulating Oil and Gas Wells Using Deformable Proppants, US Patent No. 7,322,411 B2 (2008).

Jennings, Alfred. "Navigation." Enhanced Well stimulation, 2008, www.ewstim.com/limitedentry.asp.

Kadhim, D., Imqam, A., & Dunn-Norman, S. Ceramic Proppant Transport and Placement in Heterogeneous Fracture Systems.

Kern, L. R., Perkins, T. K., & Wyant, R. E. (1959, July 1). The Mechanics of Sand Movement in Fracturing. Society of Petroleum Engineers. doi:10.2118/1108.

Lecampion, B., Desroches, J., Weng, X., Burghardt, J., & Brown, J. E. (2015, February 3). Can We Engineer Better Multistage Horizontal Completions? Evidence of the Importance of Near-Wellbore Fracture Geometry From Theory, Lab and Field Experiments. Society of Petroleum Engineers. doi:10.2118/173363-MS.

Liang, F., Sayed, M., Al-Muntasheri, G. A., Chang, F. F., & Li, L. (2016). A comprehensive review on proppant technologies. Petroleum, 2(1), 26-39.

Liu, Y., Fonseca, E. R., Hackbarth, C., Hulseman, R., & Tackett, K. A New Generation High-Drag Proppant: Prototype Development, Laboratory Testing, and Hydraulic Fracturing Modeling.doi: 10.2118/173338-MS.

M. Zoveidavianpoor, A. Gharibi, Application of Polymers for Coating of Proppant in Hydraulic Fracturing of Subterraneous Formations: a Comprehensive Review, J. Nat. Gas Sci. Eng. 24 (2015) 197e209.

Mack, M., Sun, J., & Khadilkar, C. Quantifying Proppant Transport in Thin Fluids: Theory and Experiments. doi: 10.2118/168637-MS.

Malhotra, S., Lehman, E. R., & Sharma, M. M. (2013, February 4). Proppant Placement Using Alternate-Slug Fracturing. Society of Petroleum Engineers. doi:10.2118/163851-MS.

McDaniel, B. W., Willett, R. M., & Underwood, P. J. (1999, January 1). Limited-Entry Frac Applications on Long Intervals of Highly Deviated or Horizontal Wells. Society of Petroleum Engineers. doi:10.2118/56780-MS.

McDaniel, G. A., Abbott, J., Mueller, F. A., Anwar, A. M., Pavlova, S., Nevvonen, O., . . . Alary, J. Changing the Shape of Fracturing: New Proppant Improves Fracture Conductivity. doi: 10.2118/135360-MS.

Miller, C. K., Waters, G. A., & Rylander, E. I. (2011, January 1). Evaluation of Production Log Data from Horizontal Wells Drilled in Organic Shales. Society of Petroleum Engineers. doi:10.2118/144326-MS.

Novotny, E. J. Proppant Transport. doi:10.2118/6813-MS.

Palisch, T., Wilson, B., & Duenckel, B. New Technology Yields Ultrahigh-Strength Proppant. doi: 10.2118/168631-MS.

Parker, M. A., Ramurthy, K., & Sanchez, P. W. New Proppant for Hydraulic Fracturing Improves Well Performance and Decreases Environmental Impact of Hydraulic Fracturing Operations. doi: 10.2118/161344-MS.

Peirce, A., & Bunger, A. (2015, April 1). Interference Fracturing: Nonuniform Distributions of Perforation Clusters That Promote Simultaneous Growth of Multiple Hydraulic Fractures. Society of Petroleum Engineers. doi:10.2118/172500-PA.

Rickards, A. R., Brannon, H. D., & Wood, W. D. High Strength, Ultralightweight Proppant Lends New Dimensions to Hydraulic Fracturing Applications. doi:10.2118/84308-PA.

Roussel, N. P., & Sharma, M. M. (2011, May 1). Optimizing Fracture Spacing and Sequencing in Horizontal-Well Fracturing. Society of Petroleum Engineers. doi:10.2118/127986-PA.

Sahai, R., Miskimins, J. L., & Olson, K. E. (2014, February 4). Laboratory Results of Proppant Transport in Complex Fracture Systems. Society of Petroleum Engineers. doi:10.2118/168579-MS.

Schmidt, D., Rankin, P. E. R., Williams, B., Palisch, T., & Kullman, J. Performance of Mixed Proppant Sizes. doi: 10.2118/168629-MS.

Sinclair, A. R., Graham, J. W., & Sinclair, C. P. Improved Well Stimulation With Resin-Coated Proppants. doi: 10.2118/11579-MS.

Stipp, L. C. and Williford, R. A., 1967. Pseudolimited Entry: A Sand Fracturing Technique for Simultaneous Treatment of Multiple Pays. SPE 01903.

Tong, S., & Mohanty, K. K. (2016). Proppant transport study in fractures with intersections. Fuel, 181, 463-477.

W.C. Krumbein, L.L. Sloss, Stratigraphy and Sedimentation, second ed., W. H. Freeman and Company, San Francisco, 1963, p. 660.

Warpinski, N. R. (2010, November 1). Stress Amplification and Arch Dimensions in Proppant Beds Deposited by Waterfracs. Society of Petroleum Engineers. doi:10.2118/119350-PA.

Wu, K., & Olson, J. E. (2015, April 1). Simultaneous Multifracture Treatments: Fully Coupled Fluid Flow and Fracture Mechanics for Horizontal Wells. Society of Petroleum Engineers. doi:10.2118/167626-PA.

Zhang, G., Li, M., Guo, T., Li, Y., & Chen, Z. (2016). Characterization of proppant effective settlement diameter falling in non-Newtonian fracturing fluids. Advanced Powder Technology, 27(2), 486-495.

VITA

Shail Janakbhai Soni was born in Gujarat, India. He received his bachelor's degree in Petroleum Engineering from Pandit Deendayal Petroleum University in 2014. Shail joined Missouri University of Science and Technology in January 2016. He joined proppant transport research group under direct supervision of Dr. Shani Dunn Norman and Dr. Abdulmohsin Imqam. He received his master's degree in Petroleum Engineering in May 2018 from Missouri University of Science and Technology.